Douglas, Katie (2022) *Tunable three-dimensional hydrogels for pancreatic cancer investigations.* MRes thesis.

http://theses.gla.ac.uk/82762/

Tunable Three-Dimensional Hydrogels for Pancreatic Cancer Investigations

Katie Douglas

Prof. Manuel Salmeron-Sanchez

Centre for the Cellular Microenvironment

University of Glasgow

Prof. Laura Machesky

Beatson Institute for Cancer Research

Glasgow

Table of Contents

List of Tables

List of Figures

Definitions/Abbreviations

2D	Two-Dimensional
3D	Three-Dimensional
AFM	Atomic Force Microscopy
BCA	Bicinchoninic Acid
BSA	Bovine Serum Albumin
CAFs	Cancer Associated Fibroblasts
DMEM	Dulbecco's Modified Eagle Medium
DMEM-Cys	DMEM without Cysteines
E	Young's Modulus
ECM	Extracellular Matrix
ERK	Extracellular Signal-Related Kinase
FA	Focal Adhesion
FBS	Foetal Bovine Serum
FN	Fibronectin
GF	Growth Factor
IAA	Iodacetamine
iCAFs	Immortalised Cancer Associated Fibroblasts
LM	Laminin
MMPs	Matrix Metalloproteinases
M-PEG-SVA	Maleimide-PEG-Succinimidyl Valerate
Mt	Matrigel
OCT	Optimum Cutting Temperature
PBS	Phospphate Buffered Saline
PDAC	Pancreatic Ductal Adenocarcinoma
PEG	Poly-Ethylene Glycol
PEG-4-MAL	4-Arm PEG-Maleimide
PEG-8-MAL	8-Arm PEG-Maleimide
PEG-FN	PEGylated Fibronectin
PEG-LM	PEGylated Laminin
PEG-SH	PEG Di-Thiol
PF	PEG-Fibronectin Hydrogel
PFA	Paraformaldehyde
PFL	PEG-Fibronectin-Laminin (Bi-Protein) Hydrogel
PL	PEG-Laminin Hydrogel
PO	PEG-Only Hydrogel
SH:MAL	Di-Thiol:Maleimide ratio
TGF-β1	Transforming Growth Factor Beta 1
ULA	Ultra-Low Attachment
VPM	Degradable Cross-Linker
WR	Working Reagent
YAP	Yes-Associated Protein
α-SMA	α-Smooth Muscle Actin
ξ	Mesh Size
ρ_c	Effective Cross-Link Density

1 Introduction

1.1 Cancer

The term 'cancer' describes diseases whereby abnormal cells evade apoptosis and undergo uncontrollable and often rapid division. Cancer can spread from its initial site to other sites throughout the body and induce metastatic disease. Cancer remodels the tissue structure and the microenvironment surrounding the cells, alters the genetics of the tissue, and ultimately deems it dysfunctional and ineffective.

This work focuses on Pancreatic Cancer, with a particular interest in the tumour microenvironment and the transition from dormant to metastatic pancreatic cancer.

1.1.1 Pancreatic Cancer

Pancreatic cancer is the term which describes a cancer that has originated in the pancreas. Pancreatic Ductal Adenocarcinoma (PDAC) is among the most deadly cancer malignancies, less than 8% of those diagnosed surviving past 5 years[1,2]. This poor prognosis is the result of a combination of factors including limited treatment response and the likelihood that the cancer has already reached an advanced, inoperable stage before diagnosis[3,4]. The majority of cancer related deaths are caused by metastatic disease[5,6], where the cancer cells have left the initial tumour mass and spread elsewhere in the body. PDAC begins in the pancreas but spread locally into the surrounding tissues and also metastasise to the liver and lungs[7]; this unfortunately removes the option of surgical intervention as a treatment. PDAC most commonly develops from pancreatic intraepithelial neoplasia (PanIN). PanINs present a range of morphological changes and dysplastic growth in the ducts of the pancreas, and in their later stages a mutation in the tumour suppressor p53 gene is commonly observed[7].

Given the development of PDAC from these neoplastic regions, and the effect that such dysplastic growth can have on the surrounding cells and environment, we must pay close attention to the environmental factors which allow and encourage cancer growth.

1.1.2 The Tumour Microenvironment

In order to understand, study, and treat this disease, it is important to understand the environment in which it develops and persists. The extracellular matrix (ECM) is the structure consisting of myriad proteins and molecules within which cells attach, develop, grow, move, and communicate with one another. The stiffness of this matrix is of key interest in cancer research, with tissue stiffness being measured as the elastic modulus, or Young's Modulus (E), which is calculated by stress exerted divided by the resultant strain[8]. Cell-ECM interactions and matrix mechanics are critical for many cellular processes: differentiation, migration, proliferation, growth, cell viability, and development[9,10]; therefore for tissue to function normally, tissue and cellular architecture ensuring normal cell morphology, cell-cell and cell-ECM interactions must be maintained[11], with suggestions that for tissue to ensure normal architecture, tensional homeostasis must be maintained. If matrix stiffness is increased for extended periods, for example due to chronic inflammation or persistent injury, there will be an enduring increase in cytoskeletal tension which may eventually lead to perturbations in tissue architecture. Similarly, a sustained increase in ERK (extracellular signal-related kinase) activity may cause these perturbations in tissue architecture[12]. These microenvironmental disturbances act to increase cellular tension, FA (focal adhesion) assembly, and ERK activation, triggering various epigenetic processes leading to irregular cell growth, malignant transformation, and tumour initiation[9,13].

The tumour microenvironment is often stiffer than that of normal tissues[14,15]; architectural changes, fibrosis, and interstitial pressure increases lead to increased stromal stiffness and cellular tension[9], for example in mouse models of mammary gland tissue, stromal stiffness has been found to be in the range of 1 kPa with the tumour itself reaching > 4 kPa, whereas normal mammary gland tissue stiffness is <200 Pa[9].

A prominent desmoplastic region is characteristic of pancreatic cancer, with a large percentage (often up to 90%) of PDAC tumour volume consisting of fibrous ECM and vasculature, immune cells and cancer associated fibroblasts (CAFs). Pancreatic CAFS, often derived from pancreatic stellate cells (PSCs - prominent

components of the desmoplasia), produce soluble factors (IL-6, IL-11, αSMA among others) and ECM components which aid in the progression of the cancer[2]. Investigations into type IV collagen (col-IV) expression in human adenocarcinoma by Öhlund et al. concluded that col-IV could be viewed as a stroma-related biomarker for pancreatic cancer, with post-operative circulating levels as a potential predictor for disease relapse[16].

Tumours require oxygen, nutrients, and energy to sustain their heightened proliferation and growth rates, so must recruit a vascular system. Irregularities in the recruited network mean that vascularisation varies between tumour regions, leaving oxygen and nutrients unevenly distributed throughout[17]. This poor vascularisation coupled with the oxygen diffusion limit of 200 μm results in hypoxic regions in up to 60% of solid tumours[11]. As previously mentioned, pancreatic cancer displays a limited response to treatment, with its dense ECM and poor vascularisation holding partial responsibility as they physically impair the effective delivery of drugs throughout the tumour[2,3]. Further, investigations into the effects of the tumour ECM on anti-cancer drug activity saw that when various ECM components were added to 2D monolayer cell culture the sensitivity of the cancer cells to the anti-cancer drugs was altered compared to non-ECM controls[14]. This indicates the importance of the tumour microenvironment in therapeutic efficacy.

It is not only the tumour microenvironment which is of such importance the development of, recognition of, and therapeutic efficacy on pancreatic cancer. Another very important factor is the genetics and mutations of the cells which make up the tumour mass.

1.1.3 The Genetics of Pancreatic Cancer

PDAC tumours are generally genetically heterogenous[18], however there are some characteristic mutations of PDAC, all of which have been formerly associated with metastasis. These are mutations of KRAS (occurring in over 90% of PDAC, important in initiation and maintenance of primary and metastatic tumours, helping sustain survival in low nutrient environments[5,4]), p16[INK4A] which also appear in over 90% of PDAC, TP53 appearing in ~70% of PDAC, and SMAD4 appearing in 55% of PDAC[4]. PDAC are most frequently believed to develop from PanINs, where lesion progression and early KRAS mutations lead to malignant,

invasive disease[4,19]. Work on a mouse model of reversible PDAC by Lin et al. found that the down-regulation of the c-Myc oncogene led to macroscopic remission of the primary tumour as well as cell death at the metastases, however residual cells were capable of reinitiating the cancer when c-Myc was re-expressed[20]. Ying et al. found that the removal of the Kras oncogene led to rapid tumour regression, and a reduction in the number of PSCs[19]. Oncogene removal also led to the downregulation of certain metabolic pathways, a reaction later confirmed in work by Viale et al. who, as well as demonstrating the characteristic heterogeneity[21] of PDAC tumours, described the dependence of pancreatic cancer cells on mitochondrial function[22]. Öhlund et al. produced an organotypic system by co-culturing pancreatic organoids described by Boj et al.[3] with PSCs or cancer associated fibroblasts (CAFs) in Matrigel, further demonstrating the intratumoural heterogeneity of pancreatic cancer and its related stroma with the identification of two CAF subtypes: myofibroblastic and inflammatory[2].

Both the genetic make-up of the tumour itself and the signals and influences coming from the tumour microenvironment have an effect on the behaviour of the cancer.

1.2 Tumour Behaviour

Given the above discussion of the genetic heterogeneity and plethora of environmental signals which are available to cancer cells, it is understandable that not all tumours, or even cells within or related to the tumour, behave similarly. Some cancers may lie quietly dormant, some may be malignant and actively metastatic. Both of these cases will be described below.

1.2.1 Dormancy

In relation to cancer, dormancy can describe three separate conditions; angiogenic dormancy, immune-mediated dormancy, and cellular dormancy[23]. The first two ensure that the tumour mass is unable to grow; cell proliferation is matched by cell death either due to poor vascularisation or immune-mediated cytotoxicity, with the resulting non-proliferating mass being described as an 'indolent metastases'[5]. Unfortunately dormant, or very slowly developing, endogenous tumours are often not recognised by the immune system, therefore

are able to evade immune-mediated death[24]. However, work on mouse models of melanoma by Elyes et al. demonstrated the role of CD8+ T cells in the immunosurveillance of primary and metastatic lesions; depletion of these cells increased the likelihood of metastasis formation, whereas without this immune depletion the number of cells expressing the Ki67+ proliferation marker was low, indicating CD8+ T cells are active in inhibiting proliferation[25]. The third dormancy condition described is when cells undergo cell cycle arrest and become quiescent. This can relate to cells within the tumour mass that are non-proliferative; their state is dictated by availability of oxygen and nutrients so as the mass grows, supply available to core region decreases, resulting in a structure which has high levels of proliferation close to the blood supply and regions of reduced proliferation, dormancy, or even cell death deeper within the mass. Cellular dormancy may also relate to single disseminated cells which have become quiescent[26].

A recent review by Gay and Malanchi discusses the mechanisms permitting metastatic latency (time between dissemination and outgrowth), and how the microenvironments of distant tissues affect disseminated tumour cells. An adaptive environmental niche is required to maintain the progression of metastases, as the requirements of the metastatic cells change with time. A dormant niche on the other hand, must remain stable to keep the cells in a quiescent state. They also discuss signalling pathways of importance in dormancy and proliferation; p38 activity is associated with dormancy, Akt mediates survival, ERK activation is high in proliferating cells[5]. Until recently, the main method for dynamic measurements of single cell kinase activity was with Förster resonance energy transfer (FRET) sensors, however recent work carried out by Regot et al. has produced a series of fluorescent biosensors able to report kinase activity (kinase translocation reporters (KTRs)) within living cells[27]. Lifeact, another technology for cell visualisation, in this case of the actin cytoskeleton, was described by Riedl et al.[28]. These novel technologies should allow improved measurement, analysis, and understanding of cellular signalling and kinase activity within single live cells, as well as visualisation of the cellular structure, demonstrating how biotechnological advances and novel engineering solutions are furthering the understanding of cancer, dormancy, and metastasis.

1.2.2 Metastasis

Metastasis is characteristic to malignant disease. It is the process by which cells move through the basement membrane, escape the primary tumour, travel through blood and lymphatic vessels as circulating tumour cells (CTCs), invade, and remain in distant sites as disseminated tumour cells (DTCs), where they can initiate secondary lesions[4-6,23]. A vital step in this process is ECM and basement membrane breakdown by matrix metalloproteinases (MMPs)[6]. Another proposed key step is the epithelial to mesenchymal transition (EMT), wherein carcinoma cells convert from differentiated epithelial-like cells with characteristic cell-cell adhesions, polarity, and minimal motility, into stem cell (SC)-like cells with mesenchymal features; increased resistance to apoptosis, increased motility, and invasive properties[29].

There is some controversy in the field regarding when in disease progression metastasis occurs, with some describing the disease evolution as linear, with metastasis as a late event[30], and others suggesting dissemination may occur early in tumour formation[24]. Eyles et al. found a match between the genetic signature of the primary tumour and that of the cells within metastatic lesions in mouse models of melanoma[25], and even when the disease is in the PanIN stage there has been evidence that some cells expressing cancer SC markers have been shed into circulation from this premalignant site[4], supporting the hypothesis that dissemination may occur early, and in parallel to tumour progression.

Mathematical analysis of patient data allowed Haeno et al. to investigate progression, dissemination, and metastasis kinetics in pancreatic cancer, predicting all primary tumours contain a fraction of cells capable of metastasising at the point of diagnosis[31]. Rhim et al. also investigated the kinetics of dissemination and EMT using novel cell tracking to observe pancreatic epithelial cells in a mouse model of PDAC. They found that cells were entering the circulation and disseminating early in tumour formation, again supporting the view that dissemination and tumour growth occur in parallel[24,25]. They also induced pancreatitis to assess how inflammation may affect EMT, finding an increase in EMT, circulating cells and dissemination, and interestingly pancreatic cells without oncogenic mutations undergoing EMT and beginning to

circulate[32]. From this, it can be concluded that inflammation may encourage EMT and dissemination to aid in cancer progression, providing evidence that environment is important as a driver of metastasis.

1.2.3 Therapy and Resistance

Cancers are highly dangerous in their metastatic state, and in their dormant state they are, by definition, only dormant and can become active and dangerous in response to various factors. As such, finding efficient and effective therapies to treat cancer is highly important.

Cancer therapy aims to fully remove the known tumour mass and prevent cancer recurrence while concurrently stopping dissemination of malignant cells to distant sites[33], with cytostatic drugs being of particular interest[26]. Drug resistance, either *de novo* or acquired, limit treatment response, with acquired resistance arising due to genetic heterogeneity, drug pharmacokinetics, the actions of the cancer cells in clearing the drugs, and potentially cellular dormancy[26]. Anti-proliferative drugs can be ineffective in eradicating dormant cells, with cell cycle arrest (at the G0-G1 phase - a marker of single cell dormancy) being partially responsible, along with expression of ATP binding cassette (ABC) transporters[33,34]. Wenzel et al. recently described a cancer spheroid model *(1.2.2 – Three Dimensional Models)* for high content drug screening. The central, dormant regions of these models with limited oxygen and low glucose levels were found to be more responsive to drugs inhibiting the respiratory chain[26]. Grandhi et al. found, using a dormant 3D bladder cancer environment model, that dormant cells could survive proliferation-targeting chemotherapeutic treatments, however these dormant environments could be ablated with drugs inducing chronic stress in the endoplasmic reticulum[35].

Unfortunately, palliative treatment often remains the only course of action for pancreatic cancer patients[5,6], however there is a great deal of ongoing work into models of pancreatic cancer and dormancy in attempts to find new therapeutic targets to improve the prognosis of this malignancy.

1.3 Engineering solutions

Cancer research relies on in vitro models to better understand the disease and investigate potential treatment techniques and drug efficacies. Over the years these models have evolved from 2D cultures in glass dishes to much more complex 3D tumour models. What is still to be developed is a highly reproducible model able to incorporate more of the surrounding tumour microenvironment and signalling molecules in a controlled manner. This would allow for more accurate investigations and drug testing, as the influence of the surrounding cells and environment would also be taken into account.

1.3.1 Two Dimensional Models

Traditionally 2D cell culture has been used, and is still widely used, as the main method for (pre-clinical) drug testing due to the lack of suitable 3D *in vitro* models[17], with the first record of tissue culture published by Harrison et al. in 1907[36] with developments and improvements producing the process we know today; cells are grown, fed, and sub-cultured as monolayers in plastic tissue culture flasks[11]. However, repeated passaging on hard, flat plastic tissue culture-ware leads to the formation of a selective, homogeneous monolayer of cells with increased survival on said substrate and rapid proliferation rates; this monolayer poorly represents the heterogeneous 3D population, and could respond more strongly to anti-proliferative drugs, giving false expectations leading into *in vivo* trials[17]. Many sources report that culture on hard, flat glass or plastic do not closely mimic the mechanical or biochemical environment that cells experience *in vivo*, nor are they able to reproduce *in vivo*-like morphology, architecture, receptor expression, soluble factors, cell-cell or cell-ECM interactions; as such conclusions drawn from 2D cell culture may not translate to 3D culture or *in vivo* implementation[11,13,14,17,37]. For example, it has been reported that various tumour cells have been found to be less sensitive, equally sensitive, or more sensitive to anti-cancer drugs in 3D when compared to 2D for the same drug and cell type, with studies revealing significant genetic differences between cells as well as changes in protein expression when cultured in 3D compared to 2D[14]. As such, the development and implementation of 3D models has been necessary.

1.3.2 Three Dimensional Models

With increased cell-cell and cell-ECM interactions, variations in proliferation, oxygen and nutrient gradients throughout the volume, and increased stromal ECM with the possibility of stromal cell addition, 3D cultures present a more realistic environment, and therefore drug response, than traditional monolayer culture[14].

There are various possible 3D models, ranging from *in vitro* 3D scaffolds or cultures to the *in vivo* animal models. Xenografts allow for the study of human cancers within a more physiologically relevant environment, however these are not without issue; the animal tissue microenvironment is not identical to human tissue therefore cells do not behave exactly as they would in human patients[17]. The use of patient-derived xenografts and genetically engineered mouse models to investigate PDAC has given insight into the disease, however these methods are expensive, time consuming, and highly complex due to the plethora of signalling molecules and pathways presented[3,17]. Implementing a 3D scaffold or culture system allows analysis of cells in an environment that closely mimics the composition and architecture of the physiological tissue without the need for animal models [14].

A commonly implemented 3D model for cancer research is the multicellular tumour spheroid. Tumour spheroids are spherical cellular aggregates between 20 μm and 1000 μm in diameter and display an increase in ECM deposition compared to monolayers, more cell-cell contact, and importantly regional variations in viability, metabolism, and proliferation rates[14,17,26]. Wenzel et al. produced breast, prostate and colorectal cancer spheroids (~400 μm Ø) with anoxic cores, dormant regions of intermediate oxygen, and proliferative outer regions of sufficient oxygen and glucose. They saw that hypoxia and slow nutrition responsive genes were up-regulated within the 3D spheroids compared to the same cells in 2D culture, emphasising the need for more 3D *in vitro* models[26].

Spheroids can be formed by a variety of methods[17]. Some are anchorage independent; liquid overlay, hanging drop, spinner flasks, and rotary wall vessels[14]. Spheroids produced via overlay culture display notable differences in many characteristics; such as morphology, growth rate, viability, and diffusion,

however the surface modifications necessary can be time consuming or costly[11,38]. Hanging drop culture can result in highly reproducible spheroids, however the they are easily disturbed during production[11]. Spinner flasks and rotary wall vessels can produce high numbers of spheroids but with inconsistencies in spheroid size, specialist equipment required, and sheer forces affecting the formation, these systems have their drawbacks[11,17]. There are also anchorage dependent methods such as culturing within hydrogels; cancer cells are known to aggregate within 3D scaffolds or gels, however there can be issues with spheroid distribution and overlap[11]. Other issues that may arise when working with 3D samples are the difficulties encountered when attempting to accurately image the thick, highly scattering samples[13], as well assess drug response, viability, and proliferation; traditional monolayer assay protocols may need to be altered to allow diffusion of the reagents throughout the full volume of the model, and also to account for the variations in viability and proliferation in different regions of the model[17].

Hydrogels, mentioned above as a scaffold for anchorage dependent spheroid formation, are versatile networks which can be used as a 3D cell culture platform for a variety of purposes, ranging from cancer investigations to bone regeneration.

1.3.3 Hydrogels for Three Dimensional Models

Hydrogels are swollen hydrophilic 3D networks of polymers, synthetic or biological, which can be used for a variety of purposes, including controlled substance release and cell encapsulation. In terms of mechanical properties, polymer gel stiffness can be controlled by polymer density or cross-linking density; these changes also lead to alterations in the mesh size which in turn affect the spatial restrictions and diffusional properties within the gel[10]. Synthetic scaffolds, while providing precisely tunable mechanical properties, lack the inherent biological cues of a biological scaffold. Biological scaffolds, such as collagen, and Matrigel biopolymers[10,17], provide a plethora of biological information, however the signals provided can often be too many to pin-point which signals are causing which activities, and Matrigel, although commonly used, has high instances of inter-batch variability. The ideal scaffold should have the mechanical tunability provided by synthetic materials while

incorporating the biofunctionalties of interest, such as adhesive sites, growth factor binding domains, or degradable sites to produce environments that closely mimic those *in vivo* while remaining structurally controllable[39-41]. For a 3D culture system to allow embedded cells to grow, migrate, and remodel the matrix as required, this element of degradability must be factored in, often in the form of a protease-degradable crosslinker[10].

Poly-ethylene glycol (PEG) is a synthetic polymer which has been widely utilised in hydrogels due to its high biocompatibility and its low toxicity and inflammatory reactions *in vivo* which, when coupled with its low protein adsorption, ease of functionalisation, versatile physical characteristics, and distinct physical structure, results in high standard hydrogels which have proven safety *in vivo*. A further benefit of using PEG is that it can be cross-linked in non-toxic conditions either by Michael-type addition or by photoinitiation, therefore gelation can occur in the presence of cells [10,41,42].

As PEG is a widely used and versatile component, there is a wide range of previously implemented PEG-based gels. Raeber et al. describe 4-arm PEG-Vinyl Sulfone based gels sensitive to MMPs or plasmins for cell migration studies, finding cell viability, morphology and migration to be comparable to those within the more commonly implemented biopolymer matrices[37]. When investigating cross-linking in various PEG based gels, Phelps et al. found that functionalising 4-arm PEG with maleimide end groups (PEG-4-MAL) produced hydrogels able to fully cross-link in ≤5 minutes (rapid gelation is desirable in terms of cell distribution as it allows less time for cells to sink), with stiffness comparable to natural microenvironments, and efficient peptide incorporation compared to other hydrogel variations[42]. Cruz-Acuña et al. utilised PEG-4MAL functionalised with the cell-adhesive RGD peptide sequence to generate and grow human intestinal organoids from intestinal spheroids, with similar viability to those grown within Matrigel[10]. Trujillo et al used PEG-4-MAL to produce functionalised hydrogels, PEGylating FN monomers and producing tunable hydrogels able to retain growth factors in a controlled manner[43]. Almany et al. also functionalised their PEG gels by polymerising PEGylated fibrinogen (PEG-diacrylate), finding that the incorporation of fibrinogen lowered the elastic moduli of the gels as fewer crosslinking sites were available, however varying the PEG-diacrylate amount allowed control over stiffness. These gels are an

improvement upon those described by Phelps et al.[42] as they implement a natural protein backbone as opposed to solely the adhesive peptide chain, and they were found to be able to promote both cellular adhesion and extension of endothelial cells as well as provide sites for proteolytic degradation of the scaffold, while attaining the desired mechanical properties[41].

A variety of 3D dormancy studies have been carried out recently implementing various PEG-based and non-PEG-based gels. Cultrex® basement membrane extract (Trevigen Inc., MD[44]) was employed by Barkan et al. to investigate the influence of type I collagen (col-I) enriched fibrosis in breast cancer dormancy, finding it encourages the awakening of dormant cells, and their subsequent proliferation[45]. Grandhi et al. developed an aminoglycoside-derived hydrogel "Amikagel", and were able to produce dormant 3D bladder cancer tumour environments, with Live/Dead® (Molecular Probes, Inc.[46]) staining revealing that they consisted of an outer layer of metabolically active cells, with the central cells under stress and displaying high levels of cell death. They demonstrated the importance of the tumour microenvironment when the transfer of the dormant environments to softer, adhesive gels led to cell escape and micrometastasis-like nodule formation[35]. To investigate environmental effects on dormant and proliferating breast, pancreatic and colorectal cancers, Fang et al. used Col-Tgel (101Bio, CA[47]) of varying stiffness to reveal that the doubling time of these cells was slower in 3D culture than in 2D monolayer culture, and that morphology, activity and cell number varied within each cell line depending on the substrate stiffness[48]. However with an upper stiffness of 50 kPa in this[48] case, and all "Amikagel" systems[35] having stiffness greater than that of bone, these systems may not truly represent the *in vivo* microenvironment. Further work is still required to accurately recreate the dormant niche for studies into dormancy and reawakening of all cancers, including pancreatic.

1.4 Objectives

Given the poor prognosis for many pancreatic cancer patients, and the need for more research and testing into possible therapeutic targets and drugs, there is a requirement for a more accurate and reproducible model of pancreatic cancer.

The base objective of this work is to produce a controllable, synthetic, physiologically relevant, 3D model for pancreatic cancer investigations; namely, gaining a better understanding of PDAC behaviour in specific environments, and assessing therapeutic effect in 3D compared to 2D.

Much work has been carried out utilising hydrogels with cell adhesive ligands (such as RGD and IKVAV) or other bioactive peptides[40,49,50], however examples of synthetic hydrogels containing full proteins are limited. Using full proteins will allow more functionalities to be incorporated into the system simultaneously, with cell adhesive sites and a range of domains for binding various molecules. This system is a platform which should allow the incorporation of many proteins relevant to the cancer microenvironment.

In this work, the proteins that will be incorporated are fibronectin (FN) and laminin (LM); FN is abundant in the ECM, with key roles in cell adhesion, migration, growth and differentiation[51], and LM (specifically LM 332) is important in sustaining CAF phenotype[52] and has a range of growth factor (GF) binding domains[53], combining to promote carcinoma cell invasion. Incorporating these proteins into PEG-Based hydrogels will provide a mechanically controllable, biofunctional, and more physiologically accurate model of PDAC for future investigations.

More specifically, this work aims to begin investigations into the use of these hydrogels as an in vitro PDAC model by carrying out the following work:

- Assess the suitability of PEG-based hydrogels for investigations with PDAC cells.

- Assess the behaviour of PDAC cells in response to varying conditions of PEG-based hydrogels.

- Explore the effect that cancer related cells have on the behaviour of PDAC cells within these hydrogels.

- Alter the hydrogel composition to incorporate laminin into the network and determine the success of this incorporation.

- Assess the behaviour of both cell types in the new bi-protein hydrogels.

- Introduce growth factors into the hydrogel system, determine the hydrogel composition with the most GF uptake, and observe the effects of the GF on PDAC cells.

Following this work, conclusions will be drawn as to the suitability of this system as an in vitro model of pancreatic cancer.

2 Materials and Methods

2.1 Cell Culture

All cell culture reagents were purchased from Thermo Fisher Scientific.

C2C12, PDAC cells (line B, isolated from Pdx1-Cre positive, LSL-Kras$^{G12d/+}$, LSL-Trp53$^{R172H/+}$ (KPC) mice[54]) and immortalised cancer associated fibroblasts[55] (iCAFs) were cultured in Dulbecco's Modified Eagle Medium (DMEM) (+)4.5g/L glucose (+) 0.11g/L sodium pyruvate (Gibco), (+) 2 mM L-Glutamine (Sigma), supplemented with 1% antibiotic (Gibco) and 10% foetal bovine serum (FBS)(Gibco). Cells are incubated at 37°C in 5 % CO_2. Cells are seeded in culture dishes at a density of 20,000 cells/cm^2 (1.5 x 10^6 in a T75 culture dish as standard), and passaged every 2 to 3 days, up to passage 18.

PDAC cells are encapsulated in hydrogels at 200,000 cells/ml and iCAFs are encapsulated at 400,000 cells/ml unless otherwise stated.

For PDAC spheroid and iCAF co-culture, cells were incubated with cell trackers for 1 hour before trypsinisation from culture flasks: iCAF with Cell Tracker Red (Thermo Fisher) and PDAC with Syto 13 (Thermo Fisher).

2.1.1 Spheroid production methods

2.1.1.1 Hanging Drop

Up to 500 PDAC cells (from culture dishes as described above, no higher than passage 12 for spheroid production) were suspended in the medium outlined above (DMEM (+)4.5g/L glucose, (+) 0.11g/L sodium pyruvate, (+) 2 mM L-Glutamine) on the underside of 96 well multi-well culture plates. They were cultured for 7 days, incubated at 37°C in 5 % CO_2.

2.1.1.2 Ultra-Low Attachment Plates

PDAC cells (from culture dishes as described above, no higher than passage 12 for spheroid production) were seeded in ultra-low attachment (ULA) 96 well plates (Corning) at 2500 cells per well and incubated in the medium described

above (DMEM (+)4.5g/L glucose, (+) 0.11g/L sodium pyruvate, (+) 2 mM L-Glutamine) at 37°C in 5 % CO_2 for 3 days before use.

2.2 Hydrogel Preparation

2.2.1 PEGylation of Proteins

The PEGylation of proteins is the incorporation of PEG molecules onto the proteins. This work uses site-specific PEGylation.

Fibronectin is PEGylated following the protocol by Dr Trujillo-Muñoz[56], developed from a method used by Almany et al[41]. The PEGylation of fibronectin in this case is site specific thiol PEGylation with PEG-Maleimide. The FN protein molecule is denatured to open the disulphide bonds between the two strands, exposing cysteines which are then free to react with the maleimide group by Michael-Type addition.

The laminin PEGylation performed here is amino group reactive PEGylation. A PEG molecule with maleimide for crosslinking throughout the hydrogel network and succinimidyl valerate (an active ester) for binding the laminin was utilised in this case. The succinimidyl valerate forms an amide linkage with the free amines of the Laminin molecule, and the maleimide is later required to react with the cross-linker to bind to the hydrogel structure.

2.2.1.1 PEGylation of Fibronectin

Fibronectin (FN) (Yoproteins, 50 µg/50 µl hydrogel) was denatured by mixing with an equimolar amount of TCEP (Sigma, 0.5 M Stock, pH 7), and 8 M urea (Fisher), allowing 15 minutes at room temperature. The required amount of 4-Arm PEG-Maleimide (PEG-4-MAL) (Laysan Bio, 20 kDa) was added to achieve a 1:4 FN:PEG-4-MAL molar ratio and shaken for 30 minutes at room temperature. The reaction was stopped by adding 0.5 µM NaOH. Iodacetamine (IAA) was added and shaken in darkness for 2 hours at room temperature to alkylate the protein, and solution was then dialysed against phosphate buffered saline (PBS). The protein was precipitated in ethanol and resuspended in 8 M urea to reach a final concentration of 2.5 mg/mL PEGylated FN (PEG-FN) and dialysed against PBS.

2.2.1.2 PEGylation of Laminin

Laminin (LM) (Biolamina, 10 µg/50 µl hydrogel) was dialysed against PBS (pH 8). Maleimide-PEG-Succinimidyl Valerate (M-PEG-SVA) diluted in PBS (pH 8) was added to achieve 1:10 LM:M-PEG-SVA molar ratio and shaken for 4 hours at room temperature. Solution was then dialysed against PBS (pH 7.4) and concentrated to a final concentration of 600 µg/ml PEGylated LM (PEG-LM).

2.2.2 PEG-FN Hydrogel Production

Polymer solutions were prepared by diluting the polymer powder in PBS (using DMEM without cysteines (DMEM-Cys) when cells were encapsulated). The PEG-MAL and PEG-FN (and cell suspension in DMEM-Cys when cells were encapsulated) were mixed, and the cross-linker (pure PEG-dithiol (PEG-SH) or a mixture of PEG-SH and a degradable peptide chain; VPM) added. The hydrogels were cured for 1 hour at room temperature or 30 minutes in the cell incubator, and then covered with PBS when working without cells, or cell culture media when cells were encapsulated.

Hydrogels for initial characterisation and Live/Dead assays were cross-linked with pure PEG-SH. Following this, unless otherwise stated, hydrogels were cross-linked using an 80:20 PEG-SH:VPM mix, providing 20% degradability in the hydrogel network.

For slower gelation times, the pH of the solution was lowered by reducing the pH of the DMEM-Cys used for polymer dilution and cell suspension.

See Figure 1 for schematic of PEG-FN hydrogels.
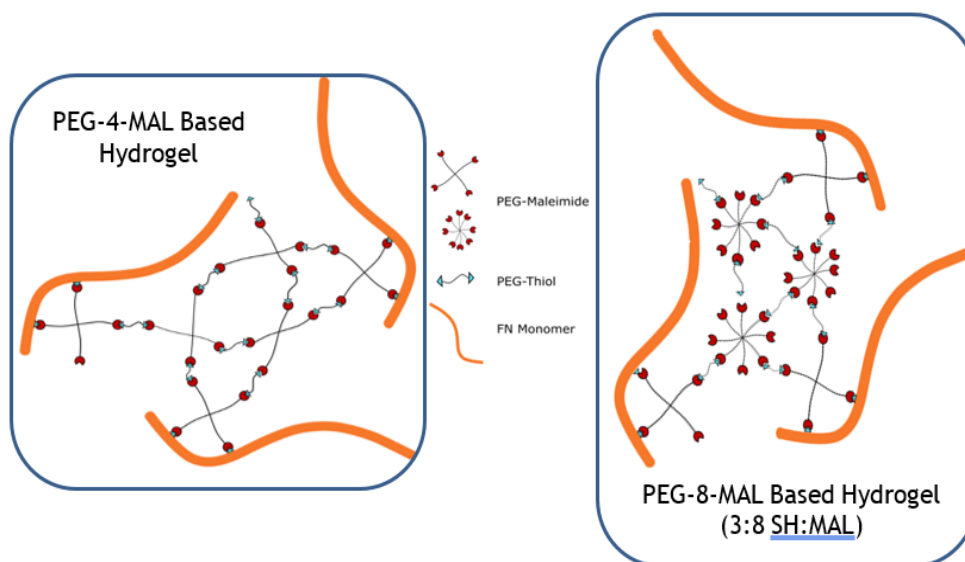
Figure 1: Schematic of 4- and 8-Arm PEG hydrogels (not to scale). These schematics show the interaction between fibronectin monomers, the PEG molecules with which they are PEGylated, and the PEG (maleimide and di-thiol) which form the rest of the network around the fibronectin.

2.2.3 PEG-LM and PEG(+)LM Hydrogel Production

As with the PEG-FN hydrogels, PEG-4-MAL, PEG-LM (or un-PEGylated LM in PEG(+)LM control) and PBS were mixed, and cross-linker added. Hydrogels were cured for 1 hour at room temperature, and then covered with PBS.

2.3 Hydrogel Characterisation

2.3.1 Atomic Force Microscopy

AFM force mapping measurements were carried out with cantilevers of 0.3 N/m or 0.03 N/m, both with 20 μm Ø spherical tips. Raw data were processed in JPK Data Processing software using the Hertz model for a spherical indenter.

2.3.1.1 Preparing Hydrogels for AFM

When prepared for atomic force microscopy (AFM) measurements, hydrogels were swelled in PBS for 24 hours post curing, then flash frozen in liquid nitrogen and embedded in Optimum Cutting Temperature (OCT) compound for sectioning. Sections (100 μm thickness) were produced with the cryotome.

2.3.2 Hydrogel Swelling Assay

Hydrogels were cured, weighed (t=0), and covered with 1 ml of MilliQ water to swell. At various timepoints, the liquid was removed, and the hydrogels were weighed. Upon confirming hydrogel mass equilibrium, the hydrogels were dried, and dry weight recorded.

2.3.3 Degradation Assay

Swollen hydrogels of each condition were covered with 50 U/mL collagenase. At various timepoints, the liquid was removed, and the hydrogels were weighed.

2.3.4 Mesh Size Calculations

AFM data and swelling data were input into calculations (based on a PhD thesis by Ting Yang[57]) in order to determine hydrogel mesh size.

2.3.5 Laminin Release

For LM release, cured hydrogels were swollen in 300 µl PBS for 24 hours, therefore maximum LM concentration per sample was 28.6 µg/ml.

2.3.5.1 BCA Assay

Bicinchoninic acid (BCA) assay (Thermo Fisher) was carried out following the user manual on the PBS supernatant following 24h swelling. Briefly, a BSA dilution was prepared for a protein standard. Working reagent (WR) was added to the BSA dilution and the hydrogel supernatant samples (150 µl WR: 150 µl sample), shaken, and incubated at 37°C for 2 hours. The absorbance was then measured on a plate reader at 562nm. A standard curve was produced from the protein standard for interpolation of sample concentrations.

2.3.5.2 TNBSA Assay

A TNBSA kit (Thermo Scientific) was used as per the instructions provided to measure free amines on LM molecules that have been PEGylated compared to

native LM to assess whether PEGylation was successful. Briefly, PEGylated and native LM were dialysed into the reaction buffer at 20 µg/mL. TNBSA solution (0.01% (w/v)) was added (0.25 mL TNBSA : 0.5 mL protein sample) and samples mixed before a 2 hour incubation at 37˚C. 0.25 ml SDS (10%) and 0.125 mL HCL (1 N) were added, and absorbance measured at 335 nm. A LM standard curve was included for quantitative analysis.

2.3.5.3 Fluorescence

The swelled hydrogels were stained for LM (Sigma). See 2.5.1, page 28.

2.4 TGFβ Incorporation

2.4.1 Reconstitution

TGFß 1 was reconstituted in MilliQ water and diluted in 0.1 % BSA.

2.4.2 Fluorescent Labelling

The GF was fluorescently labelled with DyLight® Amine-Reactive Dye, DyLight 488 NHS Ester following the provided protocol. Briefly, calculations were made following the equations in the protocol. 100 µL of DMF was added to the DyLight Ester and mixed then the calculated volume was added to protein in the reaction tube, mixed, and incubated for an hour at room temperature. The samples were then dialysed against PBS to remove non-reacted reagent, aliquoted, and stored at -20˚C.

2.4.3 TGFβ Retention in Hydrogels

PO, PF, PL, PFL hydrogels were produced as previously described. The hydrogels were swelled for 2 hours in 20 mM L-cysteine, washed with PBS, and TGFß added to each hydrogel composition at 1 µg/mL, with PBS added to control hydrogels. The hydrogels were incubated at 37˚C for 24 hours in darkness. A TGFß standard curve was produced for quantitative analysis, and the fluorescence was measured.

2.5 Cell Behaviour Characterisation

2.5.1 Immunofluorescence

Samples were washed with PBS, fixed with 4% paraformaldehyde (PFA), and washed again with PBS. They were permeablised with 0.1% Triton X-100. Samples were blocked with 1% bovine serum albumin (BSA) and incubated with primary antibody (Table 1) for 1 hour at room temperature, or overnight at 4°C. Samples were washed with 0.5% Tween20 and incubated with the secondary antibody for 1 hour at room temperature. They were again washed with 0.5% Tween20 and mounted for imaging with ProLong mountant (Molecular Probes).

Table 1: Primary Antibodies

Antibody	Clone	Source	Dilution
Anti-Ki67	**Rabbit Polyclonal**	**Abcam**	**1:800**
YAP	**Mouse Monoclonal**	**Santa Cruz Biotechnology**	**1:200**
Anti-Actin, α-Smooth Muscle (α-SMA)	**Mouse Monoclonal**	**Sigma-Aldrich**	**1:2000**
Anti-Laminin	**Mouse Monoclonal**	**Sigma-Aldrich**	**1:200**
Anti-E Cadherin	**Mouse Monoclonal**	**Abcam**	**1:400**
Anti-β Catenin	**Rabbit Monoclonal**	**Abcam**	**1:200**

2.5.2 Proliferation and Viability Assays

LIVE/DEAD ® (Molecular Probes), CCK-8 (Dojindo Molecular Technologies), and PicoGreen ® (Molecular Probes) assays were performed as per the user manuals.

2.5.2.1 Live/Dead

Briefly, samples were washed with PBS, reagents diluted in media, and samples incubated with reagents for 20 minutes at room temperature. They were then washed and covered with PBS, and immediately imaged.

2.5.2.2 CCK-8

Cells were encapsulated and hydrogels swollen. At 1, 4 and 7 days post encapsulation media was removed samples covered with 1:10 CCK-8 solution: media. Samples were incubated at 37°C for 4 hours, then absorbance measured on a plate reader at 450 nm. Samples were then kept at -80°C until PicoGreen was performed.

2.5.2.3 PicoGreen

Cell suspensions of known cell number were used to produce a standard curve. Hydrogels from the CCK-8 experiment were thawed, covered with lysis buffer, and vortexed every 10 seconds for 5 minutes, and then homogenised. Cell suspensions were lysed in the same manner. Samples were diluted in TE buffer (from PicoGreen kit), added to well plates at 1:10 sample: PicoGreen reagent, and incubated for 5 minutes at room temperature. Fluorescence was then read on a plate reader at 460 nm excitation and 540 nm emission.

2.6 PDAC Spheroid and iCAF Co-Culture

Spheroids were formed in ULA 96-well plates. 5wt% 4P(O/F) (20% degradable) were used with iCAFs encapsulated in or seeded upon hydrogels. A 1:1 Collagen:Matrigel (non-GF reduced) hydrogel mixture was used for control. Briefly, collagen gel solution and Matrigel were mixed in equal parts and 50 μl added to each control well, then gently centrifuged (300 rcf, 4°C, 5 minutes) and cured for 30 minutes in the incubator (37°C). PEG-based hydrogels were then formed (previously described) around spheroids.

2.7 Imaging

2.7.1 Equipment

Imaging was carried out using;

- Zeiss Axio Observer Z1 fluorescent microscope, with 10x, 20x and 40x objectives

- Nikon A1R Confocal microscope with Perfect Focus System, equipped with Nikon Apo ×60/1.40 and Plan Fluor ×40/1.30 objectives

- The automated IncuCyte S3 Live-Cell imaging system for long term time-lapse analysis of cultures

Imaging parameters were set up at the beginning of each experiment, and those parameters were maintained throughout all imaging for that experiment to ensure that comparisons could be made where necessary.

Confocal microscopy was carried out at the Beatson Institute under the supervision of Margaret O'Prey, in the NIS-Elements AR software. In brief, the Nikon A1R was set in the Widefield Fluorescence Laser Scanning Confocal modality. Laser power was set for each wavelength being measured individually, areas to be imaged were located manually, and Z-stacks captured for each area of interest.

2.7.2 Analysis

Analysis of images was performed in Fiji, and in the IncuCytes S3 software. Confocal images presented in this work are single slices of the Z-stacks that were captured.

2.7.3 Statistics

Statistical analyses were carried out using GraphPad Prism 6.01. Data were tested for normality using the D'Agostino & Pearson normality test. Normally distributed populations were tested with t-test or ANOVA (Tukey's multiple comparisons test) depending on the data. Populations that did not follow a

normal distribution were tested with the Mann-Whitney or Kruskal-Wallis test (Dunn's multiple comparison test) again depending on the data. Values are expressed as mean ± SD. Error bars on graphs are SD unless otherwise noted. P value symbols are as follows; ns denotes P>0.05, * denotes P≤ 0.05, ** denotes P≤ 0.01, and *** denotes P≤ 0.001.

A minimum of three discrete samples per condition were produced for all experiments throughout this work. The data sample size (n) for each set of results will be stated in the figure captions.

3 Results

3.1 Cell Viability and Density Analysis

An initial assessment of cell viability within the hydrogels was carried out to determine both viability of cells post gelation, and the optimal cell density for following work.

3.1.1 C2C12 Viability

The hydrogels used for this experiment were 3 wt% polymer (2 kPa) and 5 wt% polymer (5 kPa) PEG-Only hydrogels with 0% degradability. These hydrogel stiffnesses were selected based on their relation to PanN and PDAC stiffness; Rice et al found the Young's moduli of PanIN and PDAC to be 2 kPa and 4 kPa respectively[58]. A 0% degradable, PEG-Only hydrogel was used as this is the most difficult hydrogel composition for the cells to interact with, therefore viable cells in these conditions indicates a good level of viability in more cell interactive hydrogels. C2C12 cells were used as they are well documented and their viability in standard practice well established.

Qualitative assessment of cell viability 24 hours post-encapsulation (Figure 2, A and B) found that ~70% of cells were living, indicating that the encapsulation and hydrogel formation was successful, and that C2C12 can survive in the PEG-only hydrogels (both 3 wt% and 5 wt% polymer) for 24 hours. By 96 hours viability had reduced to ~30% for single cells and small clusters (Figure 2, C and D). Throughout the experiment the cell morphology remained rounded, which can be explained by the lack of adhesion sites in the PEG-Only hydrogels. By 96 hours there had been some larger cluster formation, suggesting that in the absence of cell-ECM adhesion, cells in close proximity were generating cell-cell adhesions, with these clusters maintaining a higher viability than single cells; as C2C12 are adhesive cells they may die via anoikis upon prolonged detachment, which explains the reduced viability at 96 hours. These results demonstrate the safety of gel formation and show that C2C12 can maintain viability up to 96 hours post-encapsulation.

**3 wt% Polymer
(2 kPa)**

**5 wt% Polymer
(5 kPa)**
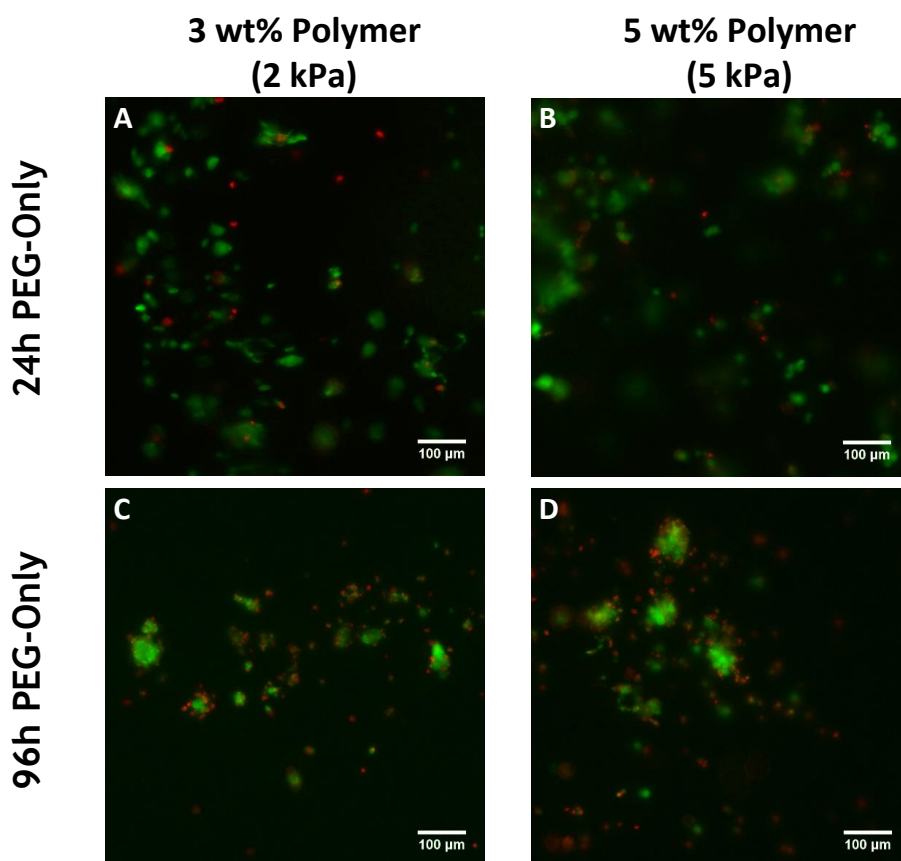
Figure 2: C2C12 are viable in PEG-only hydrogels. Green = Calcein AM (live) staining, Red = EthD-1 (dead) staining. Scale bars = 100 µm.

3.1.2 PDAC Cell Density and Viability

Following the viability results of C2C12 cells in the PEG-Only conditions, PDAC cell viability in the PEG-Only and PEG-FN hydrogels was assessed to ensure that the PDAC cells were able to survive the gelation of the hydrogels. The addition of FN into these PEG-based hydrogels does not significantly affect the stiffness of the hydrogels, as demonstrated by Dr Trujillo-Muñoz[43,56]; the PEG-Only and the PEG-FN hydrogels have similar properties, the only significant difference being the incorporation of the cell adhesion sites in the PEG-FN hydrogels. Any changes in cell behaviour between these hydrogels can therefore be attributed to the FN incorporation. As such, in following experiments the PEG-Only conditions will behave as the control, with the PEG-FN hydrogels being compared to the PEG-Only hydrogels of similar condition.

Two more controls were implemented here to ensure the reliability of the viability assay; the Positive Control and Negative Control noted in Table 2 refer to PDAC cells seeded in 2D on multi-well cell culture dishes, assessed at the same time as the experimental samples. The Negative Control cells were

treated with 100% Ethanol for 3 minutes prior to the viability assay. The controls showed that the assay worked well, with the Positive Control showing 94.2% viability, and the Negative Control showing that 0% of the cells were viable. Viability was quantified using the following equation;

$$Viability\ (\%) = \frac{number\ of\ live\ stained\ cells}{number\ of\ live\ stained\ cells\ +\ number\ of\ dead\ stained\ cells}\ x\ 100$$

with cell numbers confirmed using Dapi staining.

Quantitative assessment of PDAC cells in 3 wt% polymer (2 kPa, PanIN stage stiffness) PEG-Only and PEG-FN hydrogels found viability of cells encapsulated at each density ($1x10^6$, $2\ x10^6$, and $3\ x10^6$ cells/mL) at 24 hours (Figure 3, A-F) averaged over 50% in both PEG-FN and PEG-Only conditions (Table 2) with a monolayer viability (monolayer formed due to sunken cells) in the PEG-FN hydrogels averaging 85%. The differences in viability between suspended cells and monolayers could be due to a higher proliferation rate on the surface than within the 3D hydrogel, resulting in a faster increase in cell number, therefore more live cells, on the monolayer than within the hydrogel. By 96 hours the monolayers were highly confluent, restricting accurate analysis of viable to non-viable cells, however it was observed qualitatively that the PDAC cells appeared to have proliferated more rapidly than the C2C12 cells, and retained their high viability up to 96 hours. Another difference between the cell types was that, although some clustering occurred in C2C12, the PDAC cells were seen to form near spherical aggregates (80-225 μm Ø, averaging 145 and 152 μm Ø in the $1x10^6$ cells/mL and $2x10^6$ cells/mL in PEG-FN gels respectively). By D7 it was calculated that cells forming the monolayer in the controls had undergone a 40-fold increase from encapsulation to D7, indicating that although growth within the hydrogels could be reduced by spatial restriction, the cells remain capable of relatively rapid proliferation when on the culture plate surface. As the cell count was so high, viability assessment was inaccurate, therefore the data collected was used to assess any changes in aggregate morphology. As Table 3 shows, the aggregate diameter remained highly variable at D7, with the PEG-FN aggregates on average having a smaller diameter than the PEG-Only.

The cell encapsulation densities used in these conditions were very high, and it was queried whether the aggregates formed from clusters present at encapsulation, or from single cells. The lower value of 200,000 cells/mL was chosen for future work to minimise clustering during encapsulation and eliminate this uncertainty, as well as to reduce the formation of such a confluent monolayer.

These initial assessments show the hydrogels do not damage the PDAC cells during formation, and that PDAC cells are able to survive for at least 7 days while encapsulated in both PEG-Only and PEG-FN hydrogels. Interestingly, it was observed what while in culture in these hydrogels the PDAC cells were able to spontaneously form spheroids, a phenomenon to be investigated further. Following this, and the decision to use 200,000 cells/mL as an appropriate seeding density, investigations into the behaviour of PDAC cells in varying hydrogel conditions were begun.

Table 2: Average Viability per Condition at 24 hours.

Condition	Viability
Controls	
Positive Control	94.20%
Negative Control	0.00%
PEG-FN Gels	
1 x10^6 cells per ml	47.49%
2 x10^6 cells per ml	58.41%
3 x10^6 cells per ml	47.39%
PEG-only Gels	
1 x10^6 cells per ml	55.71%
2 x10^6 cells per ml	56.05%
3 x10^6 cells per ml	55.00%

Table 3: Aggregate Diameter at 7 days. (Average circularity = 0.95)

Condition	Average Diameter (µm)
PEG-FN; 1x10^6 cells/mL	102.51
PEG-FN; 2x10^6 cells/mL	79.22
PEG-only; 1x10^6 cells/mL	160.91
PEG-only; 2x10^6 cells/mL	120.66
PEG-only; 3x10^6 cells/mL	128.81

1x10^6 Cells/mL   **2x10^6 Cells/mL**   **3x10^6 Cells/mL**

24h PEG-Only

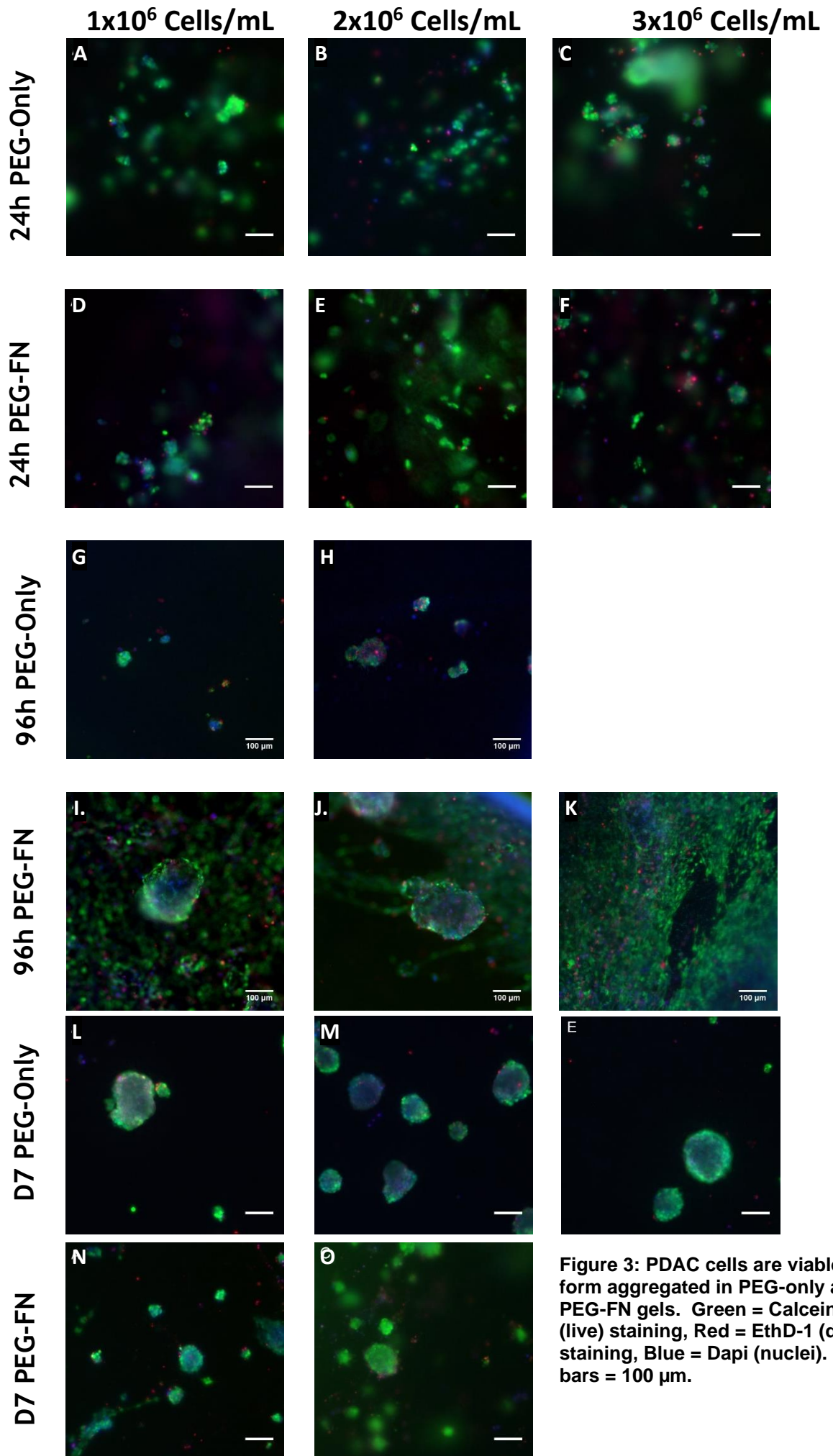24h PEG-FN

96h PEG-Only

96h PEG-FN

D7 PEG-Only

D7 PEG-FN

Figure 3: PDAC cells are viable and form aggregated in PEG-only and PEG-FN gels. Green = Calcein AM (live) staining, Red = EthD-1 (dead) staining, Blue = Dapi (nuclei). Scale bars = 100 μm.

3.2 PDAC Behaviour in Various Hydrogel Conditions

3.2.1 Varying Hydrogel Stiffness

To further assess spheroid formation, PDAC cells were encapsulated at 200,000 cells/mL PEG-only and PEG-FN hydrogels of 3 wt%, 5 wt%, and 10 wt% PEG (stiffness of 2 kPa, 5 kPa and 10 kPa). The 2 and 5 kPa stiffness were used again because of their similarity to the PanIN and PDAC environments. The 10 kPa hydrogels were introduced based on the stiffness threshold described by Elosegui-Artola et al[59], stating that on hydrogels above 5 kPa stiffness cellular force transduction is increased and the mechanosensitive transcriptional regulator, Yes-Associated Protein (YAP), is activated (translocated to the nucleus). YAP is active in inducing cancer cell proliferation and metastasis[60]. The 10 wt% hydrogels were well characterised[56] so were used to assess whether cell behaviour changes over the 5 kPa threshold in this 3D system. The hydrogels were all 20% degradable (20:80 degradable:non-degradable cross-linker ratio); the incorporation of degradability is not uncommon when working with hydrogels and is intended to afford cells the potential to remodel their environment for growth and migration[61,62].

Figure 4 (A-F) below shows representative images of spheroids formed within hydrogels at day 4. The images show strong similarities between the shape of the spheroids, with most spheroids appearing relatively spherical (Table 4). In terms of spheroid composition, there appears to be a higher concentration of actin around the edges of the spheroids in the PEG-FN hydrogels, possibly indicative of a physical interaction between the cells and the adhesive sites on FN molecules. Statistical analysis found that the only significant differences in spheroid diameter between hydrogel compositions was between the 5% PEG-Only and 5% PEG-FN hydrogel (Figure 5), however n was relatively low in this experiment, so repeats are necessary to assess this further.

By D7, there were again strong similarities between the shape of the spheroids (Figure 4, G-L, Table 4). Statistical analysis showed that all data were normal and that there were no significant differences between or within compositions (Figure 5). It was noted upon observation of the images that the spheroids formed in the PEG-only hydrogels had less well-defined edges (e.g. Figure 4,

I), with single cells occasionally protruding from the main bulk of the spheroid. At this time point the concentration of actin and the spheroid edges appeared similar between conditions. Comparing the numerical results from D7 with those from D4 it can be concluded that the spheroids in both PEG-only and PEG-FN hydrogels have grown (~80% Ø increase in PEG-only and ~50% Ø increase in PEG-FN).

As there were no consistent significant differences between spheroid diameters in PEG-Only and PEG-FN hydrogels of varying stiffness it was decided that various degradabilities should be assessed.

3 wt% Polymer (2 kPa) | **5 wt% Polymer (5 kPa)** | **10 wt% Polymer (10 kPa)**
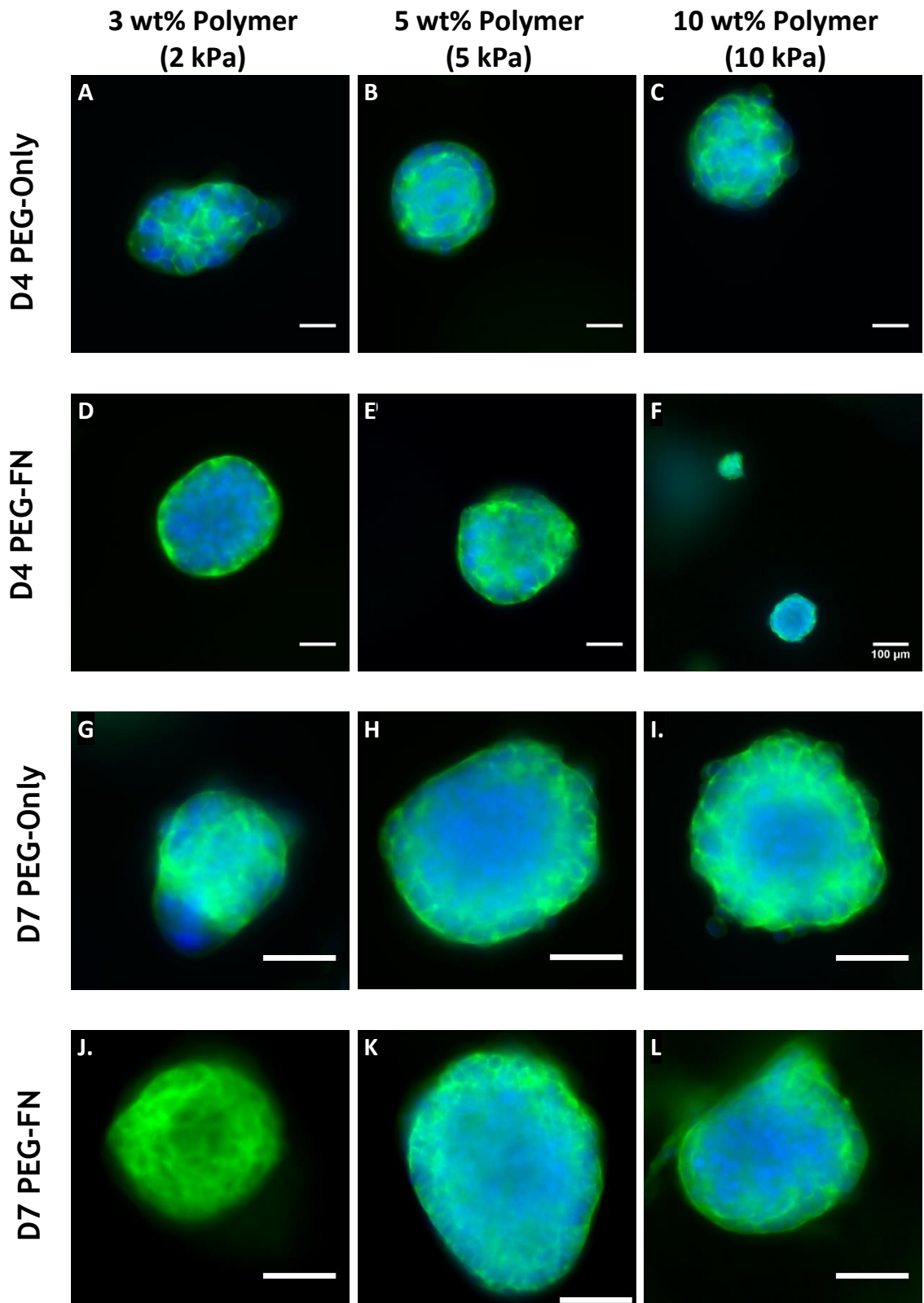
Figure 4: PDAC spheroids form in both PEG-Only and PEG-FN (1 µg/µL FN) Hydrogels. Green = Actin, Blue = Nuclei. Scale bars A-E = 25 µm, F = 100 µm, G-L = 50 µm

Table 4: D4 and D7 Average Spheroid Characteristics

Condition D4	n	Average area (μm²)	Average Circularity	Average Diameter (μm)	Standard Deviation (μm)
3% PEG-only	10	4480	0.78	72.4	22..6
5% PEG-only	16	4120	0.83	69.6	20.8
10% PEG-only	15	4990	0.81	78.5	14.7
3% PEG-FN	11	5400	0.91	81.6	15.6
5% PEG-FN	25	8390	0.88	99.7	27.8
10% PEG-FN	6	6470	0.78	87.7	25.7
Condition D7	n	Average area (μm²)	Average Circularity	Average Diameter (μm)	Standard Deviation (μm)
3% PEG-only	15	13600	0.88	131	14.7
5% PEG-only	15	14000	0.88	131	25.1
10% PEG-only	15	14100	0.84	133	15.9
3% PEG-FN	15	12300	0.83	121	33.1
5% PEG-FN	15	16000	0.86	140	29.1
10% PEG-FN	15	15400	0.81	138	23.1

A
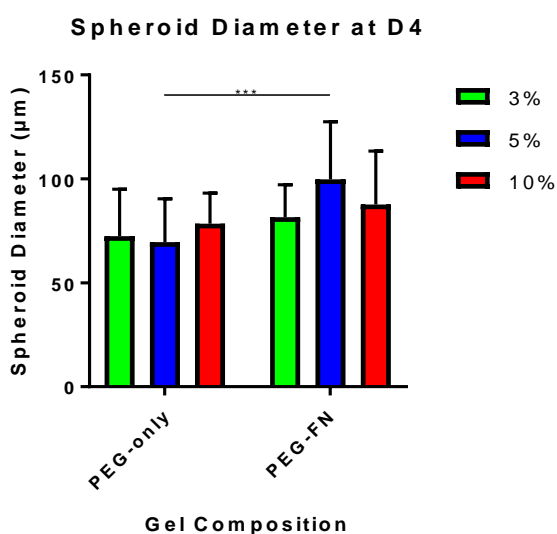
B
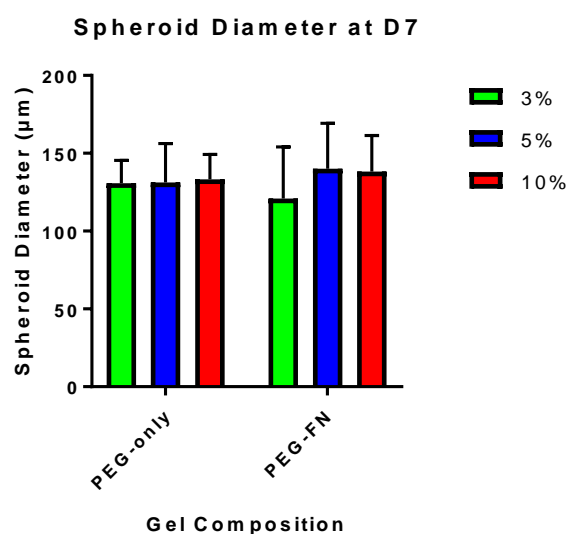
Figure 5: PDAC spheroid Diameter at D4 and D7. 2-way ANOVA with multiple comparisons (A) For PEG-only n=10, 15, and 16 for 3% (2 kPa), 5% (5 kPa), and 10% (10 kPa) respectively, and for PEG-FN n=11, 25, and 6 for 3%, 5%, and 10% respectively. All data were normal (except PEG-FN 10%; n too low for analysis). (B) n = 15. All data are normal. There are no statistically significant differences within or between the composition groups.

3.2.2 Varying Hydrogel Degradability

In order to assess the effect of varying degradabilities on PDAC cell behaviour, the 5 wt% polymer (5 kPa) hydrogel composition was used, as it is most similar to the 4 kPa PDAC tissue[58]. The 5 wt% PEG-Only and the PEG-FN hydrogels were produced to be 20%, 50%, and 80% degradable.

Assessment of PDAC cells these hydrogels again shows no clear difference in behaviour between the conditions. Figure 6 shows that, although there are some significant differences between certain conditions and timepoints, there appears to be no consistency in these differences (i.e. not all diameters increase significantly between PEG-Only and PEG-FN or between the different degradability). These results, along with past diameter analysis results, demonstrate the variability within each condition and the lack of significant differences between conditions.

Using the same conditions, spheroids were cultured and stained for the Ki67 proliferation marker, and observed with fluorescent and confocal microscopes, with confocal images undergoing subsequent image calculations. Both by observation, and by calculation, it seems that the Ki67 positive cells appear to be localised to the outer edge of the spheroid, indicating a proliferative layer around the spheroid, with a non-proliferative region within (Figure 7). This finding, however, was not consistent throughout all conditions, with some spheroids containing no Ki67 positive cells at all: taken together, the confocal proliferation data indicate that there may be variability between spheroid activity within each condition.

The Ki67 expression variability seen here could also be the result of inhibited anti-Ki67 antibody penetration throughout the full hydrogel volume. It could be that this larger antibody requires a longer incubation time than the 1 hour at room temperature which was sufficient when staining previously with Dapi and phalloidin (Materials and Methods, 2.5.1). Further, the localisation of the Ki67 expression to the outer edges of the spheroids could be due to the anti-Ki67 antibody only penetrating a certain depth into the spheroid. The protocol for immunostaining of 3D samples developed by Smyrek et al[63] that was most successful for work with multicellular tumour spheroids was similar

to the protocol used in this work, using the same fixation and permeablisation, the difference being an increased antibody incubation period and temperature. In future experiments requiring this antibody, alterations to the antibody incubation step will be implemented.

Regardless of the problems encountered with antibody penetration, the confocal imaging carried out here confirmed that high quality 3D images are attainable in these hydrogels, and as such imaging of KTRs[27] should be possible.

It is also possible that there are not consistent distinctions between the spheroids in each condition as the spheroids form spontaneously within these PEG-based hydrogels, therefore there is no control over the number of cells per spheroid. Potentially, as all hydrogels produced up to this point (varying polymer wt% and degradability) have a relatively low stiffness, we may only observe differences when cells are encapsulated in stiffer hydrogels, with the hypothesis that the spheroids will be smaller in stiffer hydrogels due to the increased cross-linking density required and the spatial restrictions that this imparts.

Another possible explanation for the lack of any consistent and significant difference between the PEG-Only and the PEG-FN conditions may be the influence of the FN in the media; so far in this work, the cell culture medium has been supplemented with 10% FBS (see Materials and Methods 2.1). It was hypothesised that the quantity of FN within the FBS added to the media may overpower the effects of the FN incorporated into the hydrogel network. As such, the following experiment assessing the effect of reduced FBS in the culture media used while cells are in the hydrogel environment was carried out.
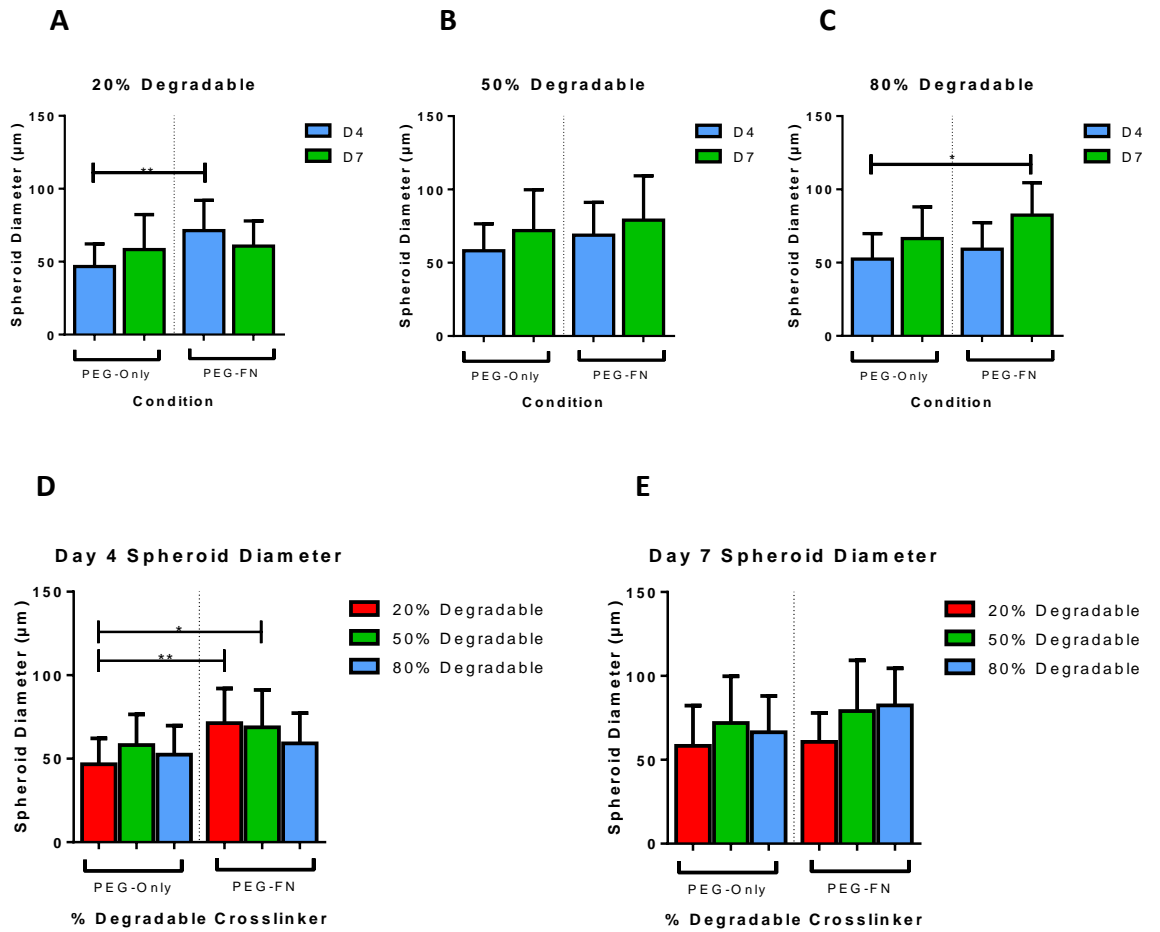
Figure 6: PDAC Spheroid Diameters Depending on Degradability. A-C compare time points. D-E compare conditions. There do not appear to be any trends in the behaviour of PDAC cells between condition.
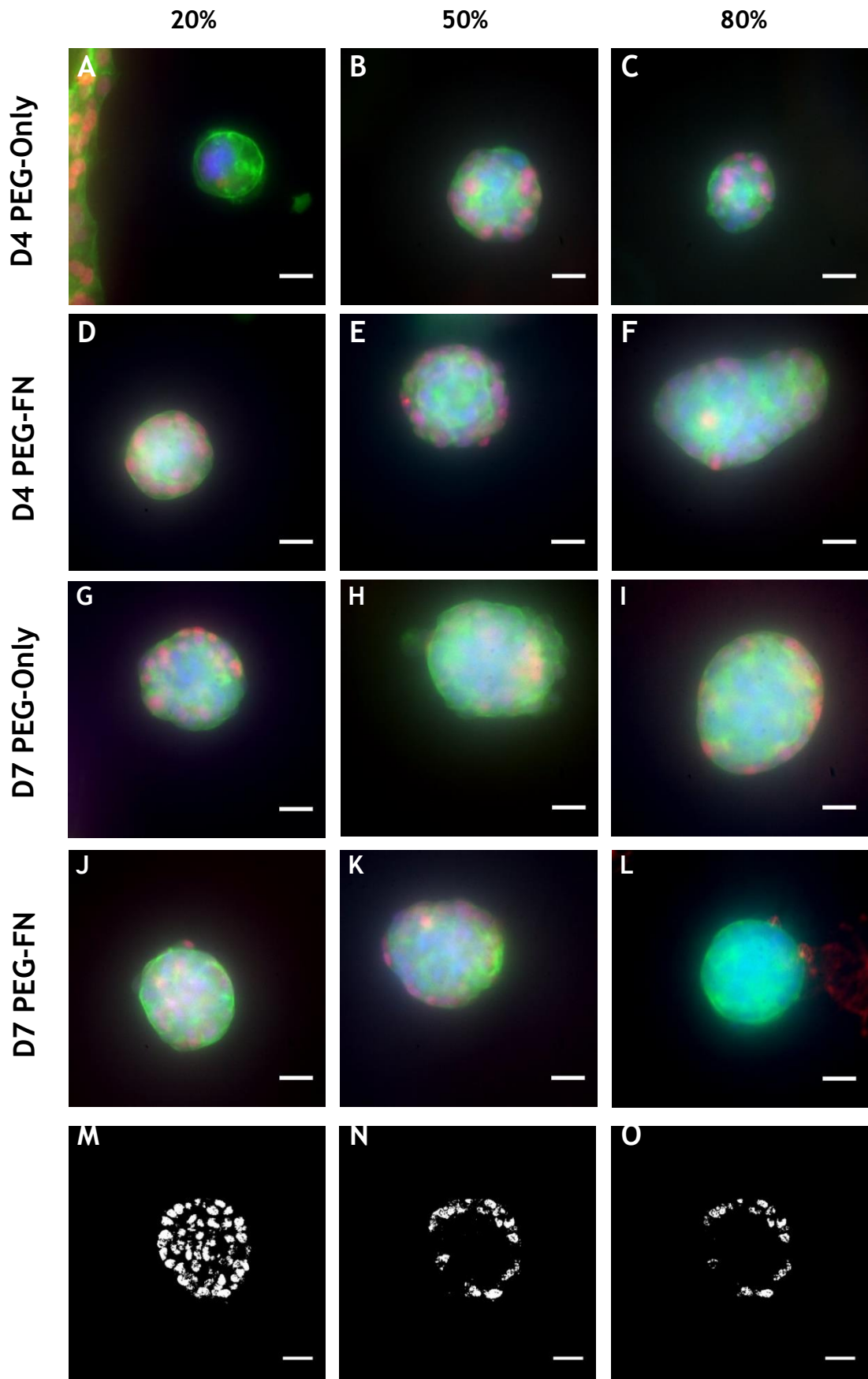
Figure 7: Proliferative cells appear to be localised to the outer edges of the spheroids. Green = actin, blue = nuclei, red = Ki67 positive nuclei. A-L = representative FL microscope images of the conditions. M-O = analysed confocal images from centre of a spheroid in 20% degradable 5 wt% polymer PEG-Only gel: M = segmented nuclei, N = Segmented Ki67 positive staining, O = Nuclei positive for Ki67. Scale Bars = 25 μm.

3.2.3 Varying Culture Media

FBS, although extremely common in all cell culture practices, is not fully characterised, contains thousands of proteins and metabolites, and batch compositions vary dependent on when and where they were produced[64]. An experiment with low FBS levels was designed to assess whether the FN content of the FBS in the media was overpowering the hydrogel incorporated FN and obscuring any potential differences between the PEG-Only and PEG-FN conditions.

The low FBS experiment was carried out using PDAC cells in 5 wt% polymer hydrogels with 20% degradability. 5 wt% hydrogels were used because as previously mentioned this condition is closest in stiffness (5 kPa) to the 4 kPa measured PDAC tissue[58], and 20% degradable because this allows cellular remodelling of the environment without the loss of too much hydrogel structure. The cells were cultured for 4 days in the medium described in Materials and Methods with only 2% FBS as opposed to the standard 10% FBS.

Upon observation of the distribution of spheroids and cells within these hydrogels at day 4, there appeared to be some single cells suspended. This could be an indication of the potential of using low FBS media to allow modelling of single cell behaviour, however further analysis of these cells would be required to determine single cell viability and activity in these conditions. It could also indicate that fewer cells were able to either establish spheroids, or come together as spheroids, given the reduction in FBS in the culture media.

Figure 8 shows that there was no significant difference between the spheroids present in the different hydrogel compositions with low FBS media. This suggests that the serum FN does not overpower the effects of the gel incorporated FN, and furthers the idea that the lack of differences observed between all conditions analysed to date may be due to the stiffness in which the cells are encapsulated, and perhaps an increase in stiffness above the 10 kPa maximum used up to this point may reveal some sort of 3D stiffness threshold above which cell behaviour is altered, as Elosegui-Artola et al found in 2D[59]. It could also be that the concentration of FN in the gels is too low to

affect the PDAC spheroid formation, which may be investigated following further assessment of the effects of stiffness. A further possibility which may need to be investigated is whether a different protein, or the incorporation of different adhesive peptides, could have some effect on spheroid formation and PDAC dormancy. Finally, it could be that the PDAC cells need to be cultured for longer in order for them to form spheroids, develop, and potentially begin more active behaviour.
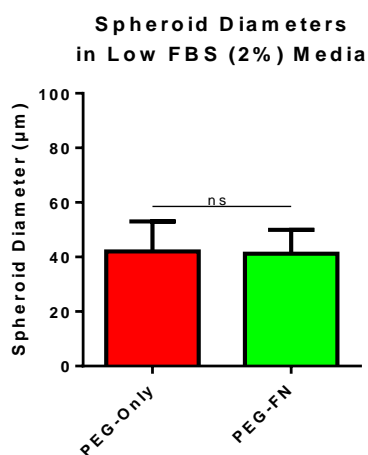
Figure 8: Spheroid Diameters under low FBS Conditions.   Data are normal, n=13. Ordinary 1-way ANOVA saw no significant differences.

3.2.4 Varying Culture Time

To assess differences in PDAC cell and spheroid behaviour over a longer period, a culture time of 14 days was chosen. PDAC cells were encapsulated in 3 wt% hydrogels with 20% degradability; media was changed at day 4 as with previous experiments, then again at day 7, day 9, day 11, and day 13. The lower wt% hydrogel were chosen this time as previous work with the 5 wt% hydrogel showed no consistent changes in behaviour between conditions. The softer 3 wt% (2 kPa) hydrogels are more similar to the PanIN environment in terms of stiffness[58], therefore the PDAC cells may be more encouraged to change their behaviour, as cells do when transitioning from neoplasia to carcinoma.

By day 14 the PEG-FN samples were largely degraded, possibly due to the proliferation of the monolayer beneath the hydrogel as well as the increase in cell number within the suspended spheroids leading to an increase in protease production, and therefore degradation of the hydrogel; this effect amplified in

the PEG-FN samples over the PEG-Only partly due to less prominent monolayers present in the PEG-Only samples, and possibly because the PEG-FN hydrogels are degradable both at the FN molecule and the incorporated degradable sequence, whereas the PEG-Only are only degradable at the incorporated degradable sequence.

Figure 9 comparison between spheroid diameter at day 7 and day 14 is not ideal as the day 7 data were from 5 wt% polymer hydrogels, however as there has yet been no definitive difference between the diameters of spheroids grown in 3 wt% and 5 wt% hydrogels, this comparison can be useful in drawing some conclusions about spheroid growth. From these data, and the increased consumption of media with time, it can be concluded that the spheroids continue to grow between days 7 and 14 and are still viable by day 14. A repeat of this experiment incorporating an immunostaining for proliferation (Ki67) and cell death (caspase) would not only confirm these conclusions, but also aid in the understanding of the activity levels throughout the spheroid volumes.
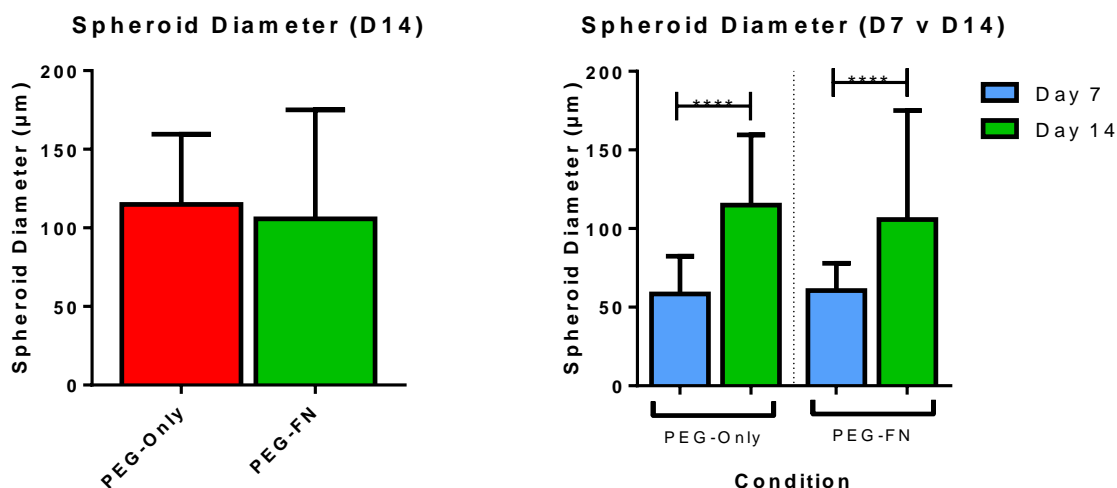
Figure 9: 14 Day Culture Analysis. Error Bars = SD. Assumed Gaussian distribution on all (n too small in PEG-FN D14 for normality test).

No significant differences in behaviour were found between PDAC cells in PEG-Only versus PEG-FN hydrogels throughout the varying hydrogel conditions (stiffness and degradability) and culture conditions (media composition and culture time). As such it is possible that there are aspects of the ECM that need to be more closely mimicked by the hydrogels.

The characteristic of the PDAC spheroids which has been assessed when varying different hydrogel conditions in this chapter (3.2) is the spheroid size., as this characteristic is a quantifiable measure of PDAC growth in these hydrogels. Another characteristic that could be of interest is the stiffness of the spheroids themselves, as tumours are stiffer than ordinary tissues[15]. The possibility of investigating this characteristic may be looked at in future work.

So far in this work no differences are being observed in the characteristic of interest throughout all variations of hydrogel composition and experimental conditions, therefore an assessment of these PDAC cells in an already established cancer model would be of use. Further, the PDAC cells do not appear invasive at any time point within the PEG hydrogels, so investigating their phenotype in a different environment would also be important.

3.3 PDAC Invasiveness Study in Matrigel

Given the lack of behavioural changes between conditions in the PEG-based hydrogels, it was decided that a commercial hydrogel used in cancer research be implemented to assess the PDAC cells interaction with the hydrogel matrix. Matrigel (a basement membrane matrix) is commonly used for cancer invasion models[65], therefore an assessment of the behaviour of these PDAC cells Matrigel could indicate possible avenues for investigation.

PDAC cells were encapsulated at different densities (20,000, 50,000, 100,000, 4,000,000 cells/mL) in 50 µl of growth factor reduced Matrigel at different cell densities. GF reduced Matrigel was chosen so that the observed behaviours could be attributed to the physical composition of the hydrogel, and not to the effects of the various soluble GFs within the Matrigel samples.

Assessment of spheroid size saw significant differences between the highest cell density and all three lower densities, possibly due to spatial restrictions imposed by the high cell density, with no significant differences between the lower densities (Figure 10). A qualitative assessment of spheroid shape was also carried out. It was hypothesised that the Matrigel would encourage an invasive phenotype, however from observation it was concluded that under no conditions did the cells appear to be branching from the spheroid and invading the Matrigel. This indicates that the invasiveness that cells in Matrigel often display may be due to the growth factors within the Matrigel rather than the basement membrane structure alone.

Inflammation may encourage cancer progression[32], and the rigidity of the ECM can induce malignancy when it is increased above homeostatic levels[59,66]. Matrigel has a very low stiffness and huge inter-batch variability (443 Pa ± 285 Pa)[67], and the stiffest PEG based hydrogel in this current system is 10 kPa. A healthy pancreas has a stiffness of 1 kPa, increasing to 2 kPa in the PanIN stages, and reaching 4 kPa when in fully developed PDAC stages[58]. The stiffness found by Elosegui-Artola et al above which force transduction is triggered in 2D *in vitro* is 5 kPa, (greater than the measured value of PDAC stiffness), however it is unknown how cell reactions to stiffness in 2D compare to cell reactions to stiffness in 3D. It is possible that in 3D *in vitro* we require

a greater measured hydrogel stiffness to mimic the internal environment PDAC cells experience *in vivo*.
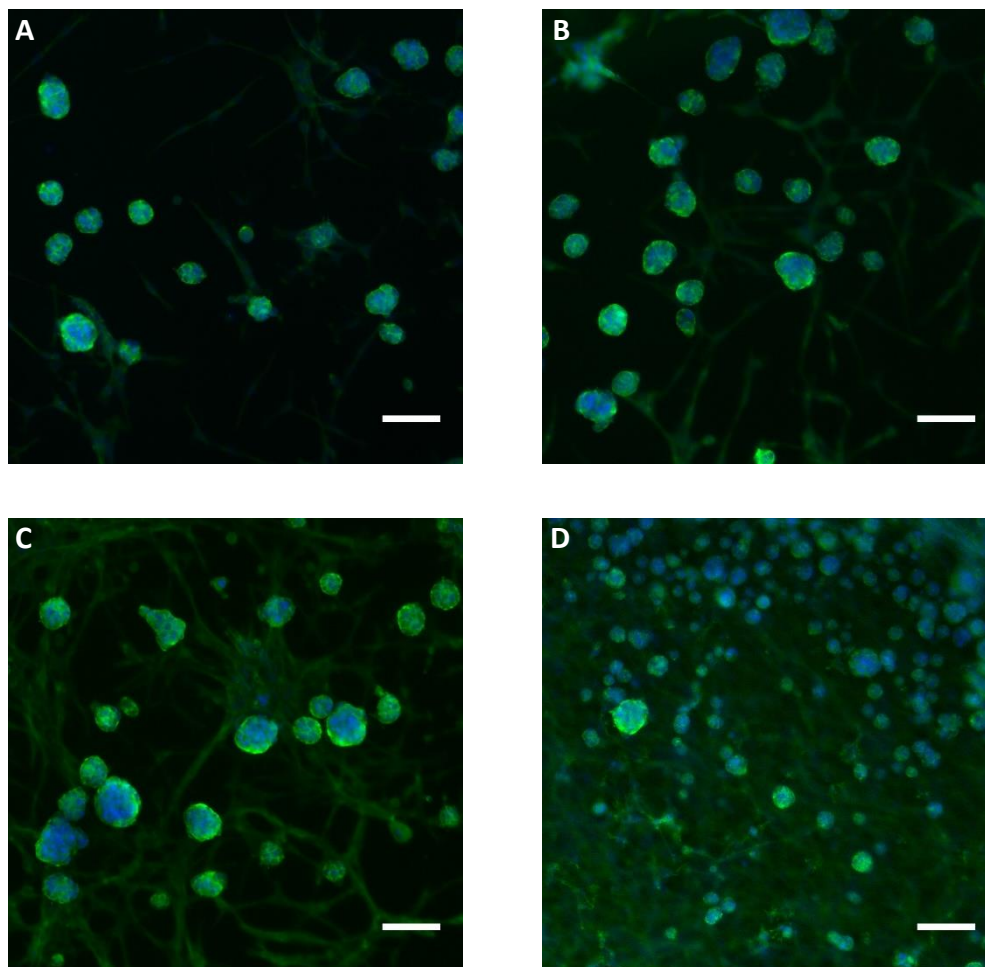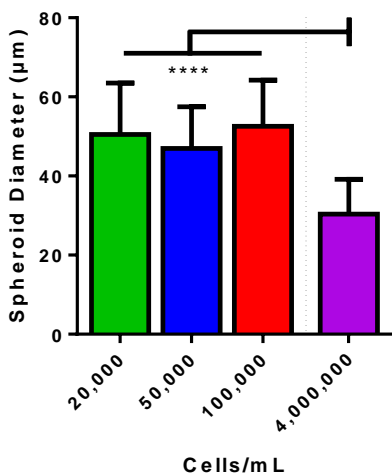
Figure 10: PDAC spheroids in Matrigel are smaller at very high densities, but do not appear invasive. Green = actin, blue = nuclei. Scale bars = 100 μm. (A) 20,000 cells/mL (1000/gel) (B) 50,000 cells/mL (2500/gel) (C) 100,000 cells/mL (5000/gel) (D) 4,000,000 cells/mL (200,000/gel) (E) Results of size assessment. n>28, not all data normal, Kruskal-Wallis comparison.

3.4 Increasing Hydrogel Stiffness

3.4.1 Increased PEG Content in 4-Arm PEG hydrogels

To explore the hypothesis that increased hydrogel stiffness would lead to differences in spheroid formation, hydrogels of increased stiffness (~40 kPa) needed to be produced. The target stiffness of 40 kPa was chosen as it is significantly higher than the previous stiffnesses implemented in this work, and it is 10 times greater than the *in vivo* PDAC stiffness value (4 kPa)[58]. It was hypothesised that this drastic increase in mechanical properties may enhance the cells response and lead to differences in spheroid formation and behaviour.

The measured stiffness values for the 3%, 5% and 10% hydrogels (Dr Sara Trujillo-Muñoz[56]) were input into MATLAB (MathWorks®) and a linear extrapolation was used to predict what wt% polymer would be required to produce hydrogels of 40 kPa (Figure 11). From this data it was predicted that a 30 wt% polymer hydrogel could have the desired stiffness of 40 kPa. The 30 wt% hydrogels were produced following the same protocol as the original hydrogels, and the stiffness of these hydrogels was determined using AFM.
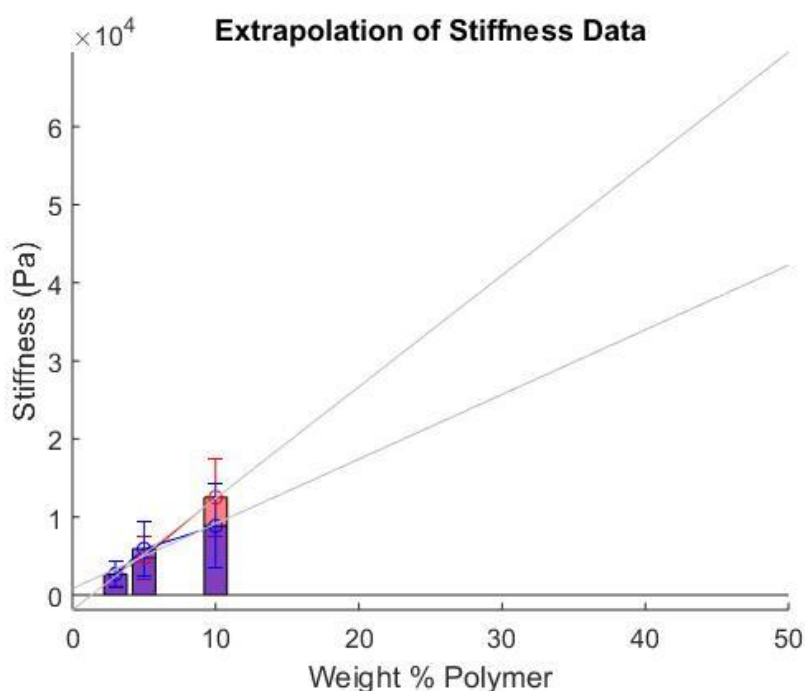
Figure 11: Extrapolation of Stiffness Data. Stiffness data (Dr Trujillo-Muñoz[56]) of 3 wt%, 5 wt% and 10 wt% polymer PEG-Only (red/pink) and PEG-FN (blue/purple) hydrogels, with a least squares prediction (grey) of polymer wt% for various stiffness.

Following AFM measurements of the 30 wt% polymer hydrogels, it was found that increasing the polymer percentages did not have the desired effect. As can be seen in Figure 12, neither of the conditions (with or without FN) produced hydrogels of sufficient stiffness, and as such the composition of the hydrogels must be redesigned.

Hydrogel stiffness is dictated both by the wt% polymer and the cross-linking density. Once the cross-linking density is at its maximum (1:1 Malemide:Thiol) as in the 5 wt% polymer hydrogels, stiffness can be further increased by an increase in wt% polymer up to a threshold, beyond which an increase in wt% polymer only leads to an increased final volume upon swelling, which has been the case for the 30 wt% polymer hydrogels. Therefore in order to produce hydrogels of a higher stiffness, more cross-linking sites are necessary: calculations were carried out (see Supplementary Information, S1) for the incorporation of 8-Arm-PEG-MAL to allow for an increase in cross-linking sites and subsequent increase in hydrogel stiffness.
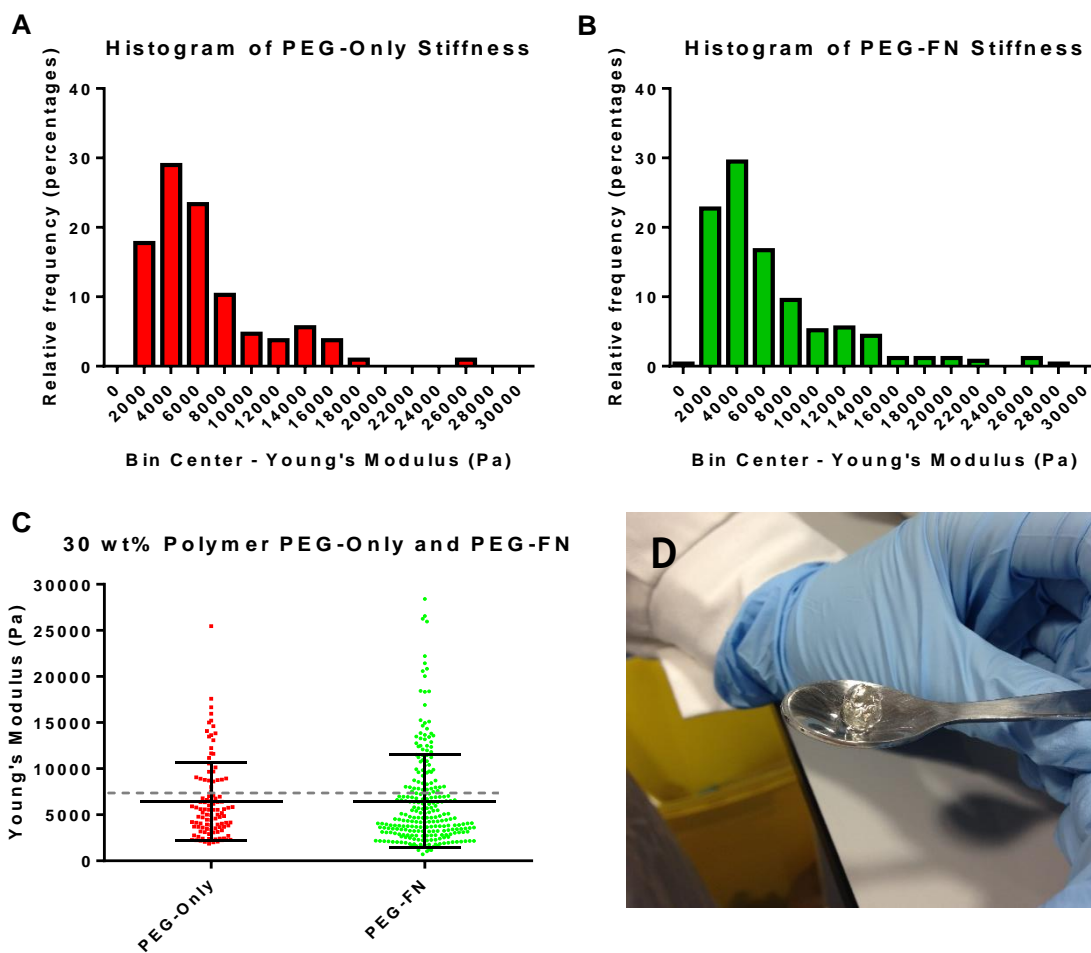
Figure 12: Stiffness of 30 wt% Polymer PEG-Only and PEG-FN gels.
(A) Histogram of PEG-Only stiffness results, (B) Histogram of PEG-FN stiffness results,
(C) Collated data, data are not normal. Mean ± SD with values shown, dotted line at 7.5
kPa. Measured values both have means of 6.5 kPa (no significant difference); both
values are significantly lower than the 40 kPa desired (p value <0.0001 in both cases). (D)
Image of PEG-FN gel (originally 50 μl volume) post swelling.

3.4.2 8-Arm PEG Hydrogels

8-arm PEG-Maleimide (PEG-8-MAL) was used in the place of PEG-4-MAL in the
hydrogel solution (PEG-4-MAL was still used for PEGylation of FN) in order to
introduce more cross-linking sites and theoretically increase the hydrogel
stiffness (see hydrogel calculations in Supplementary Information, S1). PEG-
Only (PO) and PEG-Fibronectin (PF) hydrogels (composition in Table 5) were
produced, and their Young's modulus and swelling behaviour were assessed,
their internal mesh size calculated, and PDAC viability within them was
determined.

Table 5: PEG-8-MAL Hydrogel Composition

Name	wt% PEG	Cross-linking ratio: SH:MAL
6wt% 3:8 8P(O/F)	6	3:8
6wt% 8:8 8P(O/F)	6	8:8
10wt% 8:8 8P(O/F)	10	8:8

Cross-linking ratio (SH:MAL) describes the ratio of thiol to maleimide molecules. 3:8 is minimally cross-linked in this case, with only 3 in every 8 maleimides having a thiol to bind. 8:8 is full cross-linked, with a thiol to bind every maleimide. The 8 in 8P(O/F) corresponds to the arms of the PEG molecule (4P(O/F) are PEG-4-MAL based).

3.4.3 New Hydrogel Characterisation

3.4.3.1 Youngs Modulus

AFM force mapping was used to obtain Young's modulus values for each of the hydrogel compositions mentioned above. Figure 13 and Table 6 contain the AFM results obtained. All hydrogels produced using 6wt% PEG-8-MAL were of higher stiffness than the original PEG-4-MAL maximum (10 kPa), with 6wt% 8:8 8P(O/F) hydrogels having the highest stiffness (Young's modulus (E)). The 10wt% 8:8 8P(O/F) hydrogels displayed the lowest stiffness of the PEG-8-MAL conditions, falling between the 4PO and 4PF stiffness. Cruz-Acuña et al [10] show that increasing wt% PEG-4-MAL in hydrogels leads to an increase in storage and loss moduli, however the decrease in Young's modulus seen here between the 6 and 10 wt% polymer conditions follows the same trend as the 10wt% and 30wt% hydrogels produced with PEG-4-MAL.

Figure 13: Stiffness of PEG-based hydrogels. (PEG-4-MAL data from Dr Trujillo-Muñoz[56], n>50). PEG-8-MAL hydrogels of higher stiffness than original PEG-4-MAL hydrogels were produced. All 8P(O/F) measured had a Youngs modulus > 10 kPa. Fully cross-linked (8:8) 6wt% hydrogels were significantly stiffer than 6wt% 3:8 8P(O/F) and 10wt% 8:8 8P(O/F) hydrogels. n>280.

Table 6: Numerical results of stiffness measurements

Hydrogel	Mean E (kPa)	SD (kPa)	SEM (kPa)
10wt% 4PO	12.51	4.92	0.66
10wt% 4PF	8.86	5.31	0.74
6wt% 3:8 8PO	12.72	7.50	0.44
6wt% 3:8 8PF	13.30	11.71	0.68
6wt% 8:8 8PO	24.58	13.80	0.79
6wt% 8:8 8PF	23.60	14.72	0.87
10wt% 8:8 8PO	10.49	6.77	0.33
10wt% 8:8 8PF	11.72	7.83	0.32

The increased stiffness of these hydrogels compared to the PEG-4-MAL hydrogels (Figure 13 and Table 6) allows for an assessment into whether increasing the stiffness of the PDAC cells' surroundings will encourage different behaviour to what has been seen previously in these hydrogels.

AFM was implemented successfully to measure the stiffness of the hydrogels here. As was mentioned in Chapter 3.2, it may be of interest in the future to

assess the stiffness of the spheroids themselves. The AFM protocol implemented here may be of use in determining the stiffness of the spheroids. However, given that the sections of the samples measured are 100μm thick, it is likely that the random distribution of the spheroids throughout the hydrogel volume would lead to some spheroids being split during sectioning, and some smaller spheroids having areas of hydrogel surrounding them both above and below in the AFM section. This would result in inconsistencies in the measurements, with some spheroids being measured from their centres, some from their surfaces, and some with a small layer of hydrogel on their surface. In order to assess spheroid stiffness accurately, a relatively new approach, such as the use of microtweezers, developed by Jaiswal et al[68], may be required. For this approach, the hydrogel would need to be fully degraded and the spheroids released, a procedure that will require some development and subsequent characterisation for future work.

3.4.3.2 Hydrogel Swelling

A swelling assay was performed to assess swelling and determine internal mesh size of the hydrogels. Hydrogels were weighed at different timepoints during swelling and after drying. It was seen that higher PEG content correlates with a higher water uptake (%), but a lower total degree of swelling (%) (Figure 14) in these conditions. Dr Trujillo-Muñoz saw that as PEG-4-MAL hydrogel stiffness increased, water uptake increased and degree of swelling decreased[56]. This is true of the 6wt% PEG-8-MAL results; within these conditions, the stiffer (Figure 13) 8:8 SH:MAL hydrogels uptake a greater amount of water than their softer 3:8 counterparts. However, the 10wt% PEG-8-MAL shows highest water uptake and lowest degree of swelling, while having a low stiffness compared to the 6wt% 8:8 P(O/F) hydrogels. This deviation from the trend observed in PEG-4-MAL hydrogels could relate to molecular scale changes in the network when PEG-8-MAL is used in the place of PEG-4-MAL; perhaps rheology to compare viscoelastic properties of the different conditions could provide more information.
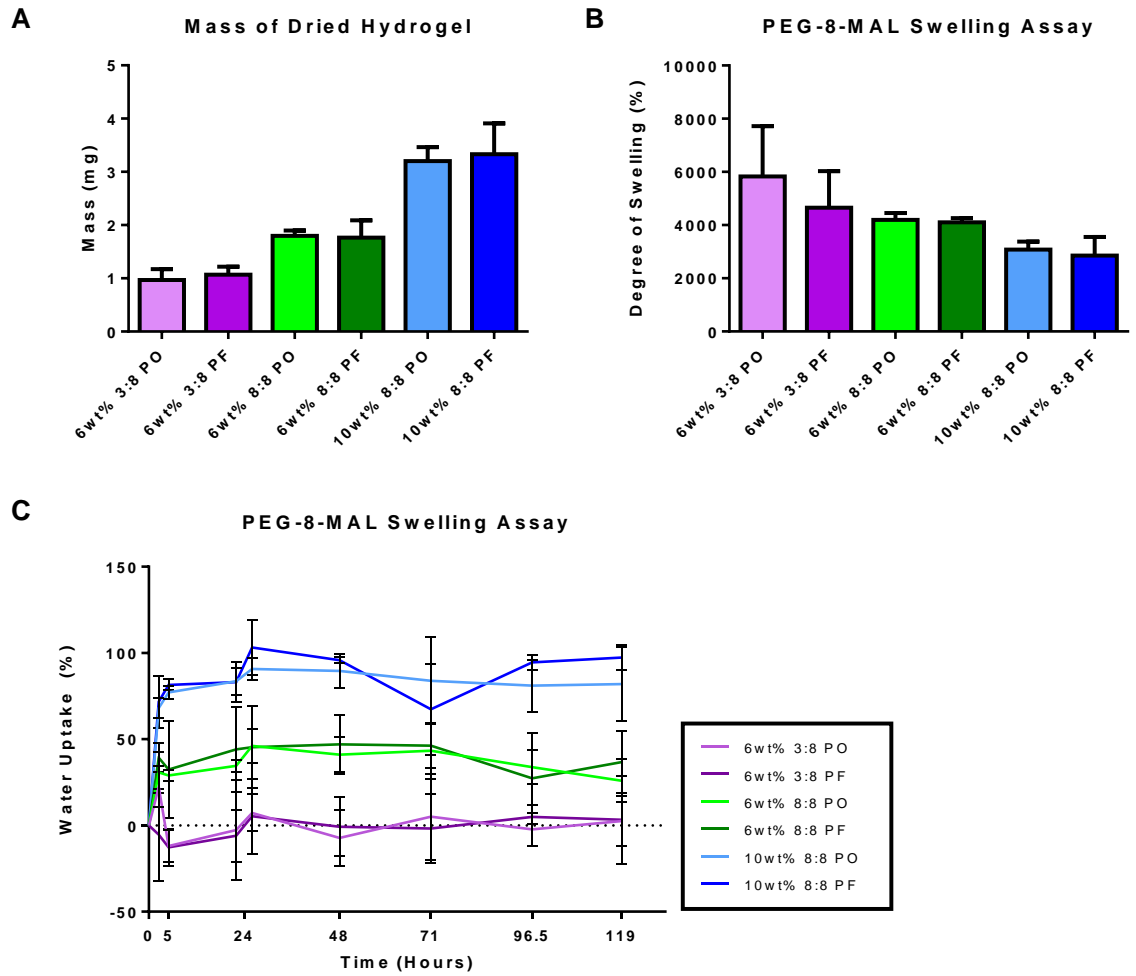
Figure 14: Degree of swelling and water uptake, with dry mass for reference. Lower cross-linking ratio and wt% polymer hydrogels uptake less water but swell to a greater degree from their dry mass. (A) Dry mass of hydrogel. (B) Degree of swelling (%) is calculated as [(mass at equilibrium - dry mass)/dry mass]*100. Equilibrium at t=26h (C) Water uptake (%) is calculated as [(mass at t – initial mass)/initial mass]*100.

3.4.3.3 Internal Mesh Size

In order to determine the internal dimensions (mesh size) of the PEG-8-MAL hydrogel network, calculations were carried out based on work by Dr Trujillo-Muñoz and a PhD thesis by Ting Yang [57], using both the stiffness and swelling results separately to produce more reliable results. The mesh size (ξ) and effective cross-link density (ρ_c) of the hydrogels were calculated (using mass at equilibrium; t-26h).

Table 7: Mesh size of PEG-8-ARM hydrogels. (M_c is molecular weight between crosslinks)

Hydrogel	ξ(nm) from Stiffness data	ξ(nm) from Swelling data	ξ(nm) from Average M_c from Stiffness and Swelling
6% 3:8 8PO	0.61	0.65	0.89
6% 3:8 8PF	0.57	0.61	0.83
6% 8:8 8PO	0.43	0.47	0.63
6% 8:8 8PF	0.43	0.46	0.63
10% 8:8 8PO	0.41	0.42	0.58
10% 8:8 8PF	0.39	0.40	0.56

Table 8: Effective cross-link density of PEG-8-ARM hydrogels. (M_c is molecular weight between crosslinks)

Hydrogel	ρ_c (mol/cm³) from Stiffness data	ρ_c (mol/cm³) from Swelling data	ρ_c (mol/cm³) from average M_c from Stiffness and Swelling
6% 3:8 8PO	0.28	0.25	0.13
6% 3:8 8PF	0.28	0.25	0.13
6% 8:8 8PO	0.47	0.40	0.22
6% 8:8 8PF	0.47	0.40	0.21
10% 8:8 8PO	0.42	0.41	0.21
10% 8:8 8PF	0.43	0.41	0.21

The results in Table 7 show the mesh size of these PEG-8-ARM hydrogels to be nanoscale, and 10x less than those of the PEG-4-MAL hydrogels calculated by Dr Trujillo-Muñoz. Comparing these values to the degree of swelling

(%)(Figure 14) shows that the more the hydrogels swell from their initial mass, the greater the mesh size, with the largest mesh size and highest degree of swelling in the 6wt% 3:8 PO hydrogels. Table 8 results confirm that the 3:8 SH:MAL hydrogels have a lower effective cross-linking density than the 8:8 hydrogels, with both 6wt% and 10wt% 8:8 hydrogels having a similar effective cross-linking density. The effective cross-linking density values calculated for the PEG-8-MAL hydrogels are 20x greater than Dr Trujillo-Muñoz's PEG-4-MAL results. The increased ρ_c coupled with the decreased ξ in the PEG-8-MAL compared to the PEG-4-MAL could lead to a more spatially restrictive area for cells, as not only is the distance between cross-links smaller, there are more cross-links, therefore more network arms around each pore. This may have implications in cell viability and interactions, as well as molecule penetration.

Given the similar stiffness and the reduced mesh size of the 10% 8:8 8P(O/F) hydrogels compared to the 6% 3:8 8P(O/F) hydrogels, only the 6wt% hydrogels were used in further work.

3.4.3.4 PDAC Viability in PEG-8-Mal Hydrogels

For viability in PEG-8-MAL hydrogels, hydrogels with 0% degradability were produced. 6 wt% PEG-8-MAL PEG-Only and PEG-FN hydrogels at 3:8 and 8:8 cross linking ratios were produced and PDAC cells encapsulated.

Figure 15 shows PDAC viability in 6wt% 8PO hydrogels to be >70% up to 4-days post encapsulation, with no decrease over time. This was to be expected; Phelps et al[42] describe high cell viability within PEG-MAL hydrogels, with C2C12 cell viability comparable to controls, and Ki et al[23] saw high PANC-1 viability (>90%) in 8-Arm PEG-Norbornene hydrogels 1 day post-encapsulation. These hydrogels are therefore suitable for use in further investigations as the changes in the inner hydrogel network from PEG-4-MAL to PEG-8-MAL do not reduce PDAC viability.

PDAC Viability in PEG-8-MAL Hydrogels
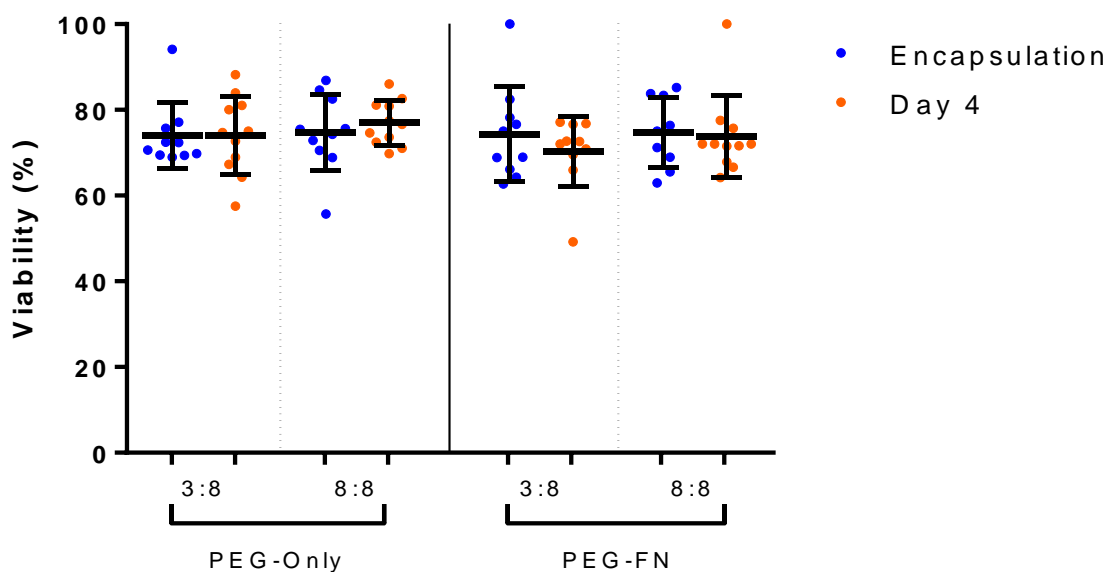
Figure 15: PDAC cells are viable up to 4 days in 6wt% 8PO hydrogels. PDAC encapsulated in both 3:8 and 8:8 SH:MAL PO and PF hydrogels show no significant cell death between encapsulation and day 4. n>8.

3.5 Comparing PDAC Behaviour in 4-Arm and 8-Arm Hydrogels

3.5.1 Soft PEG-4-Mal Versus Stiff PEG-8-MAL

In order to assess the differences in PDAC behaviour when encapsulated in the lower stiffness (5 kPa) PEG-4-MAL and the higher stiffness (24 kPa) PEG-8-MAL hydrogels, PDAC cells were encapsulated and observed in the following PEG-Only and PEG-FN conditions (Table 9).

Table 9: Soft 4-Arm and stiff 8-Arm hydrogels.

Hydrogel	Degradability	E (kPa)
5wt% 4P(O/F)	20%	5
6wt% 8:8 8 P(O/F)	20%	24

3.5.1.1 PDAC Morphology

Figure 16 shows fluorescent images of PDAC cells in both hydrogel conditions (Table 9). PDAC cells form spheroids and grow in the soft 4P(O/F) hydrogels, however remain as single cells throughout the 7 days when in the stiffer 8P(O/F) hydrogels. Given that PDAC cells are sufficiently viable in these hydrogels, these data suggest that the stiffer 8(PO/F) hydrogels are inhibiting the PDAC cells proliferation and spheroid formation. Cell behaviour on 2D hydrogels of increasing stiffness shows the opposite trend, with cells displaying more activity and surface spreading as stiffness increases[59,66]. It could be that cells respond to stiffness increases differently in 3D, or it could be that it is not the stiffness, but another internal property of the hydrogel, causing the lack of activity observed in the 8P(O/F) conditions. The difference in ρ_c (Table 8) could indicate that although the cross-linker solution was 20% degradable in both cases, the degradation profile of the hydrogels might not be the same, which could be impacting the cell behaviour.

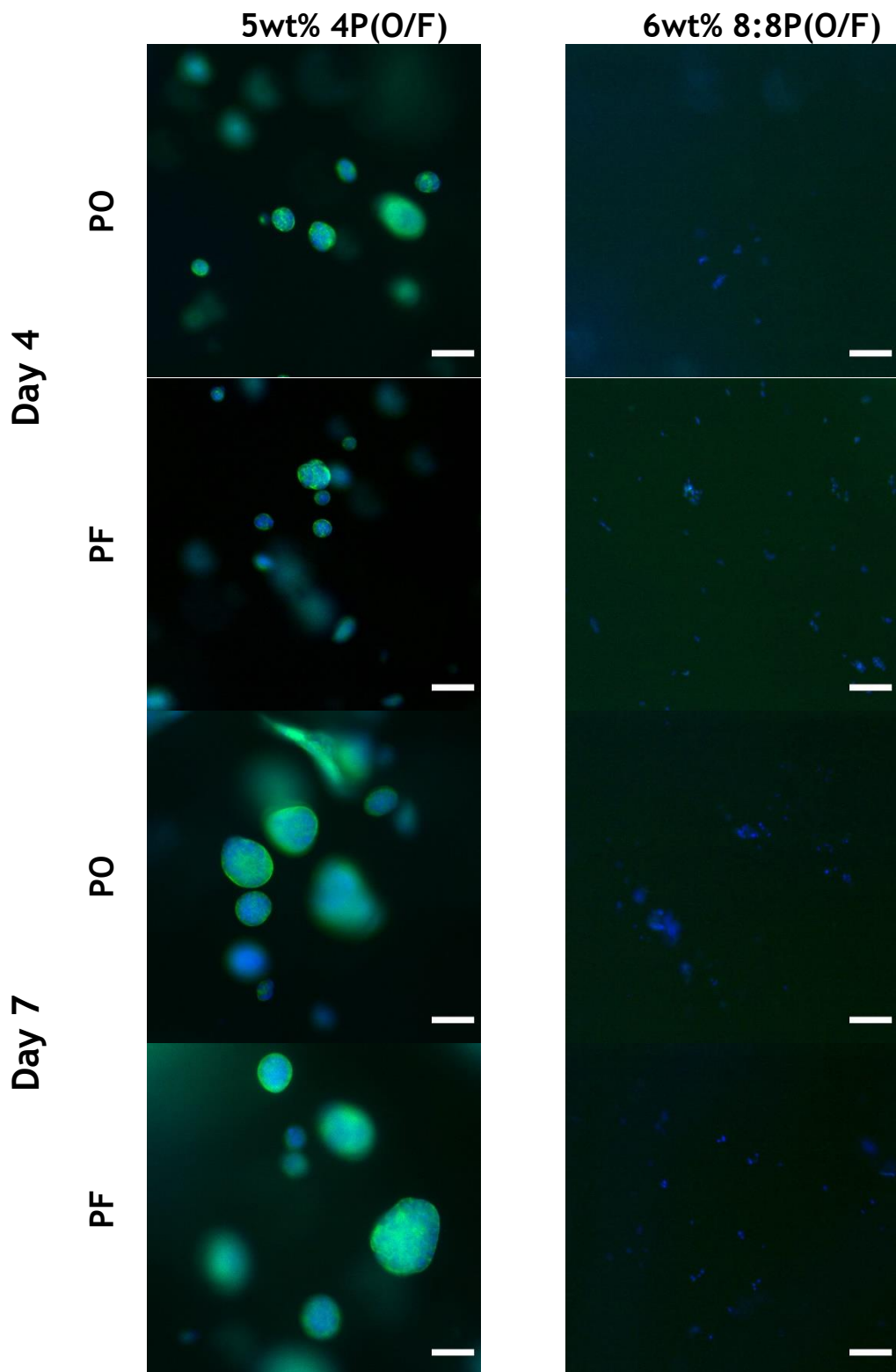**Figure 16: PDAC Cells do not grow in stiff 8P(O/F) hydrogels as they do in soft 4P(O/F) hydrogels. PDAC cells in soft 4P(O/F) hydrogels form spheroids but remain as single cells in stiff 8P(O/F) hydrogels. Scale bars = 100 μm. Blue = nuclei, green = actin.**

3.5.1.2 Visualisation of Proliferation and Mechanotransduction in PDAC

Confocal imaging was also carried out to assess proliferation and mechanotransduction in the PDAC cells in these conditions (Table 9). Ki67 was used as a proliferation marker[71], while YES-Associated Protein (YAP; nuclear during mechanotransduction, key mediator[72]) was stained to determine localisation. Antibody incubation time was increased to a 4 hour incubation at 37°C in order to remedy the varied antibody penetration seen in Chapter 3.2.2, Varying Degradability.

Unfortunately, the staining of YAP and Ki67 was still difficult to assess. Image segmentation was not carried out in the 8P(O/F) samples; PDAC remained as single cells as previously, and very few cells appeared to show any YAP or Ki67 staining, with a large amount of background staining in the images taken. It is possible that in the 8P(O/F) samples, the difficulty in visualising the antibodies was again due to poor penetration. As was described in New Hydrogel Characterisation 3.4.3.3, the internal mesh size of these 8-Arm PEG hydrogels is 10 times smaller than that in the 4-Arm PEG hydrogels, and so if there was a question of the antibody diffusing throughout the volume of the 4-Arm hydrogels, it is likely that antibody penetration in the 8-Arm hydrogels was not possible; even the relatively smaller phalloidin and the dapi were more difficult to image in the 8-Arm hydrogels.

From the images that were obtained (and analysed, Figure 17), it is clear that some spheroids in the 4P(O/F) hydrogels have proliferative cells around their outer regions, but it is not possible to say that all spheroids have these proliferative regions, as the Ki67 presentation varied vastly between and within each condition; neither size of spheroid or proximity of spheroids showed any pattern in Ki67 staining, the results were truly random. Given the alterations made to the immunostaining protocol, and the relatively small spheroid size, it is likely that the antibody was able to penetrate the volume of the spheroid, and the localisation of Ki67 represented by the immunostaining is the true localisation of Ki67 in these samples. The variety in size and number of spheroids developing within these samples could be the cause of the inconsistency in the Ki67 results, and work with pre-formed spheroids (one per hydrogel, consistent size) may produce clearer results in

terms of proliferative and other markers. Another explanation for this Ki67 presentation could be the graded nature of Ki67 levels described by Miller et al[71]; the implementation of consistent pre-formed spheroids could allow for more detailed analysis of the cell cycle phases within PDAC spheroids.

As for the YAP localisation, it appeared to be more strongly localised to the actin than the nuclei of the cells, suggesting a possible lack of mechanotransduction. However it has been shown by Lee et al[73] that mechanotransduction occurs independently of YAP in 3D breast cancer cultures, therefore it is possible that these PDAC cells behave similarly.

Another difficulty faced with these samples is imaging them. Not only is there the question of molecule penetration, even if the antibody moelcules do penetrate the hydrogel effectively, as 3D samples are relatively thick (and highly scattering)[13] the use of higher magnification objectives is restricted by working distance. Given the importance of proliferation, and the specific interest in mechanotransduction, further investigations into Ki67 and YAP localisation within spontaneously formed spheroids will be carried out.
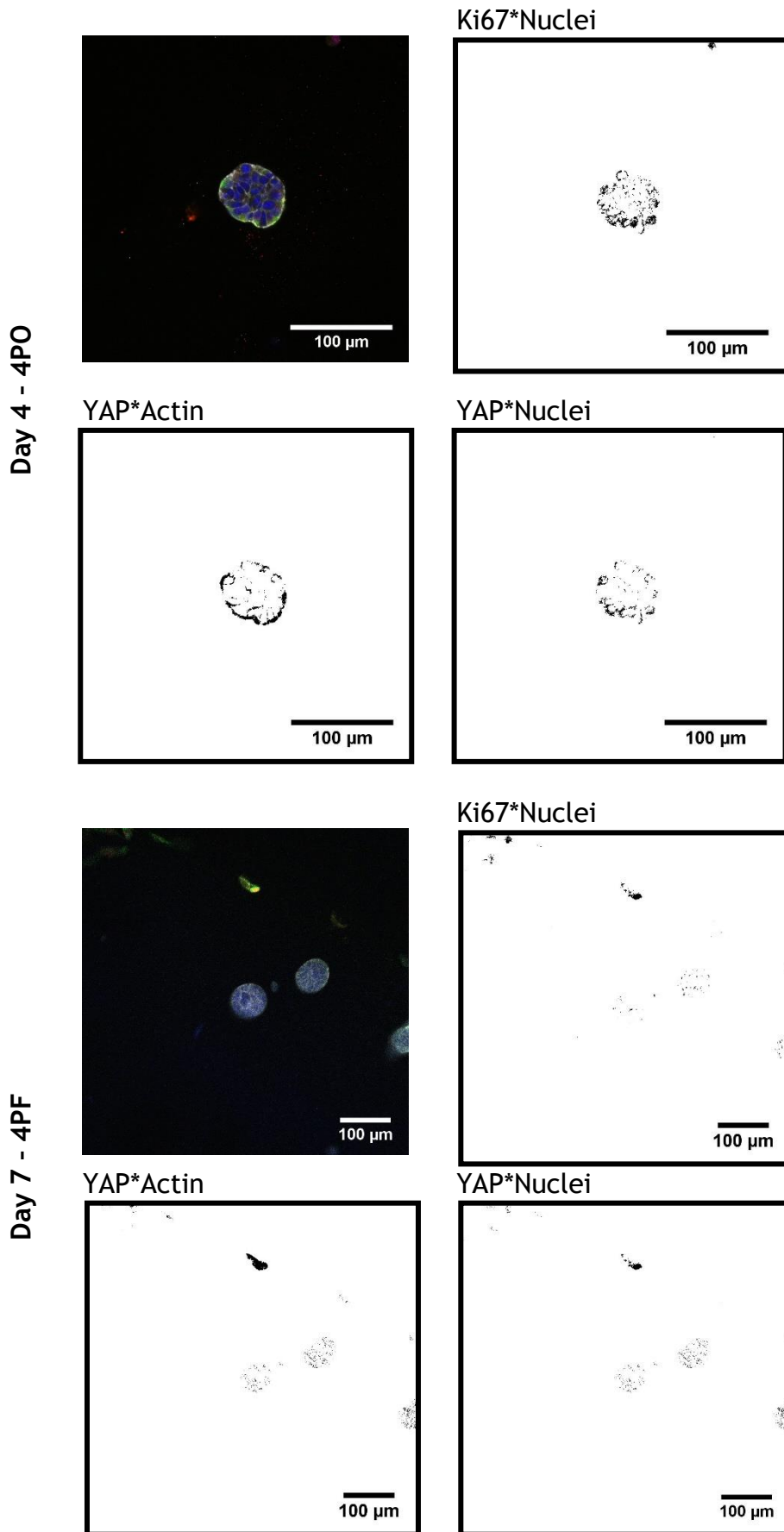
Figure 17: Image segmentation results show localisation of Ki67 and YAP. The Ki67*Nuclei images demonstrate whether the cells are expressing Ki67, and therefore are proliferative. The YAP*Actin and YAP*Nuclei images determine whether YAP is localised in the nucleus of cytoplasm of the cells. Blue = nuclei, white = actin, red = Ki67, green = YAP.

3.5.2 PEG-4-Mal Versus PEG-8-Mal of similar Stiffness

Given that the behaviour of PDAC cells in the 6% 8:8 8P(O/F) hydrogels differed significantly from their behaviour in the 4P(O/F) hydrogels, it was important to assess PDAC behaviour in the 4-Arm and the 8-Arm PEG-based hydrogels at a similar stiffness. Hydrogels of compositions and stiffness found in Table 10 were produced with PDAC cells encapsulated to determine whether it was the difference in stiffness or the difference in hydrogel composition which produced the behavioural differences between the two conditions discussed in the previous chapter.

Table 10: 4 and 8-Arm hydrogels of similar stiffness

Hydrogel	E (kPa)
10wt% 4P(O/F)	~10
6wt% 3:8 8P(O/F)	~13

3.5.2.1 PDAC Morphology

PDAC cells were imaged at 4- and 7-days post encapsulation. The results (Figure 18) show that PDAC cells behave very differently between the conditions: they form spheroids within the PEG-4-MAL hydrogels, whereas in the PEG-8-MAL hydrogels they remain small and singular. Given that these hydrogels are of similar stiffness, the differences observed here cannot be explained by stiffness, so another property must be influencing cell behaviour.

It is well known that surface topography influences many aspects of cell behaviour[74,75]. Goa et al used micropillars to show that hepatic stellate cell area and protein expression is affected by micropillar topographical dimensions, with the smallest micropillar spacing leading to the smallest cell area[76]. It is possible that PDAC morphology and activity in 4- and 8-arm hydrogels are being affected by 3D topographical differences between the conditions; with the smaller mesh size in the 8-arm hydrogels indicating smaller spacing between topographies, and possibly inhibiting cellular activity in PDAC cells.

These samples were also stained for Ki67 and YAP, but given the inconsistencies and difficulties within conditions mentioned previously (section 3.5.1.2, page 63) assessment of these arkers was not carried out.
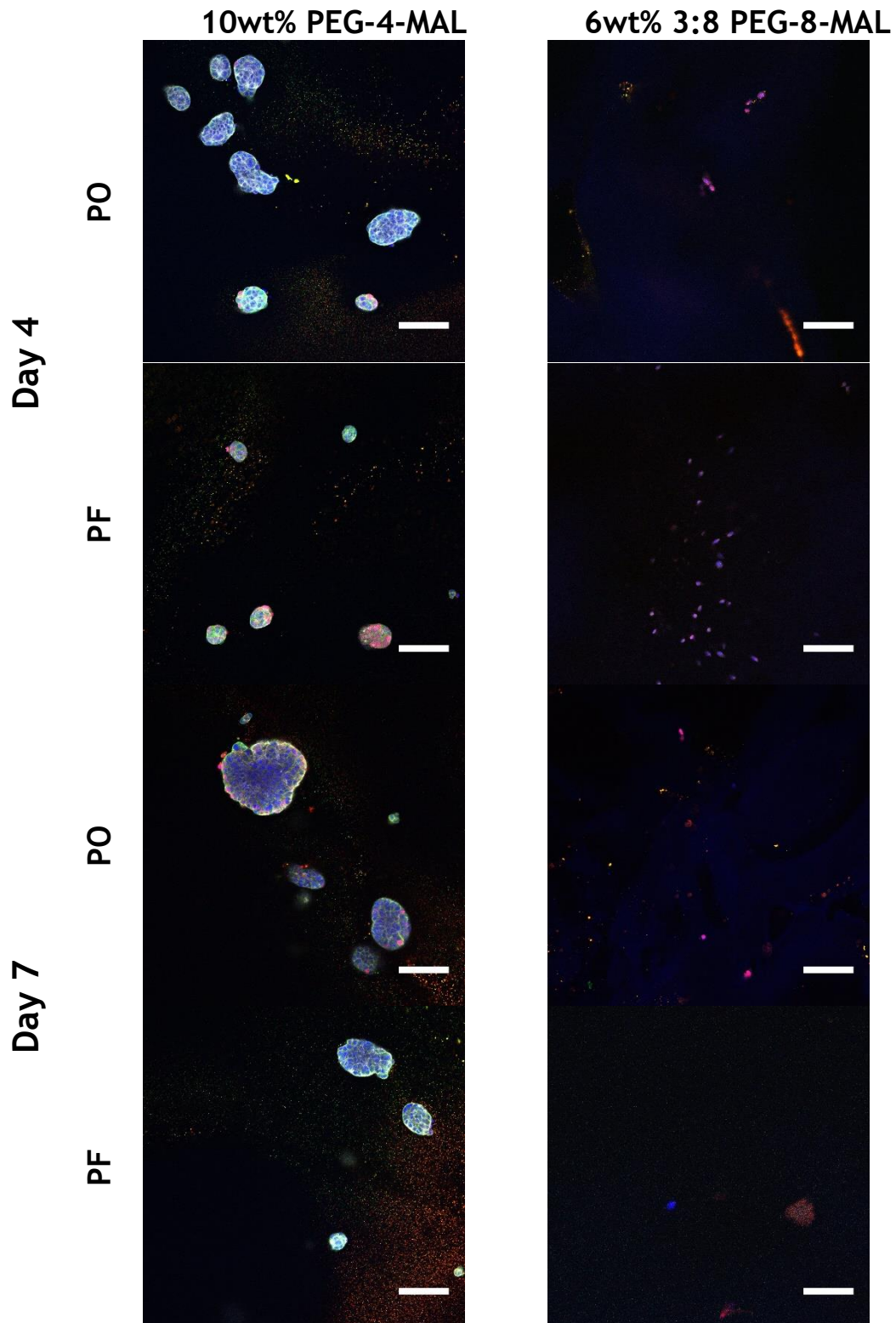
Figure 18: Cells are unable to grow in PEG-8-MAL hydrogels as they are in PEG-4-MAL hydrogels. Confocal images. PDAC cells in PEG-4-MAL hydrogels form spheroids but remain as single cells in PEG-8-MAL hydrogels. Scale bars = 100 µm. Blue = nuclei, white = actin, green = YAP, red = Ki67.

3.5.2.2 Cellular Activity

Given the apparent lack of activity seen in the PDAC cells in the previous experiment, an assay was required to determine the activity of the PDAC cells in the PEG-8-MAL hydrogels versus the PEG-4-Mal hydrogels.

CCK-8 and PicoGreen assays (quantifying metabolically active cells (using a tetrazolium salt) and total cell number (staining nucleic acids) respectively) were performed to quantitatively determine both the total and the active number of cells within PEG-4-MAL and PEG-8-MAL hydrogels at 1, 4, and 7 days post encapsulation (Figure 19).

PDAC cells are active in the 4P(O/F) conditions, as has been reported for C2C12 cells by Phelps et al[42], and appear to have proliferated between timepoints, with both total and active cell number increasing (although there are no statistically significant differences in cell number measured here, there is a clear trend). The number of active cells is consistently a fraction of the total cell number. This could be explained by the formation of spheroids which have proliferative cells in the outer regions only, with reduced proliferative activity in central cells (which could also mean reduced metabolic activity). As for the 8P(O/F) conditions, neither total nor active cell number change notably over the period. These data, and the morphology imaging (Figure 18), show that although PDAC are able to survive in the 8P(O/F) hydrogels, they are largely inactive.
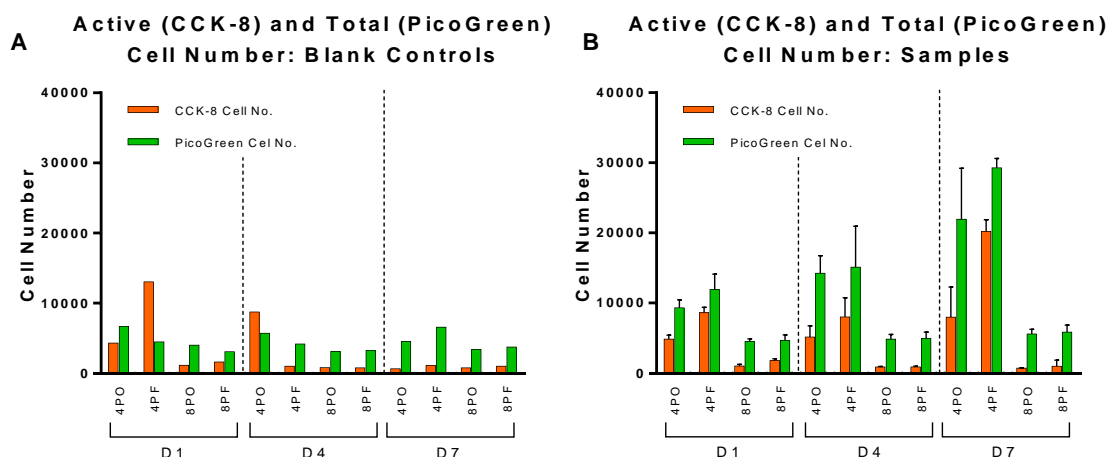
Figure 19: Total and active cell number is higher in 4-Arm than 8-Arm hydrogels. (A) Blank conditions are hydrogels without cells encapsulated. (B) Samples with encapsulated cell density of 200,000 cells/ml). Despite some anomalous CCK-8 results for the blank controls, the trend shows considerably higher total and active cell numbers within the 4-Arm samples compared to the 8-Arm samples, with this difference increasing with the timepoints. Cell number and activity appear to remain consistent throughout the timepoints in 8-Arm hydrogels.

Tan et al investigated 4- and 8-arm PEG hydrogel interaction with cells, and found that the number of cells able to adhere to the surface of 4-arm PEG hydrogels in 6 hours was significantly greater than that on 8-arm PEG hydrogels[77]. Ehrbar et al showed that in 8-Arm PEG-based hydrogels, an increase in cross-linking density impedes cell spreading and migration. They also saw that in non-degradable hydrogels, cells remained active (protruding filo- and pseudo-podia) but trapped in their higher stiffness hydrogels (>100 Pa), whereas in non-degradable hydrogels <100 Pa migration was similar to in degradable hydrogels[78]. Ki et al saw that in their 8-Arm PEG-Norbornene hydrogels, metabolic activity was higher in the softer condition than the stiffer condition, with stiffness controlled by increasing cross-linking[69,70]. The PEG molecule, cross-linking density, degradability, and stiffness all appear to have effects on cell behaviour and are largely interlinked variables.

Lee et al used PEG in culture media to increase osmotic pressure within alginate hydrogels and assessed the effect of both osmotic pressure and stress relaxation on chondrocyte cell volume and proliferation. They saw that increasing osmotic pressure decreased proliferation and inhibited cell volume

expansion. They also saw that proliferation was supressed in conditions with slow stress relaxation, and that mechanotransduction in 3D may include adhesion-independent sensing of cell volume[79]. Interstitial space and pressure affect cell behaviour and expansion[48,80], so given the lower mesh size and possibly different degradation profile of the PEG-8-MAL compared to PEG-4-MAL hydrogels, it is possible that this sensing of cell volume is at play and spatial restriction is having an effect on the PDAC cells in the PEG-8-MAL hydrogels.

The solitary spacing, and the apparent lack of proliferation and cellular activity could indicate that PDAC cells are in a dormant-like state in the 8-Arm hydrogels. This behaviour indicate the use of PEG-8-MAL hydrogels as a model for single cell dormancy, but further characterisation of the hydrogels (such as viscoelastic properties) and an improvement in immunostaining protocol would be required.

Work by Kimberley Warnock (an MEng student at the University of Glasgow whom I supervised throughout her 6 months of lab work) found PDAC tissue from the same mouse model as the PDAC cells used in this research (Pdx1-Cre positive, LSL-Kras$^{G12d/+}$, LSL-Trp53$^{R172H/+}$ (KPC) mice[54]) to have a stiffness of ~5 kPa. The 5wt% PEG-4-MAL condition (~5 kPa) is the closest to physiological stiffness of the tumour environment so will be the main hydrogel composition used in future work, with the possibility of other compositions implemented for study of single cell dormancy or pre-metastatic sites.

Initially the variable of interest in this work was hydrogel stiffness, but given the results up to this point, matching hydrogel stiffness to the PDAC tissue stiffness measured by Ms Warnock and varying other components such as CAF incorporation and hydrogel protein content could provide more insight into PDAC behaviour.

3.6 Co-Culturing PDAC with iCAF

Following the decision to move away from stiffness as the variable of interest, work was carried out to determine the effect that cell to cell communication may have on the PDAC cells. Given that the majority of PDAC tumours contain CAFs within the tumour volume[2], their influence cannot be overlooked. It was decided that incorporating immortalised CAFs into the system may bring about some changes in the PDAC cells behaviour in these PEG-based hydrogels. It is common in cancer studies to co-culture the cancer cells with relevant stromal cells, for example Sasser et al found breast cancer cell proliferation to be regulated by bone marrow stromal cells in co-culture[81], Koh et al saw that different fibroblast types had different effects on colon cancer growth, with some fibroblasts enhancing growth and some inhibiting it[82], and Yakavets et al found that co-culturing breast cancer with fibroblasts resulted in the production of ECM components and the differentiation of the fibroblasts into myoblasts[83]. Given these examples, it is important to include a co-culture in this work and assess the effect that the iCAFs have on the PDAC cells and environment.

3.6.1 iCAF Viability

Before co-culturing with iCAFs, the viability of these cells in the PEG-based hydrogels was assessed. As per Kimberley Warnock's findings, the 5 kPa hydrogel was used in this work. iCAFs were encapsulated at 200,000 cells/ml in 5 wt% 4-Arm PEG-based hydrogels, both PEG-Only and PEG-FN conditions. Figure 20 shows that up to 3 days post-encapsulation >80% of iCAFs are viable. This is an acceptable viability for the use of iCAFs both alone and co-cultured with PDAC cells within the 4P(O/F) hydrogels used here.
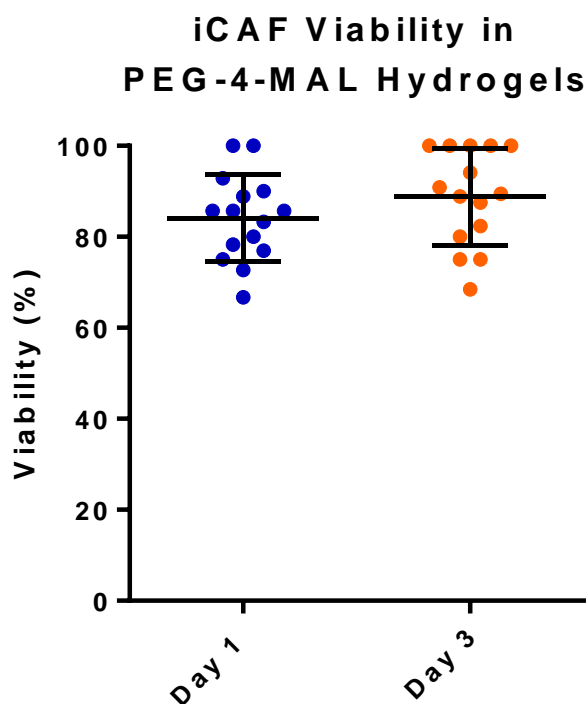
Figure 20: iCAFs are sufficiently viable in PO hydrogels. iCAF viability is >80% both 1-and 3-days post-encapsulation, with no significant difference in viability between timepoints.

3.6.2 Dispersed Cell Co-Culture

The first co-culture carried out was performed with a PDAC:iCAF ratio of 1:1, with the intention of assessing the suitability of α-Smooth Muscle Actin (α-SMA) as a specific marker for iCAFs[84]. PDAC and iCAF were co-cultured and also individually cultured in the 4-Arm PEG-Only and PEG-FN hydrogels, and stained for α-SMA. However, from the images obtained (Figure 21) α-SMA is not a suitable marker for discerning between the two cell types. α-SMA staining was apparent in the PDAC only conditions (Figure 21) where it should only be presented by the iCAF cells. It is possible that within the PDAC cell line there is a small fraction of CAFs; the process of cell isolation cannot ensure that 100% of cells are PDAC, and given that tumour cells and environments are largely heterogeneous[85], and that a large proportion of PDAC tumours consist of matrix and cancer associated cells[2], it is possible that some non-PDAC cells enter the population.

These co-culture images again show the inconsistency in spheroid growth and morphology between conditions. Observations of the spontaneous formation

of these spheroids within different environments could provide insight into the formation of both primary and secondary lesions within the body. However for the purpose of producing a consistent 3D *in vitro* PDAC model, working with pre-formed spheroids may be of more use.
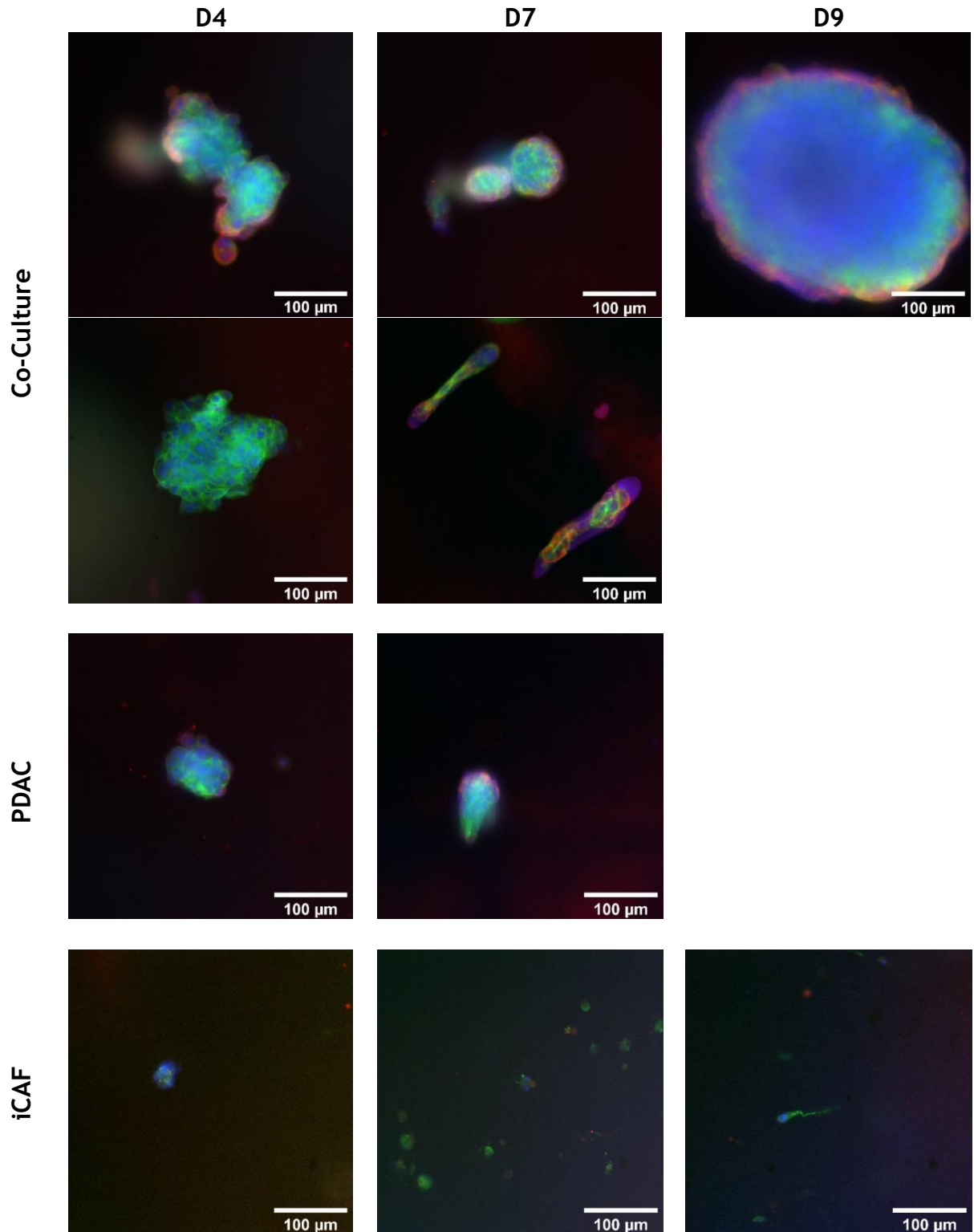

Figure 21: Co-Culture of PDAC and iCAFs. Fluorescent images. Blue = nuclei, green = actin, red = α-SMA. The α-SMA staining is most defined in the Co-Culture, with some staining of the PDAC only and iCAF only condition.

3.6.3 Spheroid Co-Culture

To solve the problem of inconsistencies within conditions, pre-formed PDAC spheroids were implemented. Both hanging drop and ULA plates were used to form spheroids, and it was found that the most consistent method was ULA plates. An experiment was set up (conditions in Table 11) to assess the effect of iCAFs on PDAC spheroid behaviour. PDAC spheroids were formed in ULA plates, cultured for 3 days, and hydrogels formed around them. The samples were imaged hourly for 5 days using the IncuCyte S3.

Table 11: PDAC Spheroid and iCAF Co-Culture Conditions

Condition	Hydrogel	iCAF Presence
Mt	50:50 Collagen:Matrigel	None
Mt+CAF	50:50 Collagen:Matrigel	On top of hydrogel (1000 cells/hydrogel)
PO	5wt% 4PO, 20% degradable	None
PO+CAF	5wt% 4PO, 20% degradable	On top of hydrogel (1000 cells/hydrogel)
PO++CAF	5wt% 4PO, 20% degradable	Within hydrogel (400,000 cells/mL)
PF	5wt% 4PF, 20% degradable	None
PF+CAF	5wt% 4PF, 20% degradable	On top of hydrogel (1000 cells/hydrogel)
PF++CAF	5wt% 4PF, 20%degradable	Within hydrogel (400,000 cells/mL)

Figure 22 demonstrates the effect of the iCAFs on the invasiveness of PDAC cells in Matrigel, with an overall increase in area that the PDAC cells cover as time progresses, the +CAF condition is consistently at a greater increase than its counterpart for each time point. Further, iCAFs do not only appear to increase the area of extension from the spheroid, but also the extension length, demonstrated by the invasive index. From this data, and the Mt images in Figure 23, the iCAFs clearly encourage the PDAC cells to spread throughout the hydrogels.

Unfortunately, the auto-focus of the IncuCyte focussed only on hydrogel features within the P(O/F) conditions so successive spheroid images were not captured in the PEG-based hydrogels as they were in the Mt condition. To assess morphology, more P(O/F) samples were prepared and imaged at day 4 on the A1R confocal microscope. The P(O/F) images in Figure 23 demonstrate the lack of invasiveness in the PEG-based hydrogels, even with FN

incorporated and iCAF influence. Given the stark contrast in behaviour of the PDAC cells in the PEG-based hydrogels compared to the Mt, alterations to the protein content of the PEG-based hydrogels may be important: PDAC spheroids behave similarly in GF reduced Matrigel and P(O/F) hydrogels suggesting that the GFs play a key role in encouraging invasion throughout Matrigel. The incorporation of a second protein into the hydrogel matrix would allow for the binding of a greater range of GFs to the hydrogel network while maintaining control of the distribution and quantity of said GFs.

Another alteration which may be necessary is the gelation rate. Some of the spheroids appear elongated or misshapen in the P(O/F) conditions (Figure 23); an issue which is likely a result of the rapid gelation of these hydrogels. This rapid gelation also means that cracks are able to form within the hydrogel (which affected the IncuCyte autofocus). Reducing gelation rate could improve the consistence of the hydrogels, minimise cracks, and stop the deformation of spheroids during encapsulation.
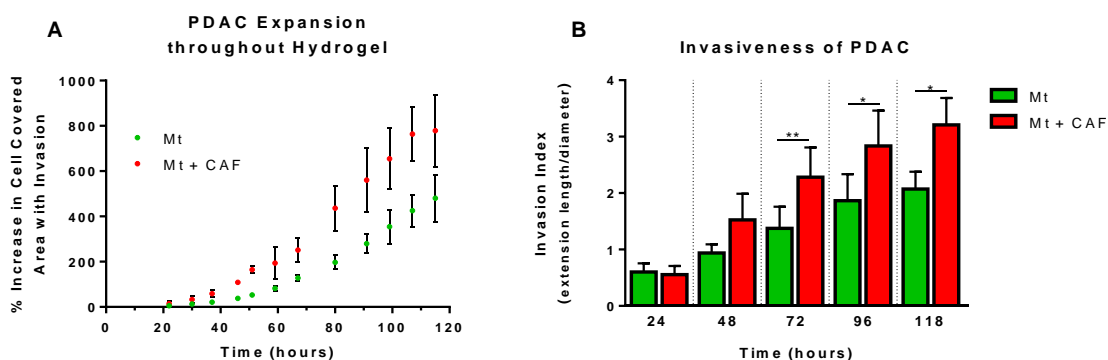
Figure 22: PDAC invasion in Matrigel with and without iCAF influence. (A) PDAC expansion showing increase in cell covered area from original spheroid area. (B) Invasion index; extension length/original spheroid diameter.
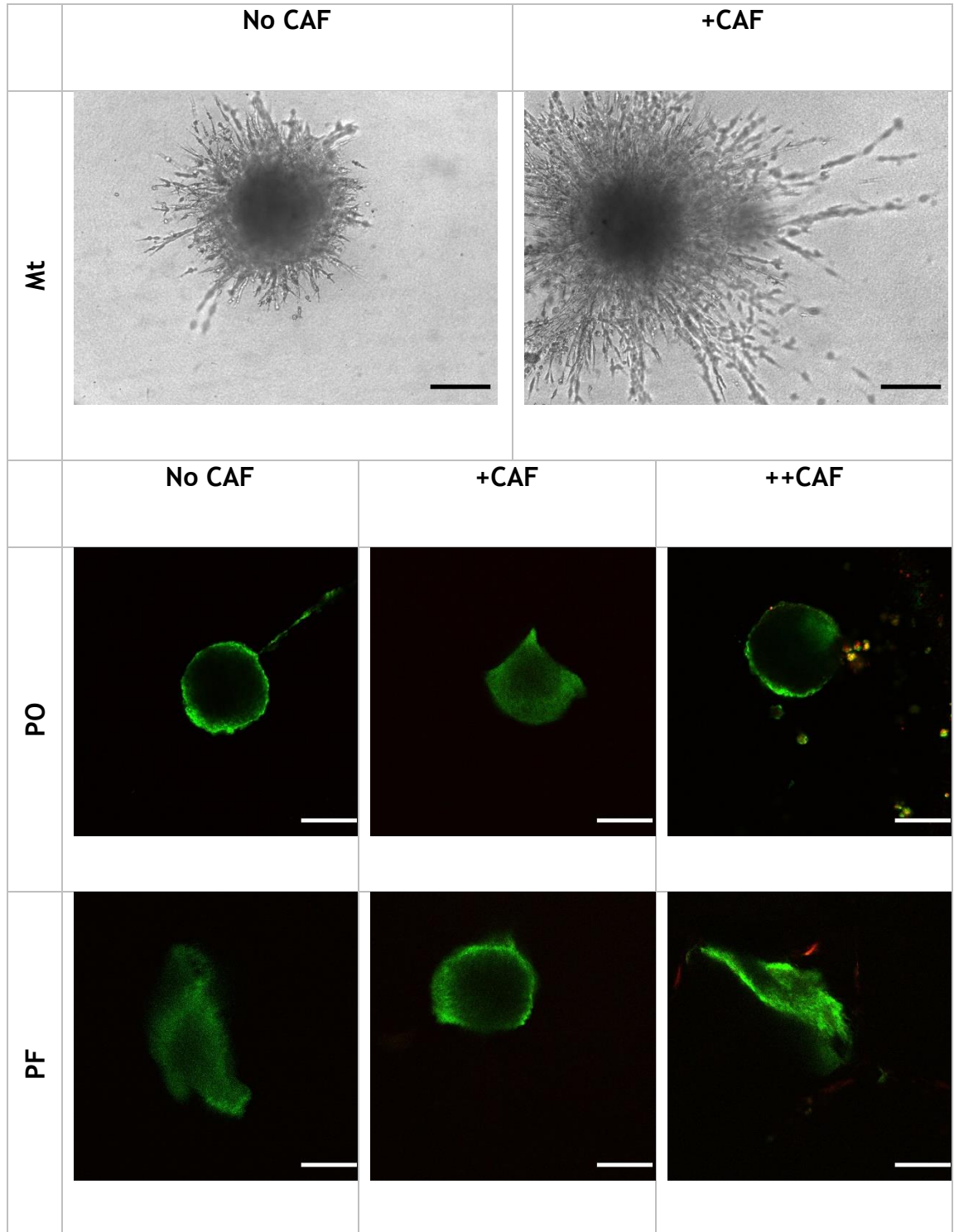
Figure 23: PDAC Spheroids in Matrigel (Mt, Row 1) and PEG-Only/PEG-FN hydrogels (Rows 2 and 3) with and without iCAF influence. Mt images are brightfield from IncuCyte at t=3d18h, PEG-4-MAL are confocal, taken ~4d. Green = Syto 13 tracker (labels nucleic acids), red = Cell Tracker Red, labelling iCAFs. Scale bars = 250 μm.

3.7 Reducing Hydrogel Gelation Rate

3.7.1 Production

As mentioned above and demonstrated in Figure 23, the rapid gelation of the hydrogels following the original preparation protocol may be causing the preformed PDAC spheroids to become elongated and deformed. Gelation following this protocol begins almost immediately, so it may be that the hydrogel components are pulling and extruding the encapsulated spheroids in a manner that does not impact encapsulated single cells in the same way, possibly due to the size difference. It is unclear whether this manual deformation could affect the behaviour of cells in the immediate area. This rapid gelation also can lead to cracks in the hydrogel; these areas can be avoided when analysing behaviour using manual microscopy, however if an automatic imager like the IncuCyte is to be implemented these areas of inconsistency cause problems. It was hypothesised that if gelation rate could be reduced then the spheroids would not be deformed, and the occurrence of cracks would be minimised.

To determine whether gelation rate could be reduced, 10 wt% 4PO hydrogels were formed with DMEM-Cys of varying pH, and the gelation times assessed. As increasing pH leads to faster reaction kinetics[86], it was expected that lowering pH would reduce gelation time. The 10 wt% hydrogels were used in this instance as it is the hydrogel condition which appears to begin its gelation most rapidly, therefore has most scope for assessment.

Table 12: Gelation of PEG-4-MAL hydrogels based on pH. (Hydrogels are 10 wt% PO, non-degradable, 10 kPa)

pH	Comments
6.98	Gelation begins immediately, cured in <30 minutes
6.05	Gelation begins immediately, cured in <30 minutes
5.23	Gelation begins at 8s, cured in <30 minutes
3.65	Able to fully mix constituents before gelation begins, cured in <1h

The PEG-based hydrogels used in this work were chosen for their rapid and efficient gelation, as described by Phelps et al[42]. In general use, this gelation

means that encapsulated cells are suspended well throughout the hydrogel volume; as rapid gelation reduces the likelihood of cells sinking through the solution. However as stated, this leads to issues when encapsulating preformed spheroids.

Table 12 shows that working at near physiological pH (6.98) as the original protocol dictates leads to gelation beginning immediately, as does lowering the pH to 6. When the pH was lowered below 6 (to 5.23) it took 8 seconds for the gelation process to begin following the addition of the cross-linker, and the hydrogel was still fully cured within 30 minutes. When the pH was further reduced to 3.65 the beginning of gelation was not as clear or rapid as in other cases, and it took longer to be fully cured than the hydrogels at higher pH, however the solution did fully cure at room temperature within 1 hour. These results showed that for the hydrogels to begin gelation more slowly and reduce the risk of spheroid deformation, a pH of <6 was necessary, and <5 was desirable.

3.7.2 Cell Viability in Reduced pH Hydrogels

Given the results of the previous experiment, the viability of cells encapsulated in hydrogels at a lower pH was assessed. The cells would need to survive in the low pH hydrogel solution for the duration of gelation, after which physiological media was added to the samples. 10wt% 4PO hydrogels were formed using DMEM-Cys of pH 3.70, 4.35, 5.45, 6.30, and 8.03, cured in the incubator, then washed and covered with media of physiological pH. A Live/Dead assay was performed 4 hours post encapsulation.

The assay found that in all cases when media of pH<5 was used for hydrogel formation, encapsulated cell viability was below 60%, and significantly less than those encapsulated in hydrogels formed with media of pH≥5.45 (Figure 24). Around 80% of cells encapsulated in hydrogels formed with media of pH>5 were viable 4 hours post encapsulation, meaning that in future work with PDAC spheroids, hydrogels can be formed in these slightly acidic (pH≥5.45, <7) conditions, reducing gelation rate, therefore reducing risk of spheroid deformation during encapsulation into the hydrogel. As the PDAC microenvironment is acidic[87] it should follow that cancer associated cells are

also viable in these reduced pH hydrogels, however viability assessments must be carried out for each cell type to be used in these conditions.
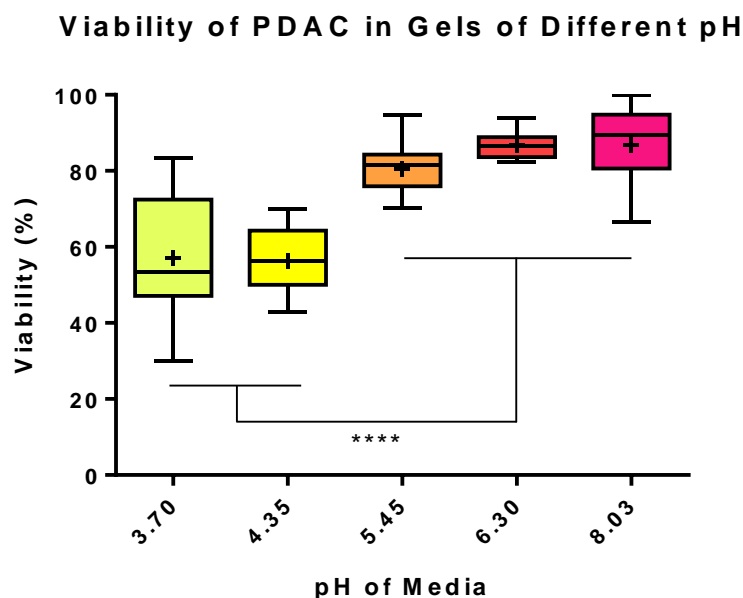
Figure 24: Cell viability is significantly reduced in hydrogels formed with media of pH <5.45. <60% of PDAC encapsulated in hydrogels formed with media of pH<5.45 are viable after encapsulation, whereas >80% of PDAC encapsulated in hydrogels formed with media of pH≥5.45 are viable after encapsulation. n>12. Box plot whiskers at minimum and maximum, + denotes mean.

Unfortunately, for hydrogels to form by Michael-type addition, the components must be combined under slightly basic conditions[88], therefore the hydrogels forming in these low pH conditions may be gelling by a different mechanism other than Michael-type addition. Therefore the resulting hydrogel may differ on a chemical level from hydrogels formed under the slightly basic pH, and as such these hydrogels would need to be characterised separately. Given the use of hydrogels formed under the physiological pH for all previous work, and the reduced cell viability at pH <5 (the desirable pH for reduced gelation rate) this method of reducing reaction kinetics will not be implemented or pursued any further in this work.

3.8 Developing a Bi-Protein (FN and LM) Hydrogel

Given the lack of PDAC invasion into the PF hydrogels observed throughout my work, and the clear differences in PDAC behaviour in Matrigel (common in 3D cancer studies[89-91]) compared to the PEG hydrogels, new hydrogels were

produced to incorporate laminin (LM), at 10μg/50μl hydrogel (1:5 LM:FN ratio). A scale size schematic of the new design can be seen in Figure 25.

As mentioned in the introduction to this work, the specific laminin chosen for incorporation into the hydrogel network was LM 332. This is because LM 332 has a range of GF binding domains[53] and is therefore useful in retaining GFs within the hydrogel for sustained interaction. Further, Cavaco et al found that LM 332 interacts with CAFs, sustaining their phenotype, and encouraging invasion of pancreatic cancer cells[52]. As such, the incorporation and characterisation of LM into these PEG-based hydrogels is essential in making a more complex pancreatic cancer model for future.
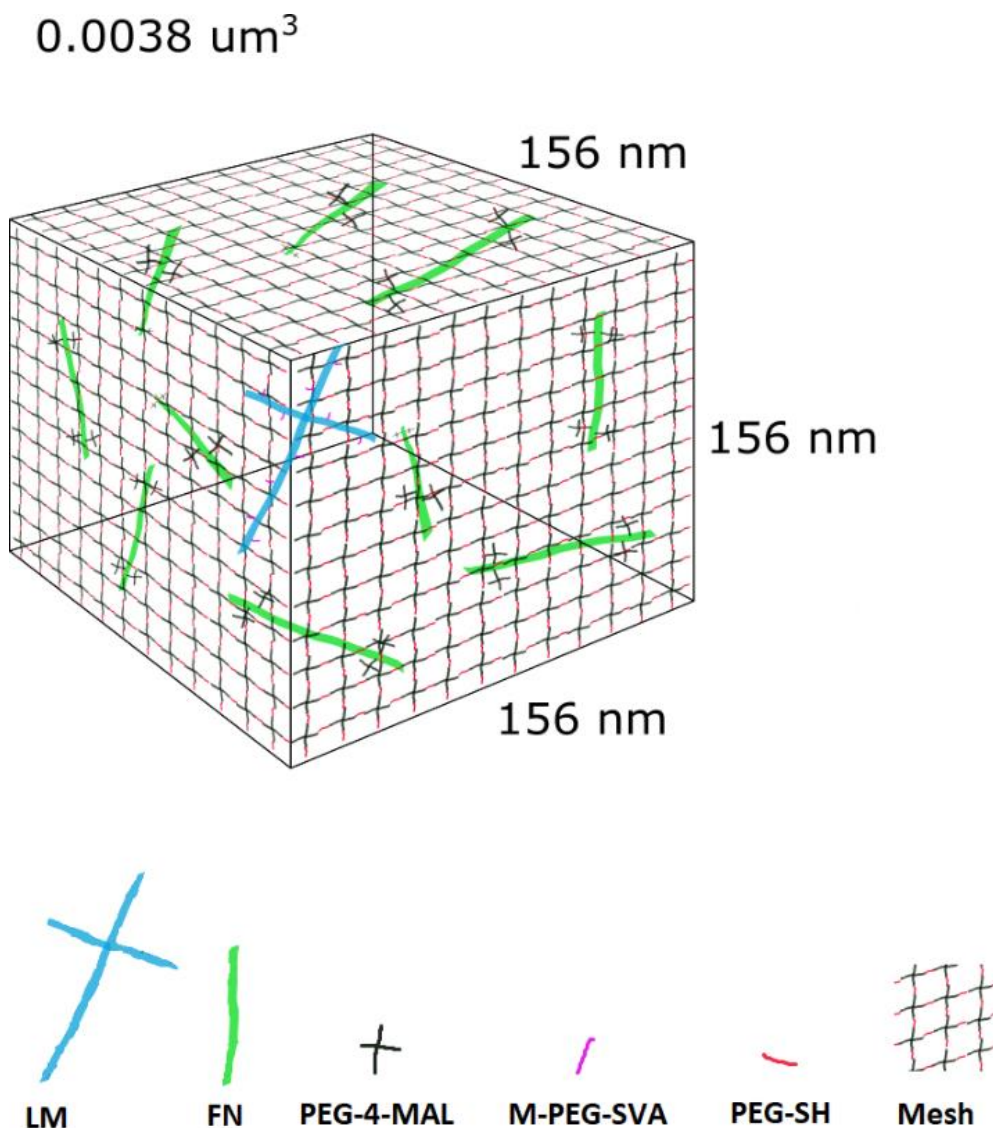
Figure 25: Scale schematic of Bi-Protein Hydrogel. A 0.0038 μm³ volume of PEG-based Bi-Protein hydrogel showing PEGylated LM protein and FN monomer, cross-linked into the PEG-4-Mal mesh.

3.8.1 LM release

The first assessment of the new LM hydrogels was to determine if the LM was being incorporated into the hydrogel network, or whether it was only encapsulated within the hydrogel and could be released.

A BCA assay was trialled to assess the LM release from the hydrogels, however it reported a higher protein release than the maximum possible concentration, suggesting the possibility that the PEG-4-MAL hydrogels interfered with the BCA assay. Therefore, analysis of LM PEGylation was made using a TNBSA Assay of the PEGylated LM. The TNBSA results (Figure 26) showed that there significantly fewer free amines in the PEGylated-LM compared to the native LM. This suggests that the PEGylation of LM was successful as the SVA in the M-PEG-SVA molecules binds the LM molecule at free amines; the reduction of these indicates SVA binding.

Following the TNBSA determination that the PEGylation was successful, hydrogels were prepared as per Table 13, swelled, and stained for LM post swelling. Fluorescence intensity results (Figure 26) demonstrate that the LM in the PEGylated condition (PL) was retained within the hydrogel, as there was a significantly greater intensity in this condition than the PO and the P+L. The results in the P+L condition were similar to that in the PO condition, suggesting that with swelling and washes, the native LM was removed from the hydrogel leaving the fluorescence results similar to the PO background results, further demonstrating the integration of the LM into the hydrogel in the PL condition, suggesting that cross-linking of LM into PEG-based hydrogel was successful.

Table 13: Hydrogel conditions for LM staining

Condition	Description
PO	PEG-Only hydrogels, PEG-4-MAL, 5 wt% polymer
PL	PEG-LM hydrogels (PEGylated-LM crosslinked into hydrogel), PEG-4-Mal, 5wt% polymer
P+L	PEG-Only hydrogels with native LM added before curing, PEG-4-MAL, 5 wt% polymer
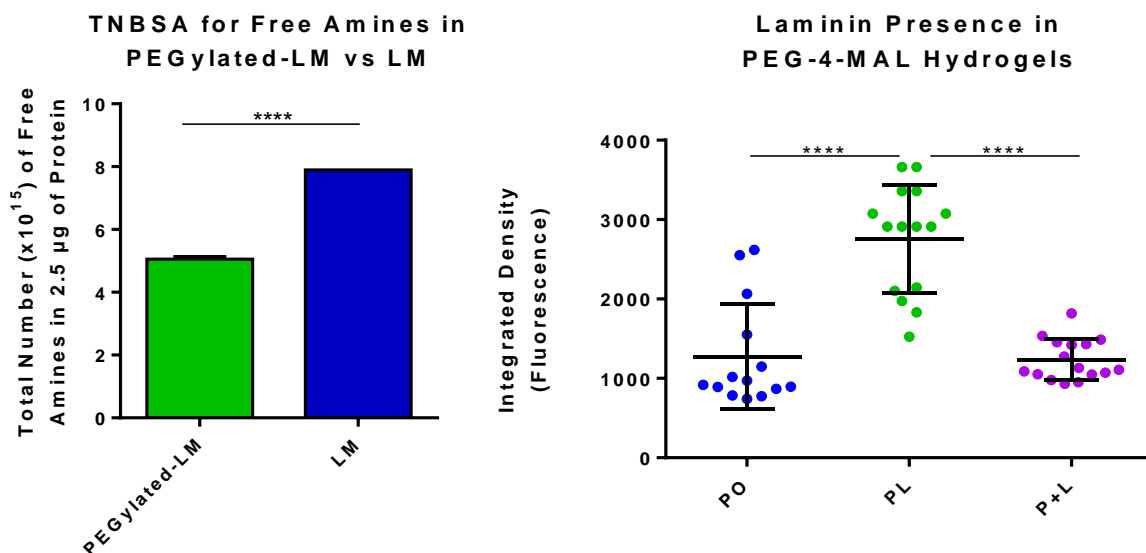
Figure 26: PEGylation of LM was successful. TNBSA results showed significantly fewer free amines in the PEGylated condition. Fluorescence results showed significantly higher intensity in PEGylated condition compared to no-LM (PO) and native-LM (P+L).

3.8.2 Hydrogel Stiffness

Hydrogels of 5 wt% polymer and 50% degradability (implemented to allow cells increased hydrogel remodelling possibility in future work) were produced as PEG-Only (PO), PEG-FN (PF), the new PEG-LM (PL), and the bi-protein PEG-FN-LM hydrogel (PFL), were produced for AFM stiffness measurements.

The results in Figure 27 show that there are no significant differences in stiffness between conditions. These values are slightly higher than those previously recorded by Dr Trujillo-Muñoz for the PO and PF hydrogels, however this is due to the addition of VPM at a higher ratio (50:50 VPM:DiSH). As the hydrogels are similar in stiffness within these 50% degradable conditions, behaviour within these different single- and bi-protein hydrogels can be compared.

Stiffness of Fibronectin, Laminin
and Bi-Protein Hydrogels
by AFM

Figure 27: AFM measurements of Youngs Modulus in PO, PF, PL, and PFL hydrogels. No significant differences.

3.8.3 Swelling and Degradation
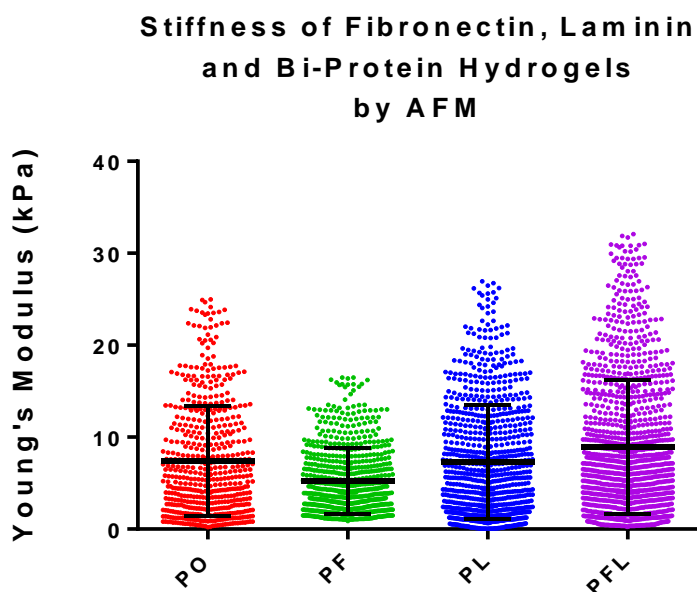
Following the AFM results showing no significant differences between the hydrogel stiffness, assays were carried out to determine how the different protein hydrogels behave in terms of swelling and degradation in comparison to each other. 5 wt% 50% degradable PO, PF, PL, and PFL hydrogels were produced for swelling and degradation assays.

The results (Figure 28) show that while water uptake and degree of swelling are similar in all conditions, the degradation of the PFL condition is significantly higher than that of both the PO and the PF conditions, with no significant difference between the PFL and the PL condition. This suggests that the LM in the hydrogels, and particularly the combination of two proteins within the hydrogel, significantly increases the degradability of the hydrogel compared to both the PO control and PF hydrogel that have been worked with to this point. Unfortunately, altering the degradability of the hydrogels by varying the VPM:DiSH ratio within the crosslinker volume leads to differences in hydrogel stiffness, so the degradability of these conditions cannot be brought in line without altering another variable; as such these conditions will be used with the knowledge that they have differing degradation profiles.
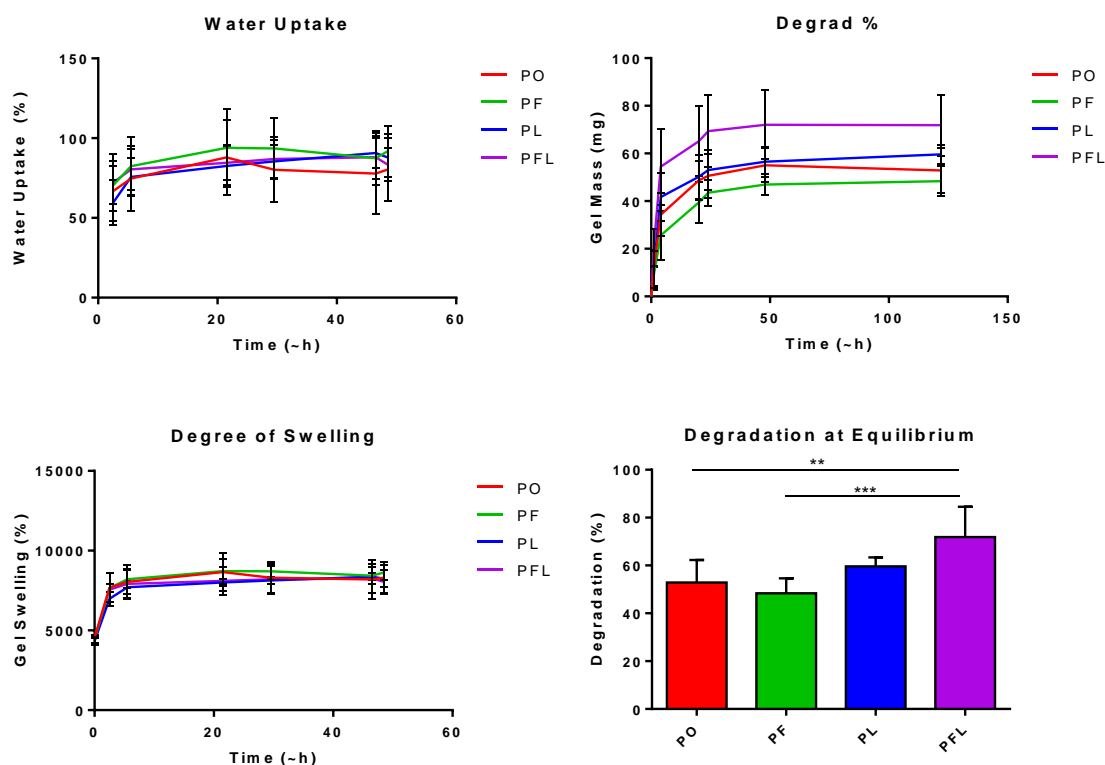
Figure 28: Swelling and Degradation of single- and bi-protein PEG-Based hydrogels. All conditions have a similar swelling profile and water uptake, however PFL degrades significantly more than the other conditions.

3.9 GF Incorporation

Given the behaviour of the PDAC spheroids in Matrigel it is clear that the uptake and retention of growth factors (GFs) into the hydrogel network is important. TGFß plays a complicated role in pancreatic cancer, but has been seen to promote metastasis, cell motility and neoangiogenesis, among other traits of late stage cancer progression[92], plays a role in the transformation of normal fibroblasts into CAFs[93], and works to maintain the CAF phenotype[94].

3.9.1 TGFβ uptake

Hydrogels of each condition (5 wt% polymer PO, PF, PL, PFL) were formed, swelled with cysteine for TGFß binding[95], and treated with 1 µg/ml fluorescently labelled TGFß. Figure 29 shows that all hydrogel compositions retained some level of TGFß, with PL showing significantly higher TGFß retention than the other conditions, retaining around 10% of the labelled TGFß. Given these results, it is possible to use these conditions to assess the

behaviour of PDAC cells in single- and bi-protein hydrogel with and without GF influence.
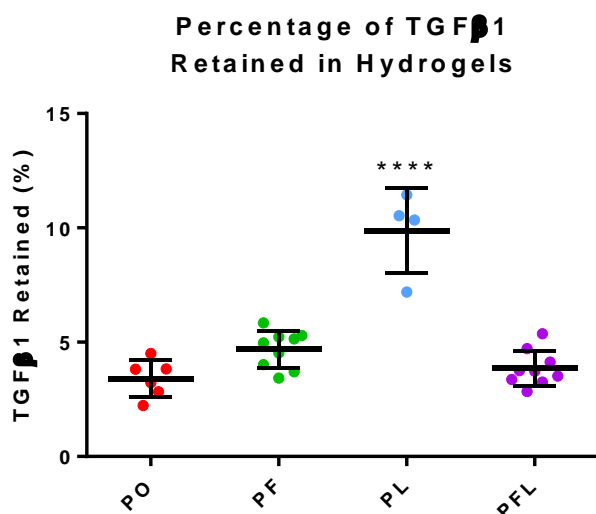
Figure 29: TGFβ retention in Hydrogels. PL hydrogels had significantly better TGFβ retention than the other conditions.

3.9.2 PDAC Cell Reaction to Bi-Protein and GF Incorporation

3.9.2.1 Determination of Optimal TGFβ Concentration

PDAC cells were encapsulated in 5 wt% 50% degradable PO and PF hydrogels (PO and PF were used in this initial assessment as they have been the most commonly implemented conditions in this work so far) and allowed 3 days to establish before treatment with various TGFß concentrations.

Figure 30 shows that in both PO and PF hydrogels, 10 ng/mL TGFß appears to have a significant effect on PDAC spheroid growth compared to the other concentrations, with the most marked effect in the hydrogels containing protein (FN). Given the significant impact of 10 ng/mL TGFß on PDAC spheroid diameter, this concentration will be used in further investigations.
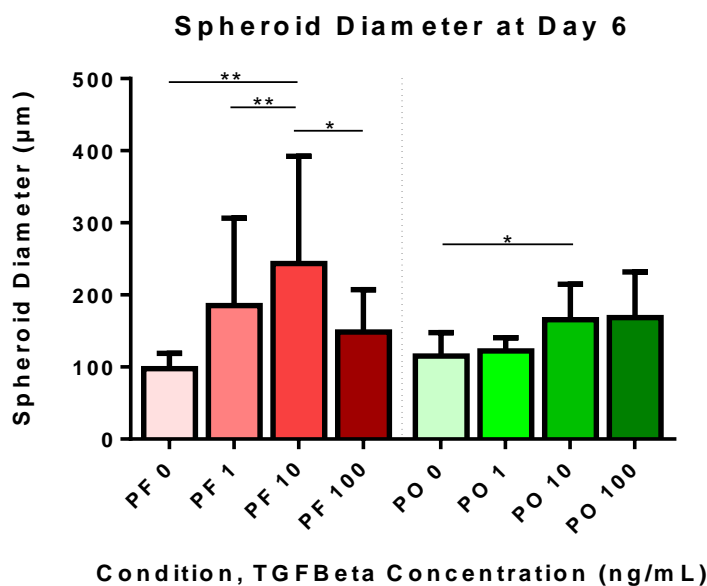
Figure 30: PDAC Spheroid Diameter following TGFβ Treatment. In both PF and PO, the 10ng/mL TGFβ condition shows significantly greater spheroid diameters than in the other TGFβ concentrations.

3.9.2.2 TGFβ Influence on PDAC Spheroids

PDAC cells were encapsulated in hydrogels of each composition (5 wt% polymer, 50% degradable, PO, PF, PL, PFL); all conditions were now included following the TGFß concentration determination. Samples were treated with 10 ng/mL TGFß, and cultured for a further 10 days.

It can be seen from the spheroid diameter results (Figure 31) that TGFß has a significant influence on the size to which PDAC spheroids are able to grow within these hydrogels. Further, it has a much greater influence in the protein hydrogels, possibly as it can interact with the hydrogel, than in the PO condition, with the PL hydrogel seeing the greatest PDAC spheroid growth. Representative images of spheroid growth in each condition can be seen in Figure 32 with spheroid size difference being visibly notable.

These samples were also stained to assess the expression of epithelial (E-Cadherin) and mesenchymal (ß-Catenin) markers within conditions[96]. Visual assessment of the confocal images (Figure 33, E-Cadherin column = green) shows that E-Cadherin appears to be expressed more clearly in the conditions without TGFß than in treated conditions (and the PO with TGFß), suggesting that TGFß treatment reduces the expression of this epithelial marker (and that

the efficacy of TGFß may rely on there being proteins to bind and retain it). The ß-Catenin in untreated samples appears to be cytoplasmic (Figure 33, PL sample is a good example of this) however in treated samples ß-Catenin appears to be localised to the nucleus, suggesting that the TGFß treatment encourages ß-Catenin activation, potentially indicating the beginning of EMT.

Another indication that these protein and GF interactions are encouraging changes within the PDAC cells is the development or irregularly shaped spheroids in GF treated protein hydrogels. Figure 34 shows representative BF images of irregularly shaped PDAC spheroids with blebbing at the surface, possibly indicating the appearance of migratory blebs[97,98] in TGFß treated samples. Khan et al have found that increased metastatic potential of prostate cancer cells correlates with increased blebbing ability[99], suggesting the appearance of these blebs could also indicate EMT. Given these potential indications of EMT, the next step will be genetic analysis of EMT genes within PDAC samples under these conditions.
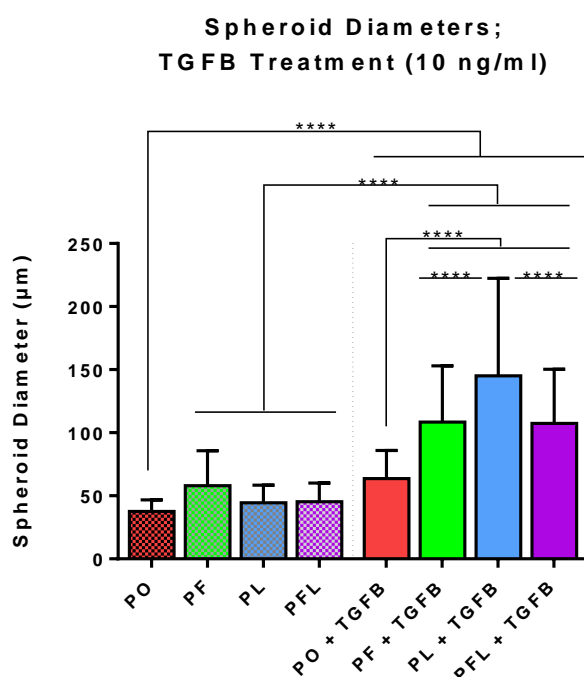
Figure 31: Spheroids are significantly larger in protein hydrogels with TGFβ treatment. PF, PL, and PFL hydrogels treated with 10 ng/ml TGFβ allowed spheroids of significantly greater diameter to form than untreated hydrogels of all compositions, and treated PO, with the PL condition producing the largest PDAC spheroids. Triplicates in each condition, >60 spheroids analysed per condition.
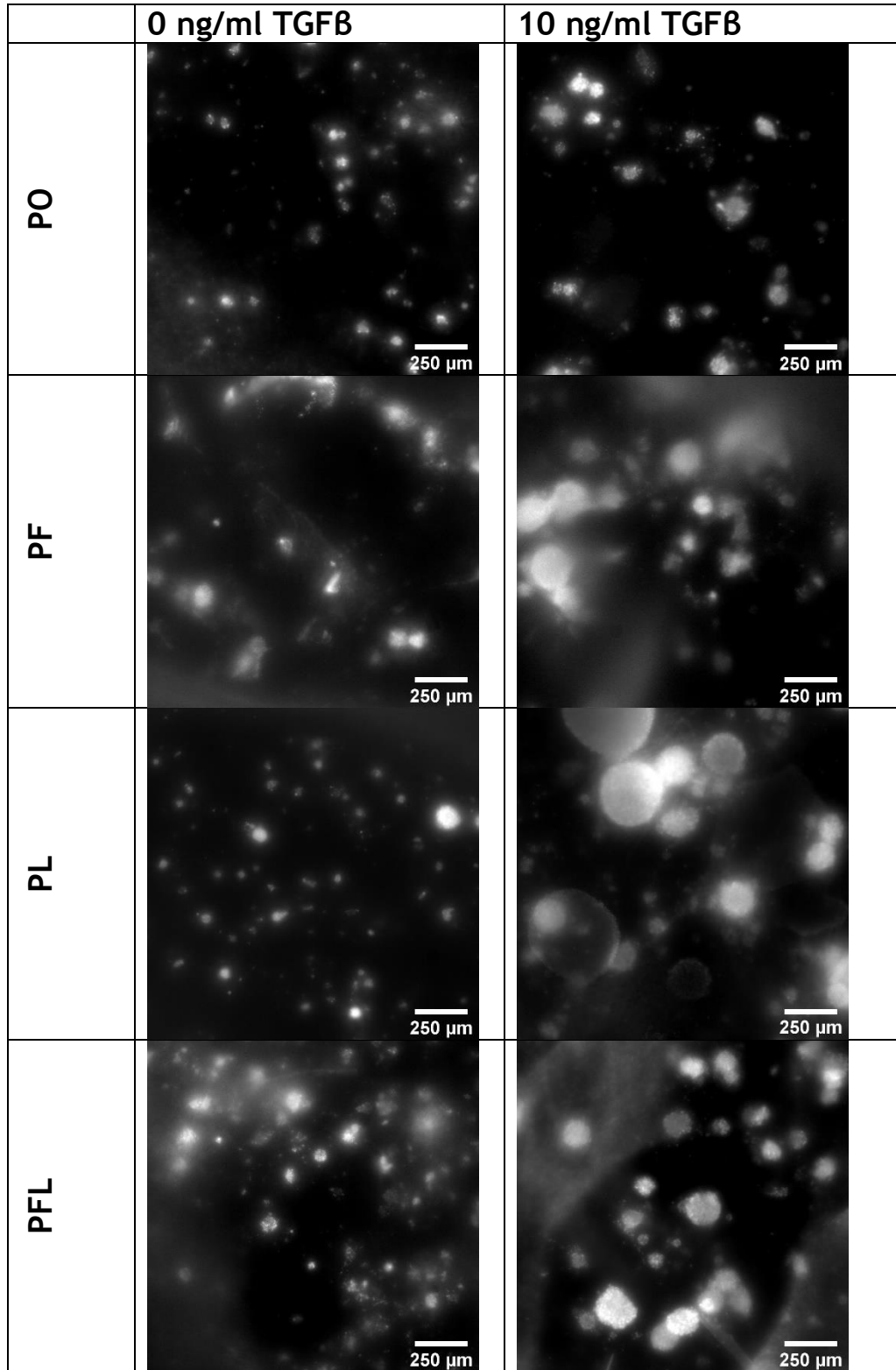
Figure 32: Representative images of PDAC spheroid sizes in different conditions. Nuclear staining. Treated protein hydrogels show considerably larger spheroids than other conditions.
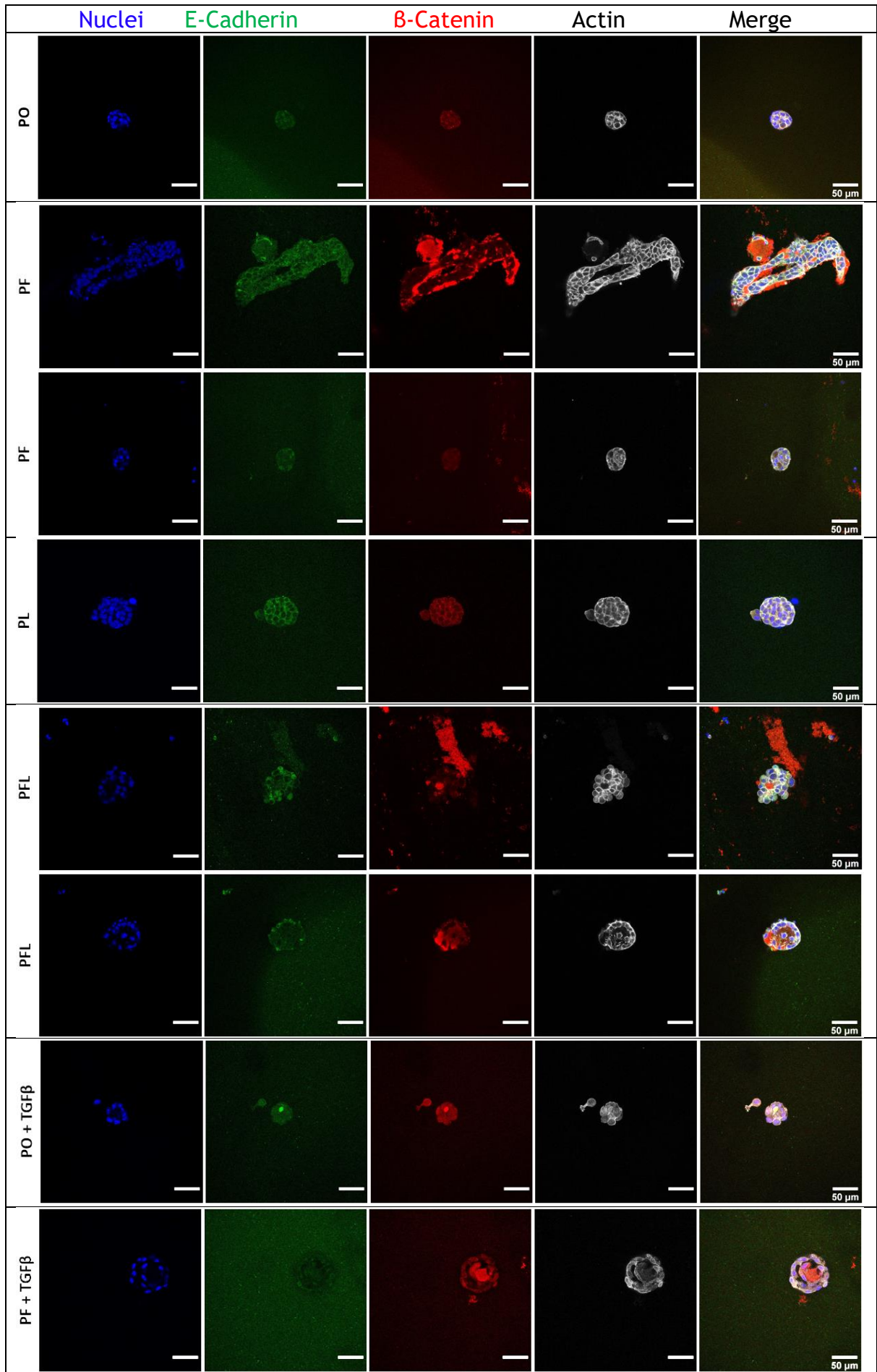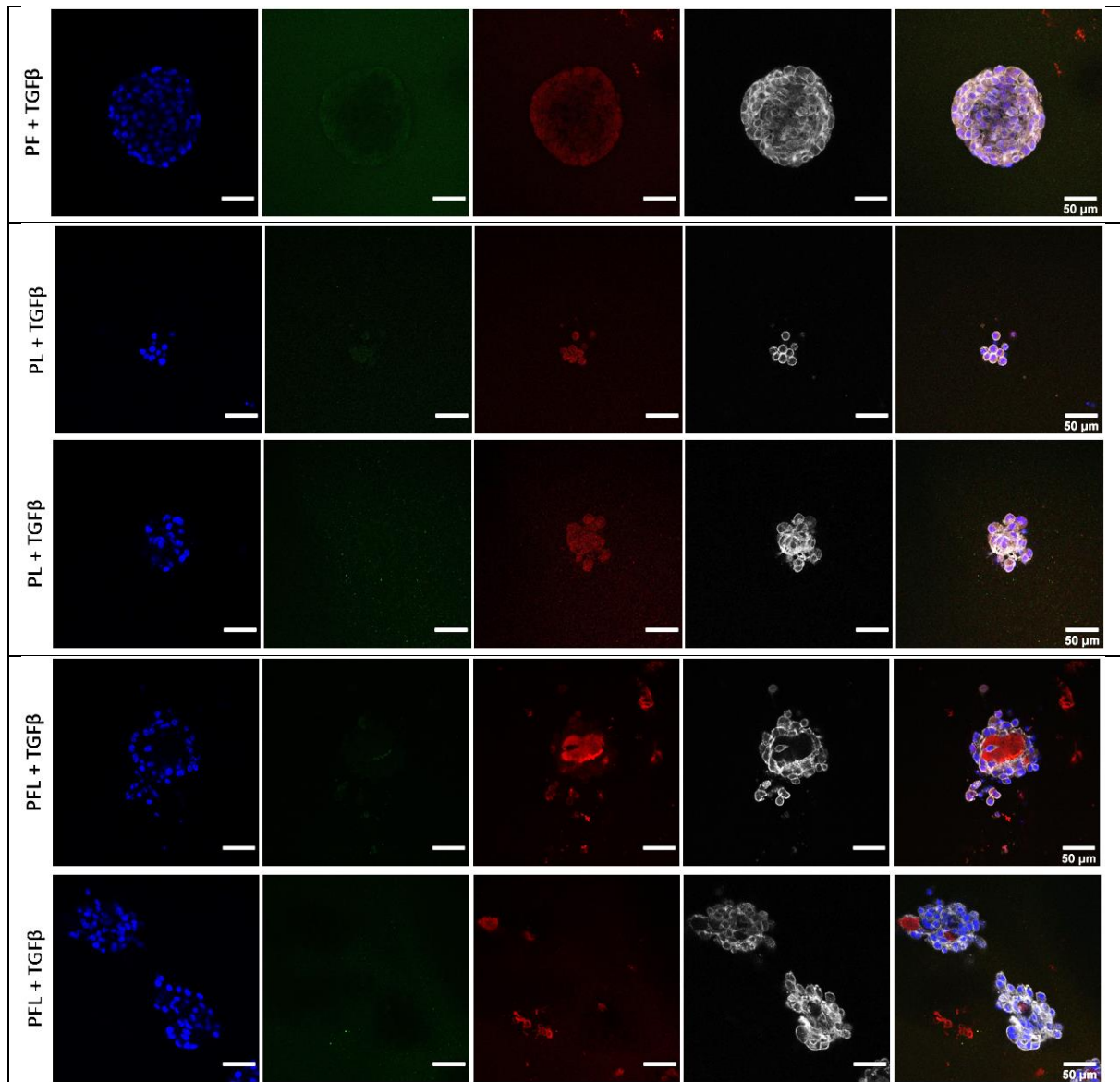
Figure 33: Representative confocal images of PDAC cells in each hydrogel condition. Stained for; blue = nuclei, green = E-Cadherin, red = β-Catenin, white = actin.
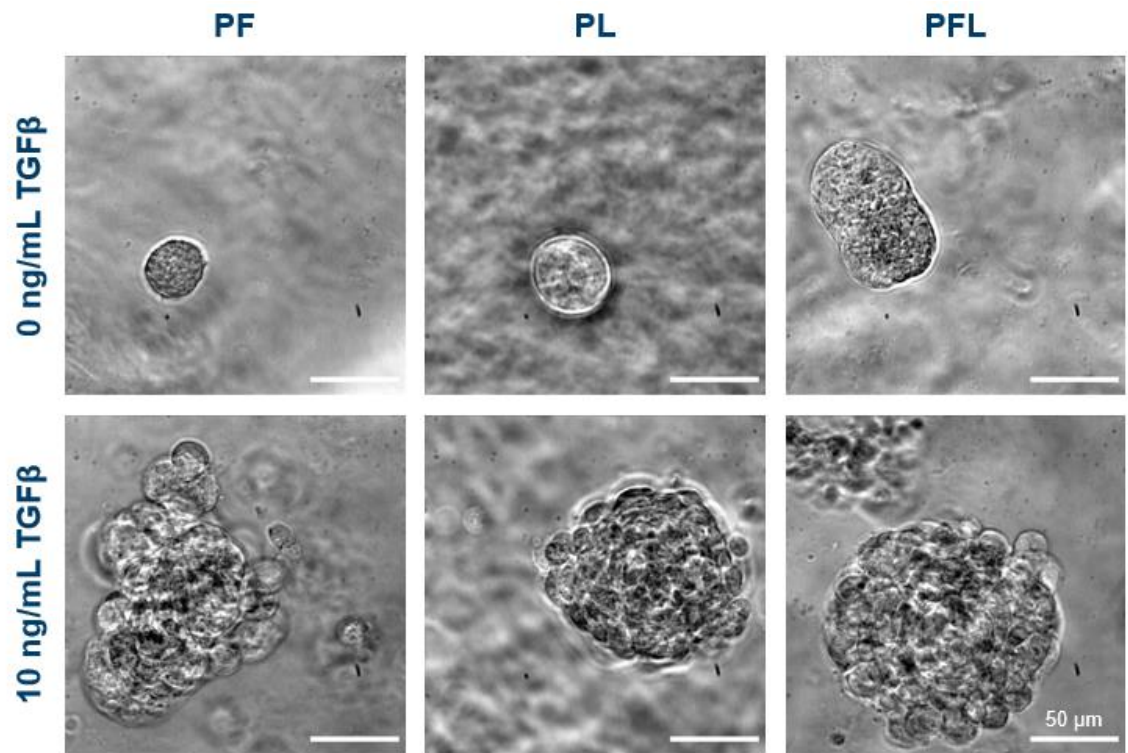
Figure 34: Irregular shape of TGFβ treated PDAC samples could indicate migratory blebbing. Bright field images.

4 Conclusion

PDAC cells react to 3D *in vitro* environments differently to how they react in 2D, with the influence of hydrogel stiffness alone having a far reduced effect in this 3D culture than in 2D literature. For example, various studies using 2D polyacrylamide hydrogels have found changes in cell adhesion[100], proliferation[101], and migration[102] all as a result of changes in stiffness, whereas no such changes appeared as a result of stiffness changes in any of the 3D work carried out in this research.

The physical effects of the matrix in terms of viscoelastic properties, the inner dimensions of the network, and the pressures, tensions and restrictions within the matrix also play an important role in the regulation of cell behaviour when cultured in 3D. Matrix pore size can affect cell phenotype[103], cellular processes are influenced by matrix viscoelasticity[104], increasing osmotic pressure has differing effects on cells in aggregates in 3D that it does on the same cells cultured in 2D[105]. Given the varying effects of each property there was much to be taken into consideration when working with these hydrogels.

Early work in varying properties of these hydrogels found that the PDAC cells behaved similarly in both the PEG-Only and the FN incorporated hydrogels throughout a range of stiffness, degradability, and over 2 weeks of culturing. Introducing a new hydrogel composition (PEG-based, using an 8-Arm PEG molecule in place of the 4-Arm PEG molecule as the basis of the network) with the intention of assessing the effects of further increasing stiffness, saw results possibly relating more to the internal network of the new hydrogel composition as opposed to the stiffness, with spatial restriction having an impact on PDAC spheroid development and growth. When working in 2D the only restriction on space is the boundaries of the culture surface, however when translating culture into 3D the space and interactions around the whole cell volume must be considered, therefore the internal dimensions of the 3D culture are extremely important and must be well characterised. It is known that interstitial space and pressure affect cell behaviour and expansion[48,80]. Lee et al showed that mechanically restricting cell volume can alter cell signalling and reduces cell growth capabilities, with chondrocytes in slow relaxing hydrogels maintaining their pre-encapsulation size[79]; the PDAC cells in

the 8-Arm hydrogels appeared to remain at a size similar to their pre-encapsulation size, suggesting that this mechanical spatial restriction could have been inhibiting their behaviour.

When returning to the original hydrogel composition and introducing iCAFs, it was found that while iCAFs have a strong impact on invasiveness of PDAC cells in Matrigel, they had little effect on the behaviour of PDAC cell in the PEG-based hydrogels used in this work. The tumour microenvironment is highly complex[106], and this demonstrates the sheer complexity of the tumour microenvironment very well; as Matrigel is derived from tumour tissue it has the correct components and architecture to encourage PDAC and iCAF interactions[107], however lacks consistency and reproducibility. Matrigel contains laminin, collagen, perlecan, epidermal GF, fibroblast GF, platelet derived GF, TGFß, MMP-2 and-9, and urokinase among other components[108]. This plethora of signals is yet to be incorporated into any *in vitro* system in a controlled manner. Introducing more complexity into the hydrogels while maintaining the ability to control their stiffness, degradability, and protein content allows for more potential cell-matrix interactions as well as the controlled integration of a range of different growth factors, while ensuring that the characteristics of the hydrogel are well defined and replicable.

Integrating LM into the hydrogel network and producing well characterised single- and bi-protein hydrogels, has allowed for GF incorporation. The results from the final experiments using these hydrogels with TGFß incorporation have been promising in possibly showing PDAC cells beginning to change phenotype from epithelial to mesenchymal, with potential migratory blebbing[97-99] visible on spheroid surfaces. Bergert et al demonstrated that the actin protrusion and myosin contraction balance within cells determine whether those cells will migrate using lamellipodia or blebs, with substrate adhesion also affecting this determination[109]; this could explain the difference observed between PDAC cells invading Matrigel with long protrusions, and the possible initiation of migratory blebbing observed in the final experiment of this work (3.9.2.2). Blebbing of the plasma membrane is known to encourage cancer cell movement away from the initial tumour site by assisting in detachment, resulting in the metastatic behaviour of said cells; as such Khan et al propose blebbing as a marker for metastatic prostate cancer[99]. The appearance of

blebs in this work is therefore an encouraging indication that these hydrogels may be able to model some aspects of EMT and metastasis. The improvement of these hydrogels with increased complexity and signalling possibilities have shown that it may be possible to produce a well characterised, reproducible, 3D environment using this system in which future *in vitro* PDAC investigations may be made.

Overall, this work has demonstrated the level of complexity needed to produce a synthetic environment able to mimic the *in vivo* reality. PDAC cell behaviour in the hydrogels used in this work differed greatly from that in Matrigel, suggesting far more intricacies are necessary for this system to be anywhere near a Matrigel alternative, with a key focus being on the chemical signals which influence cancer progression, such as growth factors. This being said, even with few of the extra complexities mentioned, the reproducibility of this system gives it merit in terms of an environment for high throughput investigations into cancer cell viability and potentially anti-cancer drug efficacy.

5 Future Work

Moving forward from this work, it will be important to develop a reliable protocol for DNA extraction from PDAC cells within these hydrogels. This will allow genetic markers for different phenotypes and behaviours, such as the possible EMT observed with GF incorporation, to be investigated in these early stage bi-protein hydrogels. Further down the line if more proteins or complexities are added to the PEG-based model, having a protocol in place would allow for genetic analyses into disease progression, interaction with and reaction to different factors, and potentially drug effects.

Introducing CAFs into the newly characterised PEG-LM and Bi-Protein hydrogels would be of great interest in assessing the effects of LM or FN-LM compared to FN alone and determine the importance of each protein in the PDAC environment as well as the iCAF influence when interacting with multiple proteins, possible GFs, and the PDAC cells.

The work with TGFβ showed that GFs can be retained withing these hydrogels depending on how they bind proteins, so work with various GFs of interest could be useful in tailoring the environment to suit the specific PDAC stage/behaviour that is being investigated.

List of References

1. Siegel, R. L., Miller, K. D. & Jemal, A. Cancer statistics, 2016. *CA. Cancer J. Clin.* **66**, 7–30 (2016).

2. Öhlund, D. *et al.* Distinct populations of inflammatory fibroblasts and myofibroblasts in pancreatic cancer. *J. Exp. Med.* **214**, 579-596 (2017).

3. Boj, S. F. *et al.* Organoid models of human and mouse ductal pancreatic cancer. *Cell* **160**, 324–338 (2015).

4. Tuveson, D. A. & Neoptolemos, J. P. Understanding metastasis in pancreatic cancer: A call for new clinical approaches. *Cell* **148**, 21–23 (2012).

5. Gay, L. & Malanchi, I. The sleeping ugly: Tumour microenvironment's act to make or break the spell of dormancy. *Biochim. Biophys. Acta - Rev. Cancer* **1868**, 231–238 (2017).

6. Curran, S. & Murray, G. I. Matrix metalloproteinases in tumour invasion and metastasis. *J. Pathol.* **189**, 300–308 (1999).

7. Ying, H. *et al.* Genetics and biology of pancreatic ductal adenocarcinoma. *Genes Dev.* **30**, 355–385 (2016).

8. Wells, R. G. Tissue mechanics and fibrosis. *Biochim. Biophys. Acta - Mol. Basis Dis.* **1832**, 884–890 (2013).

9. Paszek, M. J. *et al.* Tensional homeostasis and the malignant phenotype. *Cancer Cell* **8**, 241-254 (2005).

10. Cruz-Acuña, R. *et al.* Synthetic hydrogels for human intestinal organoid generation and colonic wound repair. *Nat. Cell Biol.* **19**, 1326-1335 (2017).

11. Breslin, S. & O'Driscoll, L. Three-dimensional cell culture: The missing link in drug discovery. *Drug Discov. Today* **18**, 240-249 (2013).

12. Dufort, C. C., Paszek, M. J. & Weaver, V. M. Balancing forces: Architectural control of mechanotransduction. *Nat. Rev. Mol. Cell Biol.* **12**, 308–319 (2011).

13. Pampaloni, F., Reynaud, E. G. & Stelzer, E. H. K. The third dimension bridges the gap between cell culture and live tissue. *Nat. Rev. Mol. Cell Biol.* **8**, 839–845 (2007).

14. Lovitt, C. J., Shelper, T. B. & Avery, V. M. Advanced cell culture techniques for cancer drug discovery. *Biology (Basel).* **3**, 345–367 (2014).

15. Butcher, D. T., Alliston, T. & Weaver, V. M. A tense situation: Forcing tumour progression. *Nat. Rev. Cancer* **9**, 108–122 (2009).

16. Hlund, D. *et al.* Type IV collagen is a tumour stroma-derived biomarker for pancreas cancer. *Br. J. Cancer* **101**, 91–97 (2009).

17. Burdett, E., Kasper, F. K., Mikos, A. G. & Ludwig, J. A. Engineering tumors: A tissue engineering perspective in cancer biology. *Tissue Eng. - Part B Rev.* **16**, 351–359 (2010).

18. Yamano, M. *et al.* Genetic progression and divergence in pancreatic carcinoma. *Am. J. Pathol.* **156**, 2123-2133 (2000).

19. Ying, H. *et al.* Oncogenic kras maintains pancreatic tumors through regulation of anabolic glucose metabolism. *Cell* **149**, 656–670 (2012).

20. Lin, W. C. *et al.* Dormant cancer cells contribute to residual disease in a model of reversible pancreatic cancer. *Cancer Res.* **73**, 1821–1830 (2013).

21. Campbell, P. J. *et al.* The patterns and dynamics of genomic instability in metastatic pancreatic cancer. *Nature* **467**, 1109–1113 (2010).

22. Viale, A. *et al.* Oncogene ablation-resistant pancreatic cancer cells depend on mitochondrial function. *Nature* **514**, 628–632 (2014).

23. Sosa, M. S., Bragado, P. & Aguirre-Ghiso, J. A. Mechanisms of disseminated

cancer cell dormancy: An awakening field. *Nat. Rev. Cancer* **14**, 611–622 (2014).

24. Röcken, M. Early tumor dissemination, but late metastasis: Insights into tumor dormancy. *J. Clin. Invest.* **120**, 1800–1803 (2010).

25. Eyles, J. *et al*. Tumor cells disseminate early, but immunosurveillance limits metastatic outgrowth, in a mouse model of melanoma. *J. Clin. Invest.* **120**, 2030-2039 (2010).

26. Wenzel, C. *et al*. 3D high-content screening for the identification of compounds that target cells in dormant tumor spheroid regions. *Exp. Cell Res.* **323**, 131–143 (2014).

27. Regot, S., Hughey, J. J., Bajar, B. T., Carrasco, S. & Covert, M. W. High-sensitivity measurements of multiple kinase activities in live single cells. *Cell* **157**, 1724–1734 (2014).

28. Riedl, J. *et al*. Lifeact: A versatile marker to visualize F-actin. *Nat. Methods* **5**, 605–607 (2008).

29. Polyak, K. & Weinberg, R. A. Transitions between epithelial and mesenchymal states: Acquisition of malignant and stem cell traits. *Nat. Rev. Cancer* **9**, 265-273 (2009).

30. Yachida, S. *et al*. Distant metastasis occurs late during the genetic evolution of pancreatic cancer. *Nature* **467**, 1114-1117 (2010).

31. Haeno, H. *et al*. Computational modeling of pancreatic cancer reveals kinetics of metastasis suggesting optimum treatment strategies. *Cell* **148**, 362–375 (2012).

32. Rhim, A. D. *et al*. EMT and dissemination precede pancreatic tumor formation. *Cell* **148**, 349-361 (2012).

33. Lin, W. C., Rajbhandari, N. & Wagner, K. U. Cancer cell dormancy in novel mouse models for reversible pancreatic cancer: A lingering challenge in

the development of targeted therapies. *Cancer Res.* **74**, 2138–2143 (2014).

34. Aguirre-Ghiso, J. A. Models, mechanisms and clinical evidence for cancer dormancy. *Nat. Rev. Cancer* **7**, 834–846 (2007).

35. Pavan Grandhi, T. S., Potta, T., Nitiyanandan, R., Deshpande, I. & Rege, K. Chemomechanically engineered 3D organotypic platforms of bladder cancer dormancy and reactivation. *Biomaterials* **142**, 171–185 (2017).

36. Harrison, R. G., Greenman, M. J., Mall, F. P. & Jackson, C. M. Observations of the living developing nerve fiber. *Anat. Rec.* **1**, 116–128 (1907).

37. Raeber, G. P., Lutolf, M. P. & Hubbell, J. A. Molecularly engineered PEG hydrogels: A novel model system for proteolytically mediated cell migration. *Biophys. J.* **89**, 1374–1388 (2005).

38. Carlsson, J. & Yuhas, J. M. Liquid-overlay culture of cellular spheroids. *Recent Results Cancer Res.* **95**, 1–23 (1984).

39. Singh, A. & Peppas, N. A. Hydrogels and scaffolds for immunomodulation. *Adv. Mater.* **26**, 6530–6541 (2014).

40. Song, H. H. G., Park, K. M. & Gerecht, S. Hydrogels to model 3D in vitro microenvironment of tumor vascularization. *Adv. Drug Deliv. Rev.* **79**, 19–29 (2014).

41. Almany, L. & Seliktar, D. Biosynthetic hydrogel scaffolds made from fibrinogen and polyethylene glycol for 3D cell cultures. *Biomaterials* **26**, 2467–2477 (2005).

42. Phelps, E. A. *et al.* Maleimide cross-linked bioactive PEG hydrogel exhibits improved reaction kinetics and cross-linking for cell encapsulation and in situ delivery. *Adv. Mater.* **24**, 64–70 (2012).

43. Trujillo, S. *et al.* Engineered 3D hydrogels with full-length fibronectin that sequester and present growth factors. *Biomaterials* **252**, 120104 (2020).

44.   Trevigen®. *Cultrex® BME*.

45.   Barkan, D. *et al*. Metastatic growth from dormant cells induced by a Col-I-enriched fibrotic environment. *Cancer Res.* **70**, 5706–5716 (2010).

46.   Invitrogen Molecular Probes. LIVE/DEAD Viability/Cytotoxicity Kit for mammalian cells. *Product Information, Catalog number: MP 03224* 1–7 (2005).

47.   Gel, C. C. *3D Cell Culture Gel (Col-Tgel)*.

48.   Fang, J. Y. *et al*. From competency to dormancy: A 3D model to study cancer cells and drug responsiveness. *J. Transl. Med.* **14**, 1–13 (2016).

49.   Wen, J. H. *et al*. Interplay of matrix stiffness and protein tethering in stem cell differentiation. *Nat. Mater.* **13**, 979–987 (2014).

50.   Lin, C. C., Raza, A. & Shih, H. PEG hydrogels formed by thiol-ene photo-click chemistry and their effect on the formation and recovery of insulin-secreting cell spheroids. *Biomaterials* **32**, 9685–9695 (2011).

51.   Pankov, R. & Yamada, K. M. Fibronectin at a glance. *J. Cell Sci.* **115**, 3861–3863 (2002).

52.   Cavaco, A. C. M. *et al*. The interaction between laminin-332 and α3β1 integrin determines differentiation and maintenance of cafs, and supports invasion of pancreatic duct adenocarcinoma cells. *Cancers (Basel).* **11**, (2019).

53.   Ishihara, J. *et al*. Laminin heparin-binding peptides bind to several growth factors and enhance diabetic wound healing. *Nat. Commun.* **9**, (2018).

54.   Morton, J. P. *et al*. Mutant p53 drives metastasis and overcomes growth arrest/senescence in pancreatic cancer. *Proc. Natl. Acad. Sci. U. S. A.* **107**, 246–251 (2010).

55.   Orimo, A. *et al*. Stromal fibroblasts present in invasive human breast

carcinomas promote tumor growth and angiogenesis through elevated SDF-1/CXCL12 secretion. *Cell* **121**, 335–348 (2005).

56. Trujillo-Muñoz, S. Engineered Fibronectin-based Hydrogels as Novel Three-dimensional Microenvironments to Promote Microvasculature Growth. (University of Glasgow, 2019).

57. Yang, T. *et al. Mechanical and swelling properties of hydrogels. Wiley* (2012).

58. Rice, A. J. *et al*. Matrix stiffness induces epithelial-mesenchymal transition and promotes chemoresistance in pancreatic cancer cells. *Oncogenesis* **6**, 1–9 (2017).

59. Elosegui-Artola, A. *et al*. Mechanical regulation of a molecular clutch defines force transmission and transduction in response to matrix rigidity. *Nat. Cell Biol*. **18**, 540–548 (2016).

60. Zanconato, F., Battilana, G., Cordenonsi, M. & Piccolo, S. YAP/TAZ at the roots of cancer. *Cancer Cell* **29**, 26–33 (2016).

61. Loessner, D. *et al*. Bioengineered 3D platform to explore cell-ECM interactions and drug resistance of epithelial ovarian cancer cells. *Biomaterials* **31**, 8494–8506 (2010).

62. Liu, H. Y., Korc, M. & Lin, C. C. Biomimetic and enzyme-responsive dynamic hydrogels for studying cell-matrix interactions in pancreatic ductal adenocarcinoma. *Biomaterials* **160**, 24–36 (2018).

63. Smyrek, I. & Stelzer, E. H. K. Quantitative three-dimensional evaluation of immunofluorescence staining for large whole mount spheroids with light sheet microscopy. *Biomed. Opt. Express* **8**, 484 (2017).

64. Gstraunthaler, G., Lindl, T. & Van Der Valk, J. A plea to reduce or replace fetal bovine serum in cell culture media. *Cytotechnology* **65**, 791–793 (2013).

65. Puls, T. J. *et al.* Development of a Novel 3D Tumor-tissue Invasion Model for High-throughput, High-content Phenotypic Drug Screening. *Sci. Rep.* **8**, (2018).

66. Elosegui-Artola, A. *et al.* Rigidity sensing and adaptation through regulation of integrin types. *Nat. Mater.* **13**, 631–637 (2014).

67. Soofi, S. S., Last, J. A., Liliensiek, S. J., Nealey, P. F. & Murphy, C. J. The elastic modulus of Matrigel™ as determined by atomic force microscopy. *J. Struct. Biol.* **167**, 216–219 (2009).

68. Jaiswal, D. *et al.* Stiffness analysis of 3D spheroids using microtweezers. *PLoS One* **12**, (2017).

69. Ki, C. S., Shih, H. & Lin, C. C. Effect of 3D matrix compositions on the efficacy of EGFR inhibition in pancreatic ductal adenocarcinoma cells. *Biomacromolecules* **14**, 3017–3026 (2013).

70. Ki, C. S., Shih, H. & Lin, C. C. Effect of 3D matrix compositions on the efficacy of EGFR inhibition in pancreatic ductal adenocarcinoma cells. *Biomacromolecules* **14**, 3017–3026 (2013).

71. Miller, I. *et al.* Ki67 is a Graded Rather than a Binary Marker of Proliferation versus Quiescence. *Cell Rep.* **24**, 1105-1112.e5 (2018).

72. Zanconato, F., Battilana, G., Cordenonsi, M. & Piccolo, S. YAP/TAZ as therapeutic targets in cancer. *Curr. Opin. Pharmacol.* **29**, 26–33 (2016).

73. Varma, S., Qi, L. S., West, R. B. & Chaudhuri, O. YAP - independent mechanotransduction drives breast cancer progression. 1–37 (2018).

74. Clark, P., Connolly, P., Curtis, A. S. G., Dow, J. A. & Wilkinson, C. D. Topographical control of cell behaviour. I. Simple step cues. *Development* **99**, 439–448 (1987).

75. Clark, P., Connolly, P., Curtis, A. S. G., Dow, J. A. T. & Wilkinson, C. D. W. Topographical control of cell behaviour: II. multiple grooved substrata.

Development **108**, 635–644 (1990).

76. Gao, X. *et al*. Regulating cell behaviors on micropillar topographies affected by interfacial energy. *RSC Adv*. **5**, 22916–22922 (2015).

77. Tan, H., DeFail, A. J., Rubin, J. P., Chu, C. R. & Marra, K. G. Novel multiarm PEG-based hydrogels for tissue engineering. *J. Biomed. Mater. Res. - Part A* **92**, 979–987 (2010).

78. Ehrbar, M. *et al*. Elucidating the role of matrix stiffness in 3D cell migration and remodeling. *Biophys. J*. **100**, 284–293 (2011).

79. Lee, H. P., Gu, L., Mooney, D. J., Levenston, M. E. & Chaudhuri, O. Mechanical confinement regulates cartilage matrix formation by chondrocytes. *Nat. Mater*. **16**, 1243–1251 (2017).

80. Hanahan, D. & Weinberg, R. A. Hallmarks of cancer: The next generation. *Cell* **144**, 646–674 (2011).

81. Sasser, A. K. *et al*. Human bone marrow stromal cells enhance breast cancer cell growth rates in a cell line-dependent manner when evaluated in 3D tumor environments. *Cancer Lett*. **254**, 255–264 (2007).

82. Koh, B., Jeon, H., Kim, D., Kang, D. & Kim, K. R. Effect of fibroblast co-culture on the proliferation, viability and drug response of colon cancer cells. *Oncol. Lett*. **17**, 2409–2417 (2019).

83. Yakavets, I. *et al*. Advanced co-culture 3D breast cancer model for investigation of fibrosis induced by external stimuli: optimization study. *Sci. Rep*. **10**, (2020).

84. Cavaco, A., Rezaei, M., Niland, S. & Eble, J. A. Collateral damage intended-cancer-associated fibroblasts and vasculature are potential targets in cancer therapy. *Int. J. Mol. Sci*. **18**, (2017).

85. Fluegen, G. *et al*. Phenotypic heterogeneity of disseminated tumour cells is preset by primary tumour hypoxic microenvironments. *Nat. Cell Biol*.

19, 120–132 (2017).

86. Mather, B. D., Viswanathan, K., Miller, K. M. & Long, T. E. Michael addition reactions in macromolecular design for emerging technologies. *Prog. Polym. Sci.* **31**, 487–531 (2006).

87. Kimbrough, C. W. *et al.* Targeting acidity in pancreatic Adenocarcinoma: Multispectral Optoacoustic tomography detects ph-low insertion peptide probes in vivo. *Clin. Cancer Res.* **21**, 4576–4585 (2015).

88. Lutolf, M. P. & Hubbell, J. A. Synthetic biomaterials as instructive extracellular microenvironments for morphogenesis in tissue engineering. *Nat. Biotechnol.* **23**, 47–55 (2005).

89. Infanger, D. W., Lynch, M. E. & Fischbach, C. Engineered culture models for studies of tumor-microenvironment interactions. *Annu. Rev. Biomed. Eng.* **15**, 29–53 (2013).

90. Li, Y. *et al.* Supramolecular Nanofibrillar Thermoreversible Hydrogel for Growth and Release of Cancer Spheroids. *Angew. Chemie - Int. Ed.* **56**, 6083–6087 (2017).

91. Lin, M., DiVito, M. M., Merajver, S. D., Boyanapalli, M. & van Golen, K. L. Regulation of pancreatic cancer cell migration and invasion by RhoC GTPase and caveolin-1. *Mol. Cancer* **4**, 21 (2005).

92. Shen, W. *et al.* TGF-β in pancreatic cancer initiation and progression: Two sides of the same coin. *Cell Biosci.* **7**, 1–7 (2017).

93. Yoon, H. *et al.* TGF-β1-mediated transition of resident fibroblasts to cancer-associated fibroblasts promotes cancer metastasis in gastrointestinal stromal tumor. *Oncogenesis* **10**, (2021).

94. Tang, X. *et al.* Autocrine TGF-β1/miR-200s/miR-221/DNMT3B regulatory loop maintains CAF status to fuel breast cancer cell proliferation. *Cancer Lett.* **452**, 79–89 (2019).

95. Li, S., Mason, C. & Melnick, A. Genetic and epigenetic heterogeneity in acute myeloid leukemia. *Curr. Opin. Genet. Dev.* **36**, 100–106 (2016).

96. Zeisberg, M. & Neilson, E. G. Review series personal perspective Biomarkers for epithelial-mesenchymal transitions. *J Clin Invest.* **119**, 1429–1437 (2009).

97. Paluch, E. K. & Raz, E. The role and regulation of blebs in cell migration. *Curr. Opin. Cell Biol.* **25**, 582–590 (2013).

98. Goudarzi, M., Boquet-Pujadas, A., Olivo-Marin, J. C. & Raz, E. Fluid dynamics during bleb formation in migrating cells in vivo. *PLoS One* **14**, (2019).

99. Khan, Z. S., Santos, J. M., Vaz, N. G. & Hussain, F. Enhanced blebbing as a marker for metastatic prostate cancer. *Biomicrofluidics* **13**, (2019).

100. Jannat, R. A., Robbins, G. P., Ricart, B. G., Dembo, M. & Hammer, D. A. Neutrophil adhesion and chemotaxis depend on substrate mechanics. *J. Phys. Condens. Matter* **22**, (2010).

101. Klein, E. A. *et al.* Cell-Cycle Control by Physiological Matrix Elasticity and In Vivo Tissue Stiffening. *Curr. Biol.* **19**, 1511–1518 (2009).

102. C.M., L., H.B., W., M., D. & Y.L., W. Cell movement is guided by the rigidity of the substrate. *Biophys. J.* **79**, 144–152 (2000).

103. Lien, S. M., Ko, L. Y. & Huang, T. J. Effect of pore size on ECM secretion and cell growth in gelatin scaffold for articular cartilage tissue engineering. *Acta Biomater.* **5**, 670–679 (2009).

104. Chaudhuri, O., Cooper-White, J., Janmey, P. A., Mooney, D. J. & Shenoy, V. B. Effects of extracellular matrix viscoelasticity on cellular behaviour. *Nature* **584**, 535–546 (2020).

105. Montel, F. *et al.* Stress clamp experiments on multicellular tumor spheroids. *Phys. Rev. Lett.* **107**, (2011).

106. Baghban, R. *et al.* Tumor microenvironment complexity and therapeutic implications at a glance. *Cell Commun. Signal.* **18**, (2020).

107. Hughes, C. S., Postovit, L. M. & Lajoie, G. A. Matrigel: a complex protein mixture required for optimal growth of cell culture. *Proteomics* **10**, 1886–1890 (2010).

108. Benton, G., Kleinman, H. K., George, J. & Arnaoutova, I. Multiple uses of basement membrane-like matrix (BME/Matrigel) in vitro and in vivo with cancer cells. *Int. J. Cancer* **128**, 1751–1757 (2011).

109. Bergert, M., Chandradoss, S. D., Desai, R. A. & Paluch, E. Cell mechanics control rapid transitions between blebs and lamellipodia during migration. *Proc. Natl. Acad. Sci. U. S. A.* **109**, 14434–14439 (2012).

Supplementary Information

S1: Hydrogel Calculations

Without revealing the quantities of each constituent of the hydrogels, the calculations for the composition of the 8-Arm hydrogels were carried out in Excel and are as follows:

- The mass of polymer required for the desired wt% polymer hydrogel was determined

    - 6 wt% = 60,000 µg/ml

    - 10 wt% = 100,000 µg/ml

- The number of moles of PEG-8-MAL and PEG-dithiol was then calculated:

    - $moles = \dfrac{mass}{molecular\ weight}$

- The number of molecules of PEG-8-MAL and PEG-dithiol was calculated:

    - $molecules = moles * Avogadro's\ Number\ (6.022x10^{23})$

- The number of maleimide groups in the determined weight of PEG-8-MAL was calculated taking into account the PEG-4-MAL used for PEGylating the FN (assuming 2 of the 4 maleimide groups in the PEG-4-MAL are no longer available following PEGylation):

    - $Total\ Maleimide\ groups = (8 * number\ of\ PEG8MAL\ molecules) + (2 * number\ of\ PEG4MAL\ molecules)$

- The number of thiol groups in the determined weight of PEG-dithiol was calculated:

    - $Total\ Thiols = 2 * number\ of\ PEGdithiol\ molecules$

- The masses of PEG-8-MAL and PEG-dithiol were then increased or decreased to achieve the correct cross-linking ratio (3:8, 6:8, or 8:8 SH:MAL) within the required total polymer mass (60,000 µg/ml or 100,000 µg/ml dependent on the wt% desired).